Photocatalytic Water Purification with Graphitic C_3N_4-Based Composites: Enhancement, Mechanisms, and Performance

Songhao Luo, †[ab] Chang Zhang, †[ab] Eydhah Almatrafi, [b] Ming Yan, [a] Yang Liu, [a] Yukui Fu, [a] Ziwei Wang, [a] Ling Li, [a] Chenyun Zhou, [ab] Piao Xu, *[ab] Zhifeng Liu, *[ab] Guangming Zeng *[ab]

[a] College of Environmental Science and Engineering and Key Laboratory of Environmental Biology and Pollution Control (Ministry of Education), Hunan University, Changsha 410082, PR China;

[b] Center of Research Excellence in Renewable Energy and Power Systems, Center of Excellence in Desalination Technology, Department of Mechanical Engineering, Faculty of Engineering-Rabigh, King Abdulaziz University, Jeddah 21589, Saudi Arabia.

* E-mail: zgming@hnu.edu.cn (G. Zeng); piaoxu@hnu.edu.cn (P. Xu) and zhifengliu@hnu.edu.cn (Z. Liu).

[1] These authors contribute equally to this article.

KEYWORDS: Graphitic carbon nitride; Single-atom catalyst; Photocatalysis; Density functional theory; Water purification; Life-cycle assessment

ABSTRACT:

Recently enormous exertions have been dedicated to modify graphitic carbon nitride (g-C_3N_4)-based photocatalysts via morphological adjustment and compositional control, providing various ways for the advance of high-efficiency catalysts in the field of photocatalytic water purification. This review summarizes the latest developments in photocatalytic removal of contaminants and sterilization in water with g-C_3N_4-based materials, highlighting the performance and mechanism of multi-component cooperative photocatalysis. We review various strategies for improving the catalytic performance of g-C_3N_4-based photocatalysts, introducing theoretical calculations to explore the relationships between basic properties and photocatalytic activity. Then the performance and mechanism of photocatalytic water purification with g-C_3N_4-based materials are discussed. Finally, we put forward the principles and ways for the enhancement and application of g-C_3N_4-based composites in the future, evaluating their full life-cycle in photocatalytic water purification.

Content

1. Introduction 4

2. Enhancement Strategies 6

2.1 Morphology adjustment and control 7

2.2 Construction of heterojunction 10

2.3 Noble metal deposition 12

2.4 Doping and defect engineering 13

3. Theoretical Investigation 16

3.1 Internal mechanism of photoactivity 16

3.2 Other basic properties 18

4. Photocatalytic Mechanism and Performance 21

4.1 Removal of antibiotics and pesticide 25

4.2 Degradation of organic dyes 32

4.3 Sterilization and disinfection 35

4.4 Reduction of hexavalent chromium 42

4.5 Metal-free Photocatalysis 46

5. Chemical and Photocatalytic Stability 47

6. Conclusions and Perspectives 48

Declaration of Competing Interest 51

Acknowledgment 51

References 52

1. Introduction

As the world's population increases and global industrialization accelerates, fresh and sustainable water supplies are under unprecedented pressure [1-3]. Large amounts of pollutants, such as antibiotics, organic dyes, pesticides, and heavy metal ions, are released daily into different types of water bodies, finally polluting raw water. These pollutants have high chemical and physical stability in the environment and are difficult to be degraded by microorganisms. At the same time, many persistent pollutants can accumulate in organisms including human beings, and cause great harm to organisms [4-8]. Therefore, the elimination of these compounds from the environment through effective methods is important. Until now, many advanced water purification technologies have been developed to convert difficult-to-biodegrade organic pollutants into less toxic or more biodegradable byproducts [9-11].

Compared with other treatment techniques, photocatalytic technology has many important features [12-14], such as mild operating conditions and fast kinetics [15-19], without secondary pollution [20,21], as well as low operating cost and high value-added production [22,23]. For water treatment applications, engineers and researchers prefer heterogeneous photocatalysts because heterogeneous photocatalytic processes avoid cumbersome separation procedures and recycling methods as well as loss of expensive catalysts [24-27]. Heterogeneous photocatalytic reaction is a complex physical and chemical process, mainly including the generation of photogenerated electrons and hole pairs, surface capture of carrier, recombination of photogenerated electron-hole pairs, and inter-interface charge transfer [28-30]. In recent years, the development of advanced materials has provided rich soil for the study of heterogeneous

74 photocatalyst.

75 The advanced materials have unique properties such as visible light responsiveness, rich
76 active sites, and controllable molecular and energy band structures. The suitable photocatalytic
77 materials have great significance to the development of photocatalyst technology. The
78 strategies for increasing the photocatalytic activity of photocatalytic materials include: (i)
79 Reducing the bandgap width of semiconductor catalysts to reduce the energy required for
80 electron transition reactions; (ii) Choosing a more suitable crystal structure to reduce
81 recombination of photogenerated carriers; (iii) Changing the morphology of the catalyst to
82 increase the catalytic active sites on the photocatalyst. Besides, attention should also be paid to
83 the catalytic stability of the photocatalyst and the external reaction conditions of the
84 photocatalytic system. Currently, semiconductor photocatalysts have been widely studied and
85 commercially valuable [28,31], including TiO_2 [32], BiOX [33], g-C_3N_4 [34], perovskite
86 materials [35], ZnO [36], and porous organic polymer [37,38].

87 Graphitic carbon nitride (g-C_3N_4) has attracted extensive interdisciplinary attention due to
88 its unique layered structure, suitable band structure, metal-free properties, and excellent
89 stability [39-41]. Above all, g-C_3N_4 allows for modification through molecular modifications
90 and surface engineering, providing various ways to prepare g-C_3N_4-based materials with
91 effective photocatalytic performance [34,42,43]. Many research groups are striving to construct
92 an appropriate g-C_3N_4-based system through the interaction between different semiconductor
93 materials to accelerate the separation of photogenerated carriers. For application, the g-C_3N_4-
94 based materials show interesting properties, especially the visible light response in nitrogen
95 fixation [44,45] and removal of contaminants [46]. Habibi-Yangjeh's group proposed an

96 enhancement mechanism for nitrogen fixation and directed the preparation of a g-C_3N_4-based
97 binary visible light induced photocatalyst with high activity and good stability for the
98 photofixation of nitrogen [44]. Meanwhile, Habibi-Yangjeh's group also constructed a g-C_3N_4-
99 based ternary metal-free nanocomposites to improve the absorption of visible light and promote
100 the separation of photogenerated charge [45], providing a new way to solve the environmental
101 issues.

102 Recently, based on a deeper understanding of the relationship between the photoelectric
103 properties and structural components of polymer-based materials, researchers delved deeper
104 into the photoresponsive g-C_3N_4-based materials, providing a new approach for efficient
105 photocatalytic water purification. Current reviews present the discussion on the g-C_3N_4-based
106 photocatalysts [34,42,47], but lack reflection on the actual water purification situation. This
107 review has conducted as a detailed investigation of g-C_3N_4-based materials for photocatalytic
108 water purification, highlighting the photocatalytic properties and mechanism models. We also
109 summarize the improvement strategies and the theoretical research to guide the synthesis and
110 design of g-C_3N_4-based photocatalysts. Finally, g-C_3N_4-based photocatalysts are favored by
111 engineers and are expected to be further applied to actual water purification modules. Therefore,
112 in the section of conclusions and perspectives, we present their future development and life-
113 cycle assessment (LCA).

114 2. Enhancement Strategies

115 Although g-C_3N_4 has many excellent properties and extensive applications, ordinary g-
116 C_3N_4 still faces three main challenges [34,42,48]: (i) The inherent energy band characteristics

of g-C_3N_4 leads to narrow light response range and low visible light energy utilization ratio; (ii) The layers of g-C_3N_4 are relatively close to each other leads to its fewer reaction sites; (iii) No direct valence bond between the molecular layers of g-C_3N_4 and photogenerated carriers produced by g-C_3N_4 with short existence life leads to the deficiency of the photogenerated charge involved in the redox reaction. The above three problems greatly limit the application of g-C_3N_4. Currently, the improvement strategies include morphology adjustment (such as preparation of materials with different dimensions) [49-51], composite modification with other semiconductor materials to construct heterojunction [52-54], surface noble metal deposition [55-57], and single-atom doping [58-60].

2.1 Morphology adjustment and control

In the process of catalytic reaction, the surface of the catalysts is usually used as the site of the reaction, so their morphology is very important for the photocatalytic process. The g-C_3N_4 has a flexible structure and can withstand high temperatures, so it is possible to prepare g-C_3N_4-based materials with different morphologies using different templates and post-synthesis modification methods during the synthesis process [34,48,61]. The special morphology of the prepared g-C_3N_4 catalysts (Fig. 1) includes three-dimensions (3D) porous flowery g-C_3N_4 [62], two-dimensions (2D) lamelliform g-C_3N_4 [51,63], one-dimensions (1D) g-C_3N_4 nanotube [49], zero-dimensions (0D) g-C_3N_4 hollow sphere [64], and novel 3D structures such as horned materials [65] and fish scale g-C_3N_4 [66].

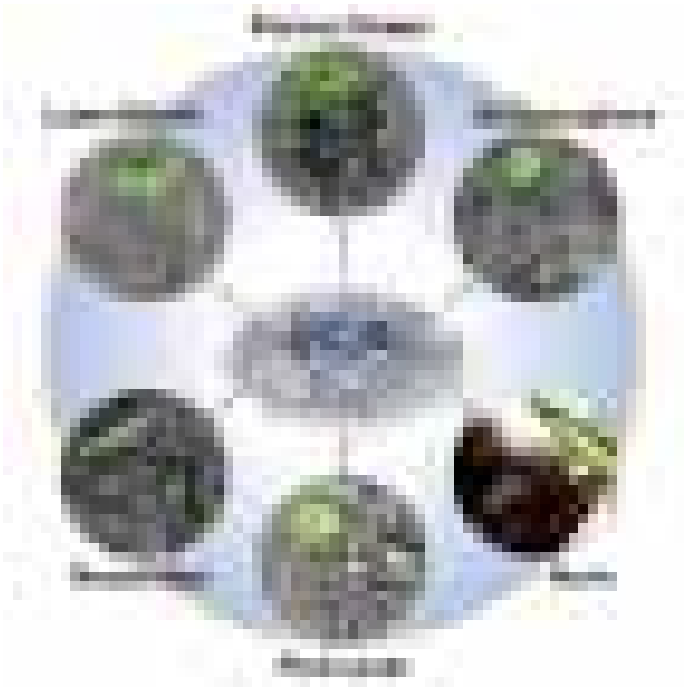

Fig. 1. Rich morphologies of the g-C_3N_4: porous flower [62], lamelliform [63], hollow sphere [64], nanotubes [49], horn [65], and fish scale [66].

The commonly used methods for preparing regular porous g-C_3N_4 include the soft template method and the hard template method [42]. Subsequent developments include the preparation of porous materials by controlling reaction conditions without adding any template agent [62]. To illustrate, Zhu et al. used melamine and hydroxyethylidene diphosphonic acid (HEDP) as reaction precursors to prepare phosphorus-hybridized mesoporous g-C_3N_4 at sintering condition of 500 °C without adding any template [62]. The obtained mesoporous P-doped g-C_3N_4 has higher photoelectric charge separation efficiency, so obtain a higher photocatalytic activity than the pure g-C_3N_4.

Flaky g-C_3N_4 can be prepared by liquid-exfoliation method and thermal exfoliation method [67,68]. Li et al. prepared the graphene-like C_3N_4 from the bulk phase g-C_3N_4 by liquid-exfoliation (Fig. 2a), and the resulting flake g-C_3N_4 was only 3-6 atomic layers thick [63]. Due

to the larger specific surface area, wider bandgap, and stronger electronic transport capacity, the obtained graphene-like C_3N_4 has enhanced photocatalytic activity. Besides, Niu et al. obtained an ultrathin g-C_3N_4 nanosheet (Fig. 2b) with a specific surface area of 306 $m^2 g^{-1}$ and thickness of 2 nm by thermal exfoliation [50], which showed higher photoresponse ability and photocatalytic activity than the bulk g-C_3N_4.

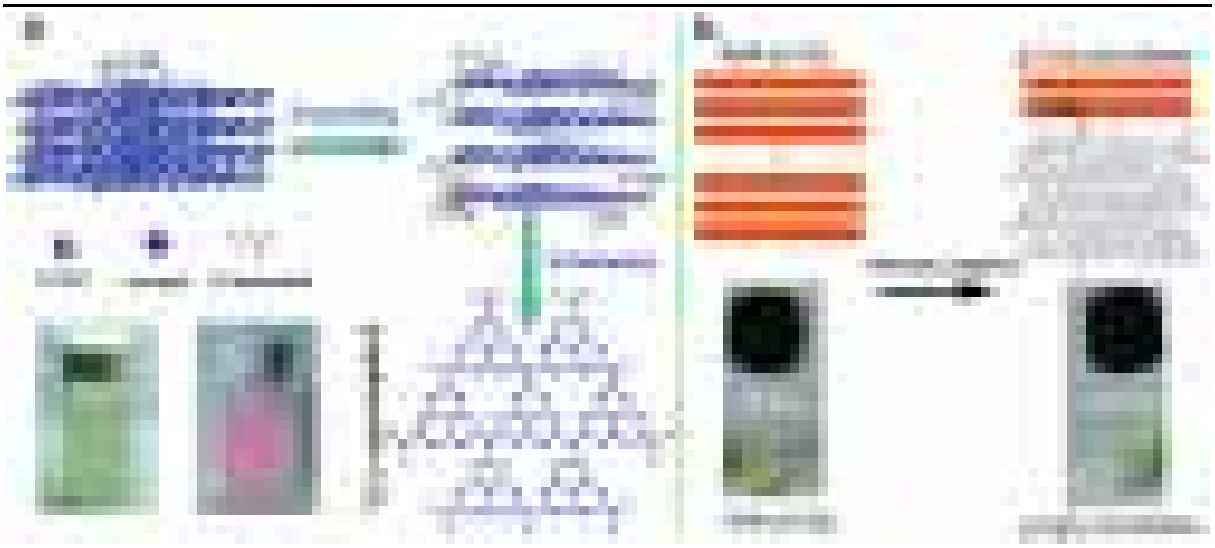

Fig. 2. Liquid-exfoliation method and thermal exfoliation method to prepare flaky g-C_3N_4. (a) The liquid-exfoliation methods for g-C_3N_4 [63]. (b) Thermal oxidation etching for the g-C_3N_4 nanosheets [50].

Horn hollow g-C_3N_4 (Fig. 1) synthesized by Liu et al. using copolymerization of melamine and ammonium bromide (NH_4Br) in the first [65]. The characteristics of hollow, mesoporous, ultra-thin, and trumpet greatly improved the efficiency of photo-generated charge separation, carrier density, and surface charge transfer. To be specific, electrons generated by the photoexcited horn hollow g-C_3N_4 migrated to the outer layer of the material, while holes migrated to the inner layer, thus achieving efficient space charge separation. Furthermore, Lin et al. obtained fish-scale g-C_3N_4 nanosheets (Fig. 1) by subsequent heat treatment of original g-C_3N_4 nanosheets with ethylene glycol, polyvinylpyrrolidone (PVP), and hexadecyl trimethyl

ammonium bromide (CTAB) [66]. For this unique fish-scale structure, photoelectrons migrate selectively along the plane to the edge of the fish-scale, which is beneficial to the detachment of photogenerated carriers, thus improving the photocatalytic efficiency.

2.2 Construction of heterojunction

The combination of different semiconductor materials comes in two main forms, one is to combine g-C_3N_4 with wide bandgap semiconductor to form heterojunctions, reducing the photoelectron-hole pairs recombination through the photogenerated charge transfer between the interface of heterojunctions [53,69,70]. The other is to combine g-C_3N_4 with narrow bandgap semiconductors (such as sulfides, metal oxides, metal halides, etc.) [71-73]. Combining g-C_3N_4 with a narrow bandgap semiconductor promotes the detachment of photogenerated carriers and improves the optical response range of composite materials owing to the excellent optical response-ability of narrow bandgap semiconductors.

In both cases, the large heterojunction interface between two semiconductors is conducive to the redistribution of charges, which significantly improves the photocatalytic performance [34,74]. In 2018, we constructed the isotypic heterojunction PCN/CN (PCN: P-doped g-C_3N_4, CN: g-C_3N_4) by attaching the lamellar CN layer to the filamentous PCN sheet containing C, N, and P elements [75]. The heterogeneous structure of PCN/CN obtain enhanced photogenic charge separation and has good energy level matching, which is beneficial to produce a stronger light response in the whole ultraviolet and visible regions. Both CN and PCN are stimulated by visible light to yield carries, and the band migration between PCN and CN can drive the transfer of photogenic carries.

Noteworthily, simulating the natural photosynthesis, select suitable semiconductor materials to form reversible donor/recipient pair with g-C_3N_4 to construct a Z-scheme heterojunction is regarded as one of the best ways to improve photocatalytic activity [76-78]. For Z-scheme g-C_3N_4-based photocatalysts, the electrons from the CB of g-C_3N_4 can maintain a strong reduction ability. Meanwhile, besides g-C_3N_4, another component of the Z-scheme g-C_3N_4 composite can also compensate for the weak oxidation capacity of holes in the VB of g-C_3N_4 [54,79]. Therefore, the g-C_3N_4-based Z-scheme systems can efficiently retain electrons and holes to greatly improve the photocatalytic performance [80-82]. Furthermore, notably, we propose a "double Z-Scheme" heterojunction for GO/ACR/CN (GO: graphene oxide, ACR: Ag_2CrO_4, CN: g-C_3N_4) [83]. As shown in Fig. 3, ACR, GO and g-C_3N_4 are all excited by visible light to produce carries in the CB or VB, then the photoelectrons in the CB of ACR shift towards the metal Ag. Meanwhile, the holes in the VB of GO or CN move to the metal Ag and binds to the electron. Finally, the formed h^+, $\bullet O_2^-$, and •OH react with organic pollutants to degrade them.

Fig. 3. Photocatalytic reaction and charge transfer mechanism of the GO/ACR/CN ternary photocatalyst under visible light irradiation. Adapted with permission from ref. [83]. Copyright 2017 Elsevier B.V.

2.3 Noble metal deposition

Surface noble metal deposition is possible to promote photocatalytic performance by the formation of Schottky barrier and surface plasma resonance (SPR) on the interface of the g-C_3N_4 matrix [57,84,85]. The Schottky barrier can capture and extend electron life, and SPR can produce photon scattering, plasma resonance energy transfer, and hot electron excitation, both of which can improve photocatalytic reaction activity [84]. In 2011, Pan et al. applied platinum (Pt) and palladium (Pd) to the functionalization of g-C_3N_4 [55], which enhanced the carrier mobility and enhanced the photogenerated electron-hole pairs separation.

Due to the presence of Ag, Ag/g-C_3N_4 composites synthesized by the surface noble metal deposition has enhanced light absorption capacity under different lighting conditions, and the built-in electric field can promote the separation of photogenerated charges [57]. As an improvement, Xue et al. attached dual noble metal nanoparticles with a particle size of 7-15 nm to the surface of g-C_3N_4 by photoreduction (Fig. 4a-c) to form Ag/Pt/g-C_3N_4 composite materials [56]. As shown in Fig. 4d, the SPR effect of Au generates many hot electrons under light conditions. These hot electrons are inserted into the CB of g-C_3N_4 subsequently. Meanwhile, the photoelectrons are transferred from the CB of g-C_3N_4 to the outward of Pt nanoparticle through the electronic bridge effect of Pt, and then a reduction reaction occurs.

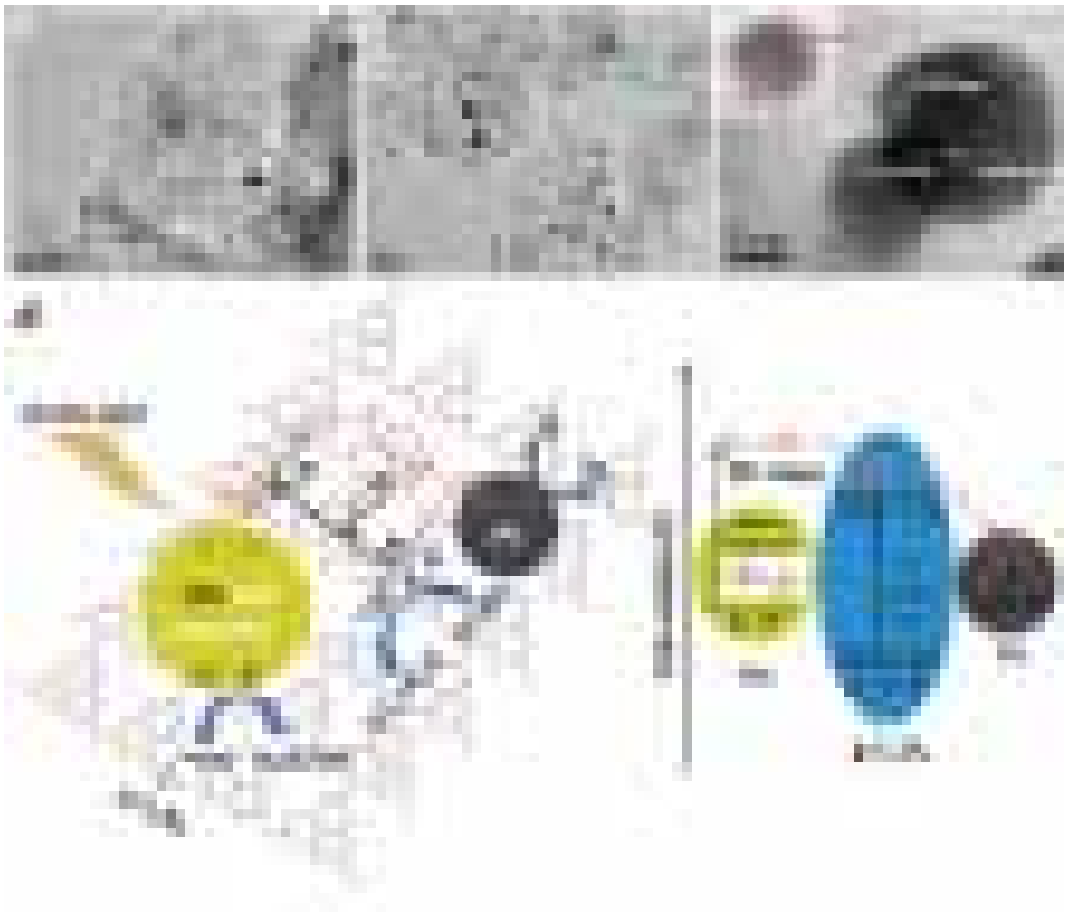

Fig. 4. Synthesis of Au/Pt/g-C_3N_4 with plasmon enhanced photocatalytic activity. Typical TEM images (a and b) and HRTEM image (c) of Ag/Pt/g-C_3N_4 nanocomposites. (d) The proposed photocatalytic mechanism for degradation of TCHCl by Au/Pt/g-C_3N_4 nanocomposites under visible light irradiation. Adapted with permission from ref. [56]. Copyright 2015 American Chemical Society.

2.4 Doping and defect engineering

Single-atom doping refers to the doping of metallic elements or non-metallic elements into the g-C_3N_4 structure, which can broaden the optical response range. As well, doping can enhance the electrical conductivity of materials, facilitate the separation and transmission of photogenerated carriers. Among them, common doped elements [59,86,87] are non-metallic elements such as sulfur (S), phosphorus (P), and boron (B), and the metallic elements such as Fe, Co, Zn, and Ni. Wang's group prepared bromine (Br)-doped g-C_3N_4 using the urea and

236 NH_4Br [88], and Br element can regulate the structure and light responsiveness of g-C_3N_4 to
237 obtain higher photocatalytic performances than the pure samples. Furthermore, P-doped g-
238 C_3N_4 also has a stronger photocatalytic ability to degrade organic dye than the g-C_3N_4 before
239 doping [60].

240 S-doping can modify the interior structure of g-C_3N_4 [89-91], for example, Liu et al. found
241 the S-doped g-C_3N_4 have an excellent photoredox effect due to the uniform substitution of S
242 for crystal lattice N and the unique electronic structure caused by the quantum confinement
243 effect [92]. Furthermore, S/P co-doping can inhibit g-C_3N_4 crystal growth, increases the
244 specific surface area, reduces the bandgap, and the O-functionalized increase the adsorption
245 capacity of g-C_3N_4 [93]. Zhen et al. introduced Fe or Cu into the g-C_3N_4 catalyst and found
246 that Fe or Cu can efficiently improve the photocatalytic performance of the overall material
247 [94]. However, noteworthily, the excessive single-atom doping could lead to electron-hole pairs
248 recombination and form more defects, which may hinder the photocatalytic process [95-97].

249 Recently, with the development of in situ meter technique, researchers have found that the
250 coordination environment of g-C_3N_4 can provide anchoring and confinement for metal atom
251 growth to form single-atom catalyst with excellent catalytic performance [98-102]. In practical
252 water treatment applications, the ideal characteristic obtained by single-atom catalysts is the
253 close to each other and uniformly dispersed of active sites in the g-C_3N_4 networks [103]. To
254 accurately locate and prove the existence of a single atomic catalyst, which usually requires the
255 advanced characterization techniques. To illustrate, aberration-corrected scanning transmission
256 electron microscopy (AC-STEM) and aberration-corrected high-resolution transmission

electron microscopy (HR-TEM) can provide the direct structural information of metal-atom [103-105]. Meanwhile, the combination of X-ray photoelectron spectroscopy (XPS), Fourier infrared spectroscopy (FTIR) and advanced computational chemistry methods, a deeper understanding of the structure of single atoms in the matrix can be provided [101,106,107].

Defect engineering is considered as an effective strategy to adjust the main structure and chemical environment of g-C_3N_4 molecules to improve their visible-light response, photoelectric charge separation, and surfactant free radical generation [108-112]. Liu's group used the template method to prepare porous g-C_3N_4 with marginal defects [113]. The extra electrons enriched at the defects of porous g-C_3N_4 give it higher interfacial oxidation activity, which is conducive to quenching the photogenerated holes and increasing the photocurrent, thus promoting the photoelectron reaction. Wu's group used the thermal treatment method containing fluorine solvent to control the defects of g-C_3N_4 [114]. Solvent heat treatment is conducive to the recondensation of terminal amino group, thus increasing the crystallinity to reduce defects. Meanwhile, the addition of fluorine promotes the formation of nitrogen vacancy thus to increases the active site. As well as, Huang et al. used in situ soft chemical treatment to synthesize g-C_3N_4 microtubules with adjustable nitrogen vacancy [115]. Nitrogen vacancy on the surface of g-C_3N_4 microtubules can adsorb and activate reactants and capture photogenerated electrons, thus enhancing photocatalytic activity. For the meantime, the porous wall structure of g-C_3N_4 microtubules can promote the diffusion of reactants, and the tubular structure is favorable for the directional migration of photoelectric charge.

3. Theoretical Investigation

In general, many materials are synthesized and modified based on "trial-and-error" research to explore the composition, structure, and properties of efficient catalytic materials. It is full of contingency, so systematically elucidate the universal law is challenging. This section mainly describes the theoretical research on the basic properties of g-C_3N_4-based photocatalysts.

3.1 Internal mechanism of photoactivity

For understanding the mechanism of photogenic carrier transfer at the hybrid interface of composite materials, density functional theory (DFT) calculation was performed [116-118]. According to the crystal structure of a single component, we constructed the O-doped C_3N_4 (OCN)/CoAl-layered double hydroxide (CoAl-LDH) heterojunction (OCAL) hybrid crystal model of lattice plane combination interface [116]. The deformation degree of the OCN lattice at the interface is far greater than that of coal-LDH, which stabilizes the Femi energy level and increases the depth of the hole, thus affecting the transfer and catalytic performance of the carriers on the interface [119]. Furthermore, the closest distance between the N atoms of OCN and the hydrogen atoms on the coal-LDH surface is 1.68Å, which may indicate the existence of obvious hydrogen bonds at the interface [120]. As well, CoAl-LDH and OCN generate the interfacial internal electric field (IIEF), which is favorable for photoinduced carrier separation [121-123]. Meanwhile, the electric field in the interface may cause the band edge to bend towards the interface [124,125] and transform the photocatalytic mechanism from the type-II mechanism to the Z-scheme mechanism [125-127]. Electrons on OCN rapidly combine with holes of CoAl-LDH through solid-solid contact interface [128], resulting in more $\bullet O_2^-$ and

298 •OH radicals generation from 2D-2D heterojunctions to degrade the organic pollutants.

299 Given that bandgap (E_g), the energy level structure, and molecular orbitals of photocatalyst
300 play a significant effect on its photocatalytic performance. Appropriate reduction of E_g can
301 make the light absorption region stronger and the electron migration faster [117,129,130].
302 Compared with CN and quantum dots (BPQDs), the TCN/BPQDs (BPTCN) composites have
303 a denser energy band curve, which indicates that BPTCN produces more photogenerated
304 carriers during the photocatalytic process. As well, the formation of a narrow bandgap in the
305 sample further moves the VBT of BPTCN up [131,132].

306 Besides, compared with CN, 2-hydroxy-4,6-dimethylpyrimidine grafted carbon nitride
307 (ACN-10) has a narrower bandgap (Fig. 5a-d) [118]. Therefore, ACN-10 has enhanced visible
308 light capture capability. Meanwhile, the HOMO and LUMO electrons of CN are both located
309 on heptazine (Fig. 5e), indicating that electrons and holes are in the same heptazine cell. As
310 shown in Fig. 5f, the HOMO of ACN is mainly distributed in the heptazine unit, while the
311 LUMO of ACN is mainly distributed in the HDMP unit, and only a small amount is distributed
312 in heptazine near HDMP [133]. Additionally, noteworthily, HOMO and LUMO energy levels
313 show a downward trend after HDMP is added to CN (Fig. 5g), which results in a bandgap
314 reduction of 0.24 eV, thus enhancing photocatalytic activity.

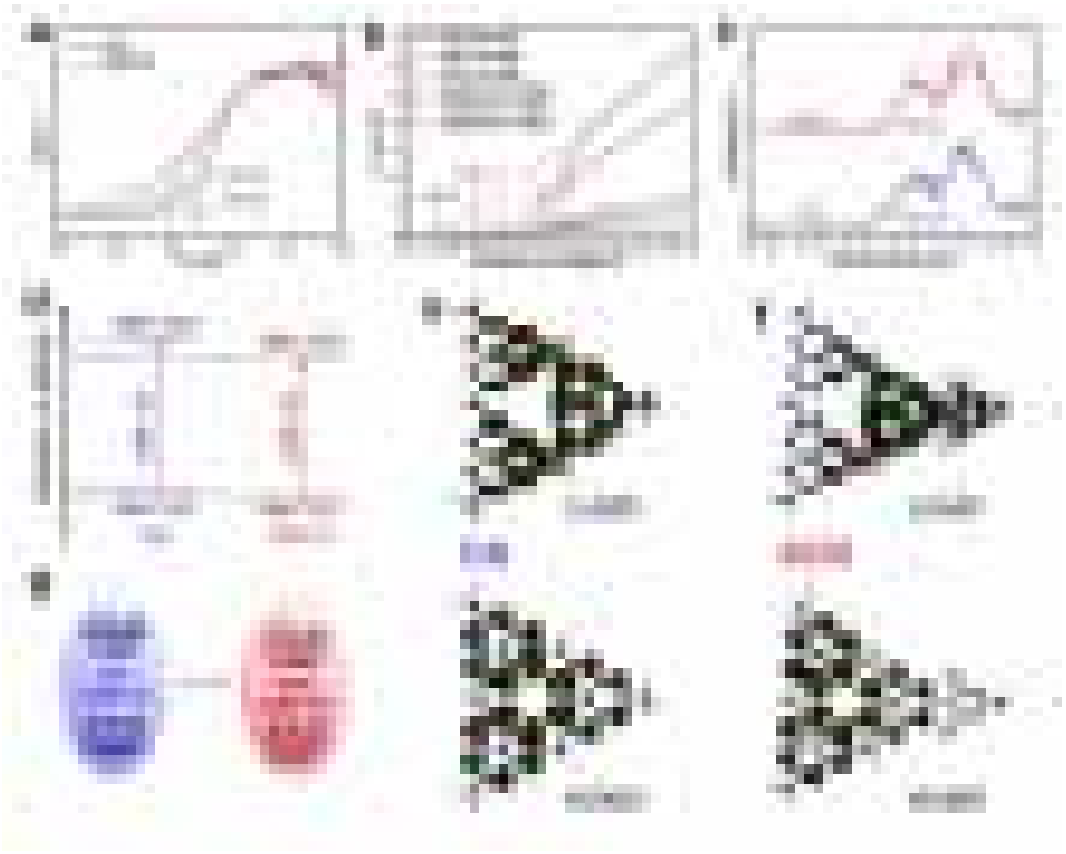

Fig. 5. Molecular engineering of polymeric C_3N_4. (a) Tauc plots, (b) Mott-Schottky plots, (c) VB XPS spectra, and (d) band structure diagrams for the CN and ACN-10; Optimized HOMO and LUMO energy levels of the (e) CN and (f) ACN; (g) DFT-calculated HOMO-LUMO band structures of the CN and CAN. Adapted with permission from ref. [118]. Copyright 2020 Elsevier B.V.

3.2 Other basic properties

Besides the basic properties mentioned above, other parameters including work function (Φ), optical absorption, and the effect of pressure also are significant basic properties of g-C_3N_4-based nanocomposites [134-136]. Work function (Φ) was defined as an escape from the Fermi level to vacuum the minimum energy [137-139]. In the theoretical calculation of photocatalytic performance, the work function is often used to assess the Fermi energy of g-C_3N_4 [138]. Normally, the work function is inversely proportional to the Fermi energy level, and when g-C_3N_4 is compounded with other materials, the relative location of their Fermi energy level can

329 be obtained by calculating their work function. The optical absorption characteristic of g-C_3N_4
330 is related to the curve of absorption coefficient (I) and photon energy or wavelength [140]. As
331 shown in Fig. 6, the g-C_3N_4 optical response range includes visible light, and the light
332 absorption curve of g-C_3N_4-based photocatalysts can be changed by the heteroatom doping and
333 doping atom change [140]. Furthermore, with the increase of pressure, the lattice constant, unit
334 cell volume, and bandgap decreased gradually, while the light absorption increases gradually
335 [141].

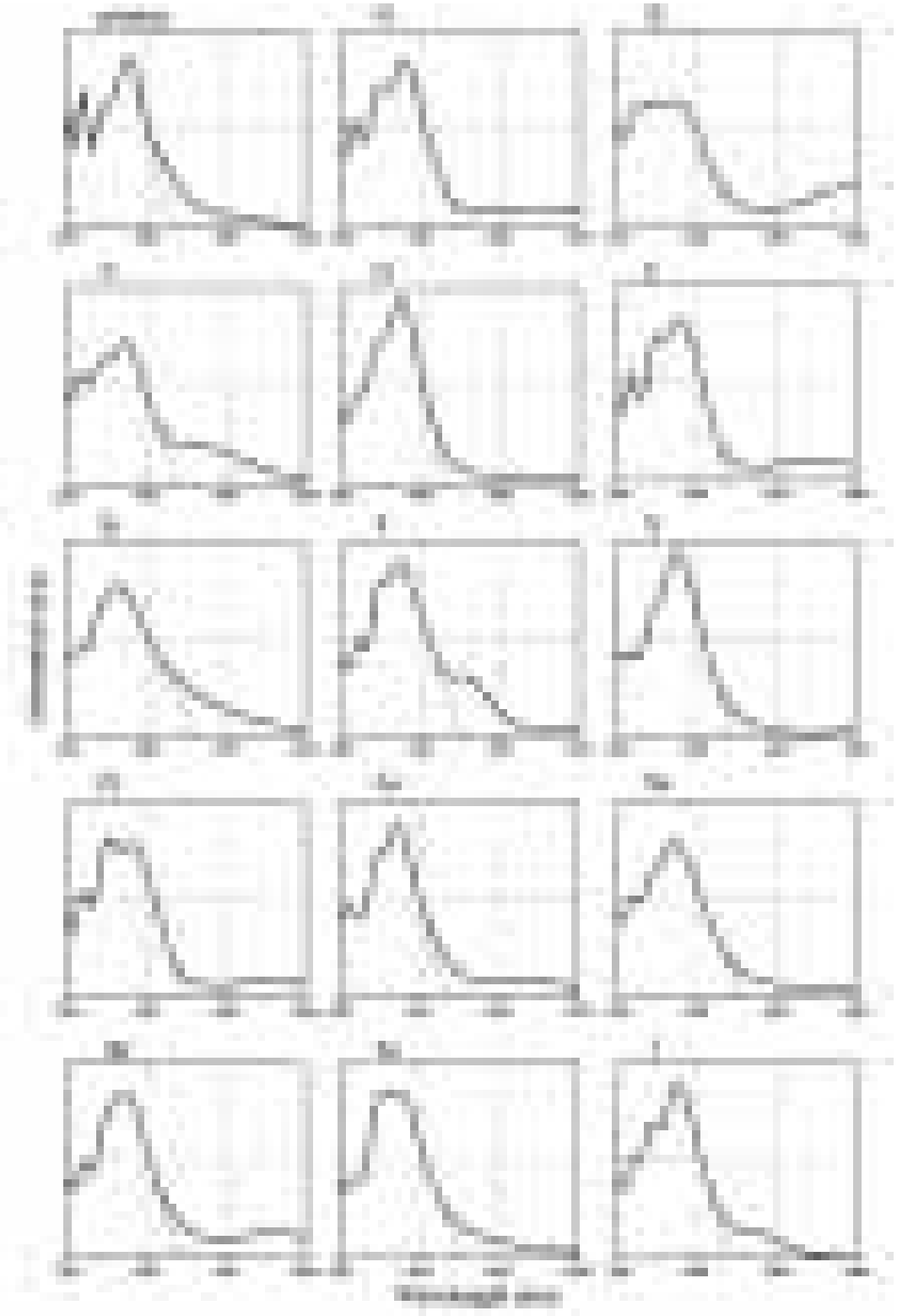

Fig. 6. Optical absorption curve of monolayer g-C_3N_4 before and after doping nonmetal atoms. Adapted with permission from ref. [140]. Copyright 2017 Elsevier B.V.

4. Photocatalytic Mechanism and Performance

Modified g-C_3N_4-based photocatalysts have attracted increasing attention owing to their promising application prospects in water purification. The state-of-art advances of photocatalytic wastewater treatment by g-C_3N_4-based materials are summarized in Table 1-4, including removal of antibiotics and pesticide, degradation of organic dyes, inactivation of water-borne pathogens, and reduction of heavy metal ion. This section describes the effect and detailed mechanism of degradation of pollutants and inactivation of pathogens by g-C_3N_4-based photocatalysts.

Table 1. Progress of g-C_3N_4-based Composites Recent Application in Photocatalytic Degradation of Antibiotics and Pesticide including Properties and Photodegradation Performance

Composites	Improvement strategy	Bandgap (eV)	Light source	Degradation efficiency					Recycling	Ref.
				Antibiotics, concentration (mg L^{-1})	Removal % (reaction time)	k_d[a] (min^{-1})	k_p[b] (min^{-1})	k_d/k_p (times)		
g-C_3N_4/Bi_2WO_6	Type-II heterojunction	2.63	300 W Xe, λ > 420 nm	IBF, 500[c]	96.1 (60 min)	0.052	0.008	6.5	5	[142]
g-C_3N_4/PCN	Isotype heterojunction	2.42	300 W Xe, λ > 420 nm	TC, 10	89.7 (60 min)	0.04392	0.01145	3.8	5	[75]
KMCN	Kalium doping	2.33	300 W Xe, λ > 420 nm	TC, 20	85.13 (60 min	0.0282	0.0058	4.86	4	[143]
BCM-C_3N_4	Carbon doping	2.02	300 W Xe, λ > 420 nm	SMZ, 10	98 (60 min)	-	-	5	4	[144]
CCN/$Bi_{12}O_{17}Cl_2$	Carbon doping and Type-II heterojunction	-	300 W Xe, λ > 420 nm	TC, 20	94 (60 min)	0.0409	0.0157	2.60	4	[145]
g-C_3N_4/WO3	Z-scheme heterojunction	-	300 W Xe, λ < 420 nm	CIP, 50	100 (120 min)	-	-	-	5	[146]
POCN	Phosphorus and oxygen cobalt doping	2.30	350 W Xe, λ > 420 nm	ENFX, 10	-	0.0236	0.0038	6.2	4	[147]
g-C_3N_4/CdS-NHCs	Type-II heterojunction	-	300 W Xe, λ > 420 nm	CXS, 10	96.46 (90 min	0.0338	0.0044	7.68	4	[129]
Nv MM CN	Nitrogen vacancy modified and morphological adjustment	2.77	300 W Xe, λ > 420 nm	NOR, 10	99.9 (20 min)	-	-	-	5	[148]
g-C_3N_4/Ag/$Bi_5FeTi_3O_{15}$	Noble metal deposit and Z-scheme heterojunction	-	300 W Xe, λ > 420 nm	TC, 20	86 (20 min)	0.0465	0.0137	3.4	5	[149]
Cu-C_3N_4	Cu doping	-	-	RhB, 10	~95%, (60 min)	-	-	-	-	[103]
HTCN-C	Sulfur doping and morphological adjustment	2.47	300 W Xe	TC, 20	82.67 (60 min	0.0293	0.0059	4.97	5	[150]
g-C_3N_4/Bi_2WO_6/AgI	Dual Z-scheme heterojunction	-	300 W Xe, λ > 420 nm	TC, 20	91.13 (60 min	0.0349	0.00846	4.13	4	[151]
UPCN/BNQDs	Morphological adjustment and	-	300 W Xe, λ > 420 nm	OTC−HCl, 10	82 (60 min)	0.0309	0.0072	4.3	4	[152]

	type-II heterojunction									
CN-SA	Morphological adjustment	2.37	300 W Xe, λ > 420 nm	SMZ, 100[c]	99 (60 min)	0.0823	0.0293	2.8	4	[153]
LCN-0.015	L-cysteine modified	2.55	300W Xe, λ > 420 nm	SMZ, 100[c]	99.7 (60 min)	0.1062	0.0086	12	4	[154]
g-C_3N_4/Co_3O_4@CoO	Dual Z-scheme heterojunction	-	300W Xe, λ > 420 nm	TC, 10	97 (120 min)	0.021	-	-	4	[155]
MCN	Morphological adjustment	2.70	300W Xe, λ > 420 nm	CFX, 2	99 (60 min)	0.0858	0.0285	3.03	5	[156]
g-C_3N_4/ZrO_{2-x}	Z-scheme heterojunction	-	300W Xe, 420 nm–780 nm	TC-H, 10	90.6 (60 min)	0.04748	0.00915	5.19	-	[157]
g-C_3N_4@PDA/BiOBr	Z-scheme heterojunction	-	300W Xe, λ > 420 nm	SMX, 2.5	~100 (60 min)	-	-	-	5	[158]
ACN	HDMP grafted	2.35	300W Xe, λ > 420 nm	OTC-HCl, 20	79.3 (60 min)	0.029	0.012	2.42	4	[118]
Co-pCN	Cobalt doping	-	300W Xe, λ > 420 nm	OTC, 20	75.7 (40 min)	0.0381	0.0103	3.7	4	[101]
SCN-CN	Morphological adjustment and type-II heterojunction	2.92	300W Xe, λ > 420 nm	TC-H, 10	82.6 (30 min)	-	-	-	5	[159]
g-C_3N_4/Ag_3PO_4/AgI	Dual Z-scheme heterojunction	-	300W Xe, λ > 420 nm	NTP, 5	95 (4 min)	0.76	0.047	16.2	-	[160]
g-C_3N_4/Fe_3O_4/Ag	Silver doping	-	UV region	DZN, 5	100 (60 min)	0.067	-	-	-	[161]
$ZnIn_2S_4$/g-C_3N_4	Type-II heterojunction	-	500 W Xe, λ> 420 nm.	2,4-D, 100	90 (180 min)	0.0129	0.0044	2.9	-	[162]

[a] The rate constant of the g-C_3N_4-based composite catalyst; [b] The rate constant of the pristine catalyst; [c] μmol L^{-1}; 300W Xe: 300W Xe lamp; SMZ: sulfamethazine; IBF: ibuprofen; PCN: phosphorus doped g-C_3N_4; TC: tetracycline; CIP: ciprofloxacin; ENFX: enrofloxacin; NHCs: hollow carbon spheres; CXS: cloxacillin sodium; NOR: norfloxacin; OTC−HCl: oxytetracycline hydrochloride; UPCN: ultrathin porous g-C_3N_4; SA: salicylic acid; LCN: L-cysteine modified carbon nitride; CFX: cefotaxime; TC-H: Tetracycline hydrochloride; PDA: polydopamine; SMX: sulfamethoxazole; ACN: 2-hydroxy-4,6-dimethylpyrimidine (HDMP) grafted polymeric carbon nitride; NTP: nitenpyram; DZN: diazinon; AC: activated carbon; PMS: peroxymonosulfate; 2,4-D: 2,4-dichlorophenoxyacetic acid.

347

Table 2. Recent Progress of g-C_3N_4-based Composites Application in Photocatalytic Degradation of Organic Dyes including Properties and Photodegradation Performance

Composites	Improvement strategy	Bandgap (eV)	Light source	Degradation efficiency					Recycling	Ref.
				Organic dyes and concentration (mg L^{-1})	Removal % (reaction time)	k_d[a] (min^{-1})	k_p[b] (min^{-1})	k_d/k_p (times)		
g-C_3N_4/MIL-125(Ti)	Type-II heterojunction	3.24	300 W Xe, λ > 420 nm	RhB, 50	95.2 (60min)	0.0624	0.0299	2.1	5	[163]
g-C_3N_4/Sb_2S_3	Type-II heterojunction	1.36	300 W Xe, λ > 760 nm	MO, 10	70 (60 min)	0.0103	0.0039	2.6	5	[164]
g-C_3N_4/h-BN	Type-II heterojunction	-	300 W Xe, λ > 420 nm	RhB, 20	99.5 (40 min)	0.13091	0.01805	7.3	5	[74]
OCN/CoAl-LDH	Oxygen doped and Z-scheme heterojunction	-	300 W Xe, λ > 420 nm	MO, 20	99.7 (60 min)	0.09568	0.0025	38.3	4	[116]
g-C_3N_4/$CsPbBrCl_2$	Type-II heterojunction	-	500W Xe, λ > 420 nm	Eosin B, 10[c]	94 (120 min)	0.0222	0.00795	2.79	3	[73]
Ag_2CO_3@g-C_3N_4	Z-scheme heterojunction	-	250 W halide lamp, λ > 420 nm	MO, 10	96.7 (54 min)	-	-	-	5	[165]
g-C_3N_4/cellulose	Heterojunction	-	350W Xe, λ < 400 nm	MB, 15	99.8 (80 min)	-	-	-	4	[166]
g-C_3N_4/Bi_2O_3	Z-scheme heterojunction	1.5	75W halogen lamp, λ > 420 nm	MG, 5	79 (60 min)	0.0191	0.0127	1.2	5	[167]
g-C_3N_4/Ag/P_3HT	Z-scheme heterojunction	-	100W LED lamp, λ < 420 nm	MO, 10	~100 (500 min)	0.01100.0057	0.00220.0015	5/3.8	5	[168]
g-C_3N_4/SnO_2	Type-II heterojunction	-	400W lamp, λ> 500nm	MB, 10	99.38 (75 min)	0.0639	0.0237	2.7	6	[169]
GO/CN	Type-II heterojunction	-	LED lamp, λ< 417 nm.	RhB, 50[c]	~100 (360 min)	-	-	-	3	[170]
O-g-C_3N_4/Zn_2SnO_4N/ZnO	Double Z-scheme heterojunction	-	500W Xe, λ > 420 nm	RhB, 5	90.14 (60 min)	0.0606	0.02886	2.10	6	[171]
D35-TiO_2/g-C_3N_4	Type-II heterojunction	-	300W Xe, λ > 420 nm	Bis-phenol A, 10	~100 (20 min)	0.285	0.099	2.88	5	[172]

g-C_3N_4-ZnO@graphene	Z-scheme heterojunction	-	300 W Xe, λ ≤ 380 nm	RhB, 20	100 (120 min)	-	-	-	4	[173]
C_3N_4/MoO_3	Z-scheme heterojunction	-	150 W Xe, λ > 400 nm	RhB, 20	- (40 min)	0.083	0.024	3.46	4	[174]
CdS/CQDs/g-C_3N_4	Z-scheme heterojunction	2.68	300 W Xe, λ > 400 nm	RhB, 10	98 (120min)	0.143	0.041	3.48	4	[175]
TNR@C_N-C_3N_4/FTO	Type-II heterojunction	2.44	Xe, λ > 400 nm	MO, 10	94.2 (180 min)	0.0160	0.054	2.96	5	[176]
SnS/g-C_3N_4	Z-scheme heterojunction	-	150 W Xe, λ > 420 nm	RhB, 6	97 (20 min)	0.18	0.016	11.25	4	[177]
xECN	Erbium-doped	2.47	35 W Xe	RhB, 5	94 (30 min)	0.0747	0.0205	3.64	-	[178]
In:CN	Indium-doped	2.74	500W Xe, λ > 420 nm	RhB, 10	~100 (60 min)	0.064	0.014	4.6	6	[179]
AgI-Ag_2S@g-C_3N_4	Double Z-scheme heterojunction	2.56	350W Xe	EB, 5	98.40 (50 min)	0.0784	0.0154	5.09	3	[180]
Ag/WO2.9/g-C_3N_4	Z-scheme heterojunction	-	500W Xe, λ>420 nm	RhB, 10	92.5 (3.5 hours)	-	-	-	4	[181]

[a] The rate constant of the g-C_3N_4-based composite catalyst; [b] The rate constant of the pristine catalyst; [c] μmol L^{-1}; MIL-125(Ti): Ti-benzenedicarboxylate composites 300 W Xe: 300 W Xenon lamp; RhB: Rhodamine B; MO: methyl orange; MB: methylene blue; MG: malachite green; P3HT: Poly (3-hexylthiophere); LED: light-emitting diode.

348

Table 3. Recent Advances in Sterilization and Disinfection by g-C_3N_4-based Photocatalysts

Composites	Improvement strategy	Amount (mg mL^{-1})	Light intensity (mW cm^{-2})	Pathogene	Concentration (CFU mL^{-1})	Radiation duration and efficiency	Rate constant (k, min^{-1})	Recycling	Ref.
F-g-C_3N_4-30-EP	Morphology adjustment and functionalization	0.50	102.23	*E. coli*, K-12, Salmonella ATCC 13076	10^6	30 min, over 99.9999%	0.14	40	[182]
PEI/C_3N_4	Morphology adjustment and functionalization	0.1	150	*E. coli*/*E. faecalis*	$2\times10^6/2\times10^4$	45min, ~100%/60min, ~100%	-	-	[183]
Ag/AgBr/g-C_3N_4	Z-scheme heterojunction	0.2	20	*E. coli*	10^8	120 min, 7.9 log	-	-	[184]
CeO_2/PCN	S-scheme heterojunction	0.010		*S. aureus*	4.51×10^7	15 min, 88.1%	-	-	[185]
Ag/g-C_3N_4	Ag deposition	0.10	271	*E. coli*	~10^7	120 min, 100%	-	-	[186]
MoS_2/g-C_3N_4	MoS_2 deposition	0.10	60	*E. coli*	2×10^3	60 min, ~100%	-	-	[187]
PDI/O-CN	Type-II heterojunction	0.2	-	*S. aureus*	10^7	180 min, 96.6%			[188]
CuS/PCN	CuS deposition	-	200	*S. aureus*/*E. coli*	-	20 min, 98.23 %/20 min, 99.16 %	-	-	[189]
O-g-C_3N_4/HTCC	Z-scheme heterojunction	0.15	40	Human adenovirus type 2 (ATCC VR-846)	10^5 MPN mL^{-1}	120 min, ~100%	-	5	[190]
$BiVO_4$/Ag/g-C_3N_4	Z-scheme heterojunction	0.25	-	*E. coli*	3×10^6	60 min, ~100%	-	-	[191]
g-C_3N_4/TiO_2	Z-scheme heterojunction	0.10	-	*E. coli*	10^3	30 min, ~100%	-	-	[192]
$MgTi_2O_5$/g-C_3N_4	Z-scheme heterojunction	0.50	1000	*E. coli*	1.2×10^7	240 min, ~100%	-	4	[193]
ACHT-CN-1000W	Morphology adjustment	5	50	*E. coli*	2.5×10^7	120 min, ~100%	-	-	[194]
PCNS	Morphology adjustment	0.4	-	*E. coli*	5×10^6	240 min, ~100%	-	-	[195]
GO/g-C_3N_4	-	0.1	300	*E. coli*	10^9	120 min, 97.9%	-	4	[196]
Bi_2MoO_6/g-C_3N_4	Type-II heterojunction	-	-	*E. coli*	2.5×10^7	180 min, ~100%	-	4	[197]

SL g-C_3N_4	Morphology adjustment	0.1	-	*E. coli*	2×10^7	240 min, ~100%	-	3	[198]

E. coli: Escherichia coli; PEI: Polyethyleneimine; *E. faecalis*: Enterococcus faecalis; *S. aureus*: Staphylococcus Aureus; PDI: perylene diimide; ACHT: Alternated cooling and heating treatment; 1000 W: denoted 1000 W microwave power; PCNS: Porous g-C_3N_4 nanosheet; SL g-C_3N_4: Atomic single layer g-C_3N_4.

349

Table 4. Recent Advances in Cr(VI) Reduction by g-C_3N_4-based Photocatalysts

Composites	Improvement strategy	Bandgap (eV)	Light source	Concentration of Cr(VI) (mg L^{-1})	Adsorption and catalytic time (min)	Degradation efficiency (%)	Rate constant (k, min^{-1})	Recycling	Ref.
PCN-S	Phosphorus doped and morphology adjustment	2.92	300 W Xe, $\lambda > 400$ nm	20	120	~100	-	5	[199]
g-C_3N_4/MIL-100(Fe)	Type-II heterojunction	-	300 W Xe, $\lambda > 400$ nm	10.0	80	97	0.037	5	[200]
PANI/C_3N_4	Acid doped and morphology adjustment	3.62	350 W Xe, $\lambda > 400$ nm	100	10	90	4.76 ± 0.058^a	3	[201]
BPTCN	Morphology adjustment	0.063	300 W Xe, $\lambda > 420$ nm	10	60	94.71	0.0404	6	[117]
Fe_3O_4/C/g-C_3N_4	Fe_3O_4 deposition	-	300 W Xe, $\lambda \geq 420$ nm	20	100	100	0.00355	4	[202]
BBC	Metal deposition	2.13	300 W Xe, $\lambda > 400$ nm	20	60	-	0.01589	4	[203]
PANI@ZFCN	PANI-sensitized	1.7	300W Xe	20	120	97.8	0.0326	4	[204]
GO/g-C_3N_4/MoS_2	Morphology adjustment and type-II heterojunctions	1.51	300W Xe, $\lambda > 420$ nm	10	120	~80	0.0123	-	[205]
g-C_3N_4/BiOI	Type-II heterojunction	-	$\lambda > 420$ nm	-	150	~100	0.0261	-	[206]
(P, Mo)-g-C_3N_x	P and Mo co-doped	2.10	300 W Xe, $\lambda \geq 420$ nm	100	120	95	0.0229	4	[207]
Ag/g-C_3N_4/V_2O_5	Noble metal deposition and Z-scheme heterojunction	2.26	Solar light	-	60	33	0.373	3	[208]
Co_9S_8/g-C_3N_4	Z-scheme heterojunction	2.42	500W Xe lamp	10	180	-	0.6311	5	[209]
BPCMSs/g-C_3N_4	Heterojunction	-	300 W Xe, $\lambda > 320$ nm	10	240	~75	-	4	[210]
g-C_3N_4/TiO_2	Type-II heterojunction	3.26	300 W Xe, $\lambda > 420$ nm	400	-	-	0.35	-	[211]
SA- g-C_3N_4/CA	Morphology adjustment	2.98	300W Xe, 380–750 nm	5	100	95	-	-	[212]
MIL-101(Fe)/g-C_3N_4	Z-scheme heterojunction	--	150W halogen cold light, $\lambda > 420$ nm	20	60	92.6	0.0432	-	[213]

[a] removal capacity ($mg \cdot min^{-1} \cdot g_c^{-1}$); 300 W Xe: 300 W Xenon lamp; PCN-S: phosphorus-doped porous ultrathin carbon nitride nanosheets; PANI: polyaniline; BPTCN: BP quantum dots (BPQDs) tubular g-C_3N_4 (TCN); BBC: Bi modified Bi_2S_3 pillared g-C_3N_4.

350

4.1 Removal of antibiotics and pesticide

For atomic-scale 2D/2D heterostructures, due to controllable molecular layer thickness [214-216] and the face-to-face contact [217,218], the photogenerated carriers can be controlled and a greater interfacial area may be formed to accelerate the separation of photoelectron-hole pairs. To illustrate, the specific degradation pathway of ibuprofen (IBF) by 2D/2D UTCB heterostructures is shown in Fig. 7a [142], major intermediate products with m/z of 238, 221, and 178 are produced during the hydroxylation process of IBF, as well as, the intermediates with m/z of 162 and 133 are produced by direct decarboxylation. The photocatalytic mechanism of UTCB-25 heterojunction obtained by DFT calculation is shown in Fig. 7b and c. The open surface $[BiO]^{+}$ layers are stimulated by light to produce holes and transferred to the surface of ug-CN to react with IBF. The middle $[WO_4]^{2-}$ layers are excited by light to produce electrons, and transferred to the edge of the monolayer for the reduction reaction. Meanwhile, the photoelectrons in the ultrathin g-C_3N_4 nanosheet are transferred to the single-layer Bi_2WO_6 nanosheet, and the electrons gather in the CB of single-layer Bi_2WO_6 nanosheet react with the O_2 to form $\bullet O_2^-$ radical, which could continuously degrade IBF.

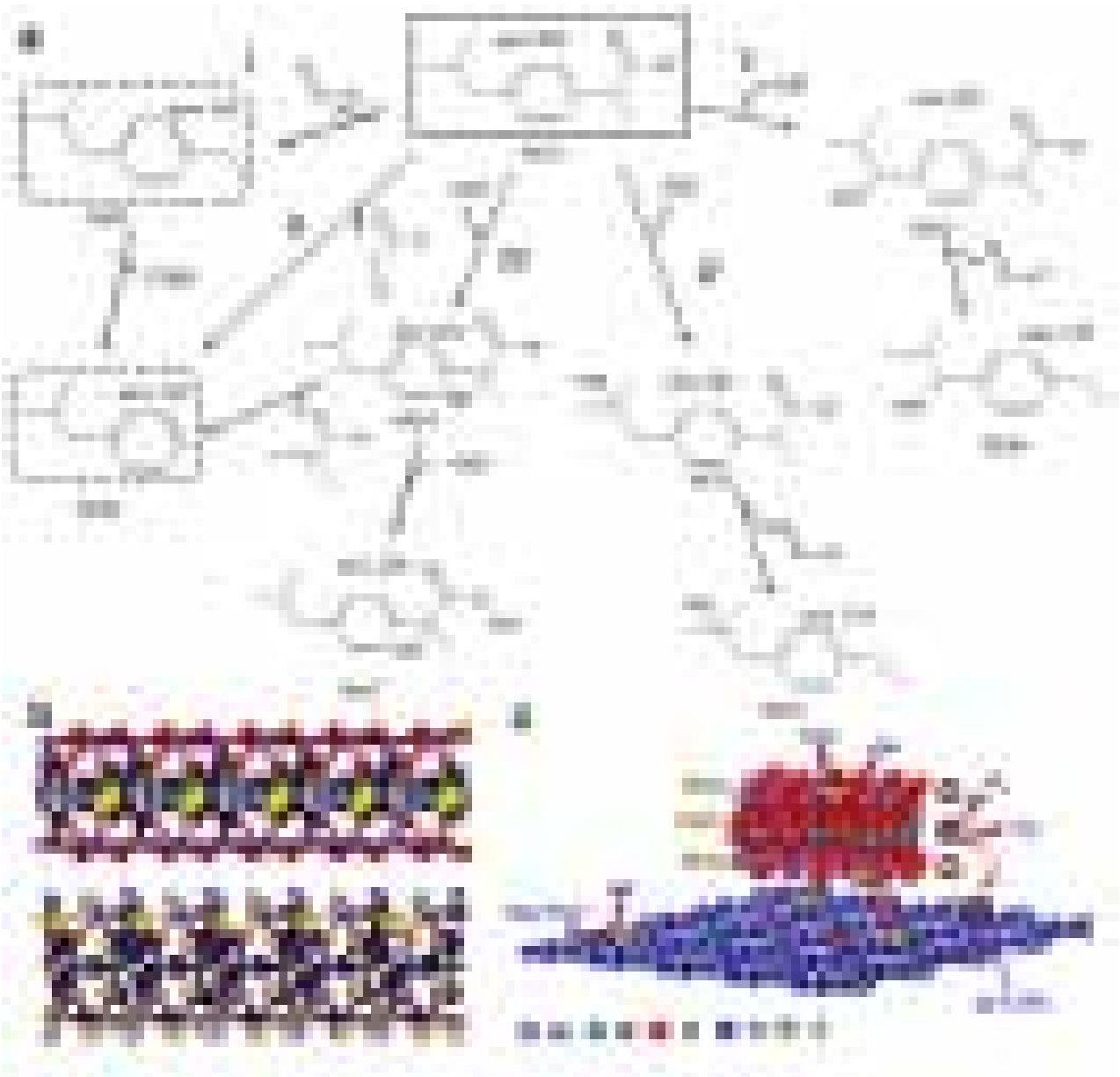

Fig. 7. Photocatalytic degradation of ibuprofen by atomic scale g-C_3N_4/Bi_2WO_6 2D/2D heterojunction. (a) Photocatalytic degradation of Ibuprofen (IBF); The LUMO (top) and HOMO (bottom) states of the monolayer Bi_2WO_6 nanosheets (b); Photocatalytic mechanism scheme of UTCB heterojunctions under visible light irradiation (> 420 nm) (c). Adapted with permission from ref. [142]. Copyright 2017 Elsevier B.V.

How to develop efficient and stable photocatalysts to obtain the widest possible spectrum of the solar spectrum is still a challenge [219-221]. To prepare photocatalysts with enhanced full spectral response range, a ternary Ag/N-doped graphene quantum dots/g-C_3N_4 nanocomposite (AGCN) was prepared for the first time in 2017 [222]. The ratio between components of the

375 composite material is very important, and the optimal ratio can obtain higher photocatalytic
376 performance [222]. The g-C_3N_4 doped with 0.5% N-doped graphene quantum dots and 2.0%
377 Ag NPs has the highest photocatalytic activity under the same condition, the photocatalytic
378 degradation rate of tetracycline (TC) reaches 92.8% in the full spectrum, and the degradation
379 rate of tetracycline can reach 31.3% under infrared light. Because the bandgap of the prepared
380 AGCN-4 has a narrower bandgap than the original g-C_3N_4 and other similar materials, AGCN-
381 4 can absorb more visible and even near-infrared light for the degradation of pollution in water.
382 Meanwhile, because of the enhanced optical response capability of N-doped graphene quantum
383 dots, the excellent electron transport capability of Ag, and the cooperative effect of both,
384 AGCN-4 has the best electronic conductivity and the lowest PL strength.

385 The following year, the P-doped CN/CN isotype heterojunction (PCN/CN) was prepared to
386 enhance the photocatalytic degradation efficiency of TC in water [75]. The built-in electric
387 field induced between CN and PCN leads to the transfer of photoelectrons from PCN to CN,
388 which promotes stronger charge detach and increases the light absorption range, thus greatly
389 enhancing the photocatalytic degradation activity of TC. Therefore, the photocatalytic
390 degradation rate of TC by PCN/CN in water was 3.8 times that of the original CN [75]. In the
391 same year, we introduced barbituric acid and melamine in the process of melamine
392 polymerization to synthesize a C-doped C_3N_4 (BC-C_3N_4) nanocomposite for the mineralization
393 of sulfamethazine (SMZ) under visible light [144]. Because nonmetallic doping changes the
394 basic properties of C_3N_4 polymers and makes them have higher photocatalytic degradation
395 capability, BCM-C_3N_4 showed a fourfold increase in the degradation rate of SMZ within one
396 hour compared to pure C_3N_4 [144].

Recently, single-atom Co-doped polymerized CN (Co-pCN) was prepared by cyclization process with urea and Co(II) acetylacetonate as precursors (Fig. 8a) for photocatalytic degradation of oxytetracycline (OTC) [101]. First, 2-hydroxy-4,6-dimethylpyrimidine (HDMP) forms by the cyclization of acetylacetone with urea and the tri-s-triazine ring forms by urea. Then, a condensation reaction was performed between HDMP and the tris-triazine ring. Finally, the Co-pCN formed by the condensation product chelates with Co^{2+}. As shown in Fig. 8b-d, monoatomic Co successfully fixed on the pCN in the form of valence bond, and the corresponding structure is also proved by the optimal DFT calculation model (Fig. 8e). The interaction between monoatomic Co and pCN expands the visible light absorption region, increases photoelectron density, and promotes photoelectrons transfer, thus significantly improving the degradation efficiency of photocatalytic OTC (Fig. 8f and g). The core active substances in the degradation process by Co-pCN photocatalyst are $^1O_2$, h^+, $\bullet O_2^-$, and •OH (Fig. 8h). Meanwhile, as shown in Fig. 8i, the photocatalytic degradation efficiency of OTC has not decreased significantly in the following four operations, which proves that the Co-PCN has excellent catalytic stability.

Fig. 8. Photocatalytic degradation of refractory antibiotics by single-atom cobalt doped C_3N_4. (a) The proposed synthetic process of Co–pCN. Co k edge XANES spectra of Co(1.28%)–pCN and other catalysts (b); Corresponding Fourier transform spectra of Co(1.28%)–pCN and other catalysts (c); EXAFS r space-fitting curve of Co(1.28%)–pCN (Insert: k space-fitting curve of Co(1.28%)–pCN) (d); Optimized DFT calculation model of Co(1.28%)–pCN (e); Photocatalytic degradation efficiency of OTC by Co(1.28%)–pCN and other catalysts under visible light irradiation (f); pseudo-first-order kinetic fitting curves and the corresponding kinetic constants (g); The corresponding kinetic constants and the relative contributions of different quenchers (h); Four cycles of degradation of OTC by Co(1.28%)–pCN (i). Adapted with permission from ref. [101]. Copyright 2020 WILEY-VCH.

Noteworthily, a "double Z-Scheme" system for degradation of antibiotic, as shown in Fig. 9a, both P-doped ultrathin CN (PCNS) and $BiVO_4$ can be stimulated by visible light to produce photoexcited carries, then, the photoelectrons generated by CB of $BiVO_4$ are transferred to the metal Ag [223]. Due to the SPR effect of metal Ag, an enhanced local electric field can be established on the surface of the Ag, which promotes the transport of photoelectrons on the Ag to the VB of PCNS. Ternary Ag@PCNS/$BiVO_4$ photocatalyst with dual Z-Scheme can degrade

CIP in water under visible light with a degradation rate of 92.6% [223]. As shown in Fig. 9b-e, the holes, •OH, and $•O_2^-$ are major active sites in the CIP degradation process by Ag@PCNS/$BiVO_4$ photocatalysts.

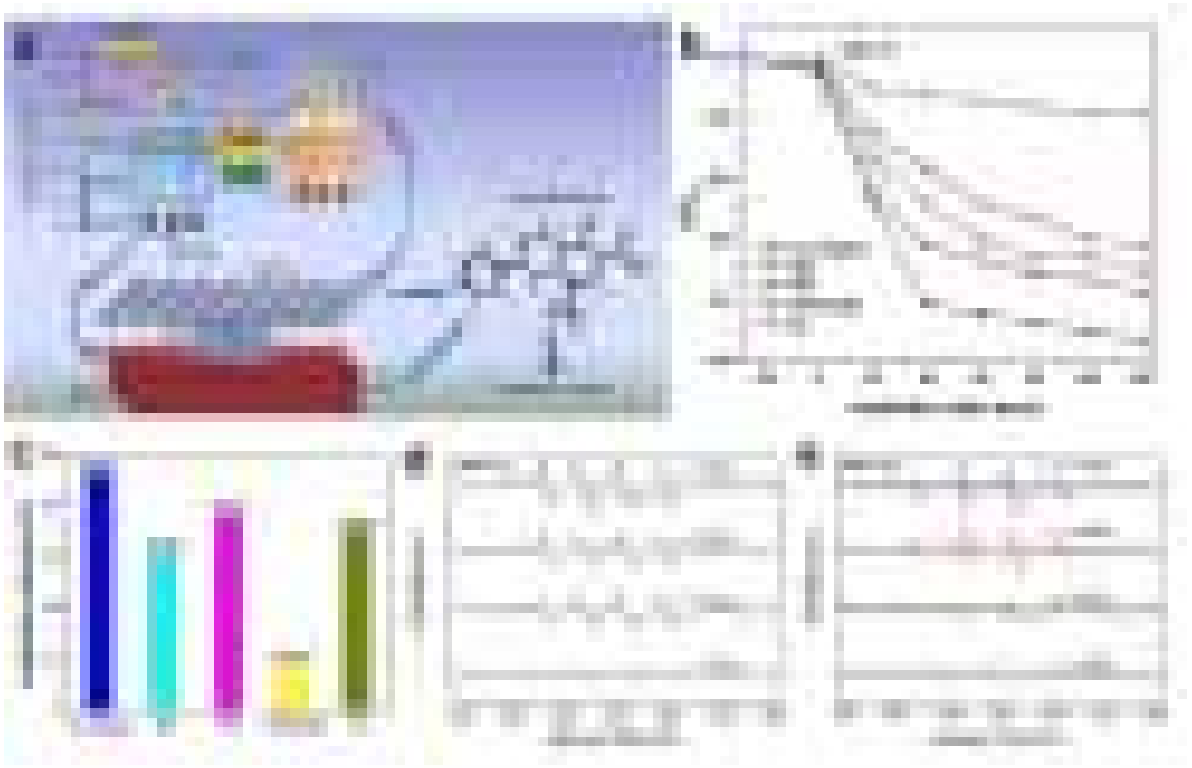

Fig. 9. The CIP degradation using Ag modified phosphorous doped ultrathin g-C_3N_4 nanosheets/$BiVO_4$ photocatalyst. (a) Photocatalytic reaction mechanism and degradation pathway of CIP by nanocomposites under visible light irradiation. (b and c) Active radical species trapping experiments for the photocatalytic degradation of CIP and the corresponding photocatalytic removal efficiency over Ag@PCNS/BiVO4 nanocomposite under visible light irradiation. (d and e) ESR spectra of radical adducts trapped by DMPO ($•O_2^-$ and •OH) in Ag@PCNS/$BiVO_4$ nanocomposite in the dark and with the visible light irradiation of 5 min, 10 min, and 15 min. Adapted with permission from ref. [223]. Copyright 2017 Elsevier B.V.

The "double Z-Scheme" system is also used for the degradation of quintessential pesticides, such as neonicotinoid pesticides. Compared with the single g-C_3N_4 and the corresponding binary materials, the dual Z-scheme AgI/Ag_3PO_4/g-C_3N_4 (AAC) composite has a better photocatalytic activity for the degradation of nitenpyram (NTP) [160]. As shown in Fig. 10a, the AAC composites synthesized by an in-situ ion exchange strategy. As the dual Z-scheme

mechanism improving the separation efficiency of photogenerated carriers (Fig. 10b), AAC generates more superoxide free radicals for photocatalytic degrading of NTP, so AAC has higher photodegradation efficiency. The apparent rate constant of photocatalytic degradation of NTP was up to 0.76 min^{-1}, which was 16.2 times that of pure g-C_3N_4 (Table 1). The possible degradation pathways of NTP are shown in Fig. 10c, which are continually attacked by the active species $\bullet O_2^-$ and eventually completely mineralized.

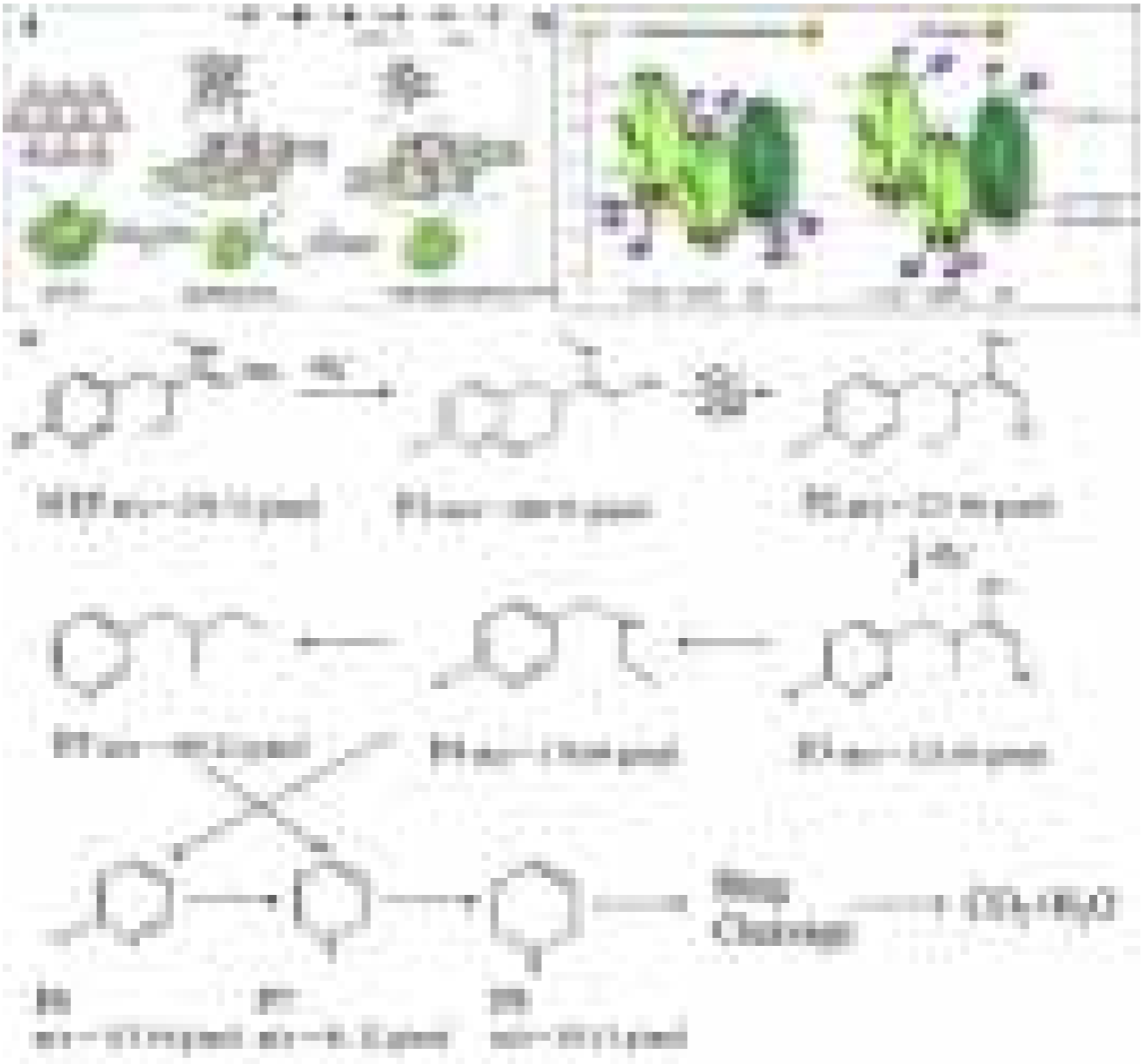

Fig. 10. Degradation of nitenpyram using dual Z-scheme g-C_3N_4/Ag_3PO_4/AgI composite photocatalyst. (a) Schematic illustration of the preparation process of AgI/Ag_3PO_4/g-C_3N_4 photocatalyst; (b) Proposed photocatalytic mechanism of AgI/Ag_3PO_4/g-C_3N_4 composite. (c)

Proposed possible degradation pathway of NTP in the presence of the AAC. Adapted with permission from ref. [160]. Copyright 2019 Elsevier B.V.

4.2 Degradation of organic dyes

Organic dyes (such as RhB, MB, azo dyes, etc.) in water mainly come from the textile industry [73,166,170]. Due to their high solubility and hard ionization, organic dyes can accumulate in aquatic organisms [73]. Meanwhile, long-term exposure of organisms to these organic dyes increases their risk of developing cancer [73]. G-C_3N_4-based photocatalysts can degrade organic dyes in water efficiently and stably. Typically, g-C_3N_4/Ti-benzenedicarboxylate composites (CMTi) were prepared by the simple solvent thermal method to degrade RhB dyes [163]. Compared with single Ti-benzenedicarboxylate composites and g-C_3N_4, CMTi has enhanced photocatalytic ability to degrade RhB dyes in visible light, and when the g-C_3N_4 content is 7.0 wt%, the composite material (CMTI-2) has the best photocatalytic degradation rate of RhB of 0.0624 min^{-1}. The main reasons for the enhancement of photocatalytic degradation efficiency for RhB may be ascribed to the synergistic catalysis of Ti-benzenedicarboxylate composites and g-C_3N_4, as well as the indirect photosensitization of RhB itself. Meanwhile, these materials can still maintain photocatalytic activity stability and crystal stability after 5 cycles of use, indicating that these materials are expected to resist photocorrosion in continuous photocatalytic water purification.

Currently, the enhancement of g-C_3N_4-based photocatalysts and their application in the photodegradation of organic dyes in water are progressing rapidly (Table 2). To illustrate, to enhance the photocatalytic degradation capability of organic dyes at near-infrared wavelengths of photocatalytic materials, we prepared a novel Sb_2S_3/ultrathin g-C_3N_4 heterostructure (CNS)

476 [164], which photocatalyst degrades methyl orange (MO) at a rate of 0.0103 min^{-1} by near
477 infrared spectroscopy. However, the specific photocatalytic degradation process, active species,
478 and degradation intermediates have not been well explained [224]. The commonly used
479 spectroscopic methods can only reflect the change of chromogenic groups with time before and
480 after the photocatalytic process, but cannot prove the photocatalytic kinetic process, and cannot
481 monitor the oxidation process of the intermediate [225].

482 For this purpose, Huang's group coupled photocalorimetry-fluorescence spectroscopy,
483 photocalorimeter, and laser-induced fluorescence spectroscopy, and studied the photocatalytic
484 kinetics, active species, and degradation intermediates of RhB in the g-C_3N_4@Ag@Ag_3PO_4
485 heterojunction system [226]. As shown in Fig. 11a, monochromatic light entered the sample
486 room and reference room through light fiber, and the photoinduced fluorescence originating
487 from the photocatalysis in the sample cell through a fiber-optic spectrometer to data collection
488 and control system. That is after the incident light is converted to parallel light through a lens,
489 it passes through a filter and a convex lens and is finally focused on the sample unit (Fig. 11b),
490 at the same time, the light-induced fluorescence is transmitted to the spectrometer through the
491 scattering pathway and the reflection of the mirror respectively (Fig. 11b). This method can not
492 only prove that photocatalysis is a pseudo-zero-order process, but also investigate
493 photocatalytic reaction pathways and rate-determining steps. During the degradation of RhB
494 by g-C_3N_4@Ag@Ag_3PO_4 photocatalysts, three major thermodynamic processes happened (Fig.
495 11c and d): (ab) photoexcited RhB molecule and photocatalyst produced superoxide radical
496 and hydroxyl group; (bc) equilibrium between endothermal photoexcitation and exothermal
497 RhB photodegradation; and (cd) unchanging exothermal RhB photodegradation process. In the

photocatalytic degradation procedure, the g-C_3N_4@Ag@Ag_3PO_4 system produced hydroxyl groups and superoxide radicals through the Z-scheme mechanism for RhB degradation. Meanwhile, corresponding to the cd stage, the final chromophore cleavage process is a rate-determining step (Fig. 11e), which leads to the photocatalytic degradation process of RhB.

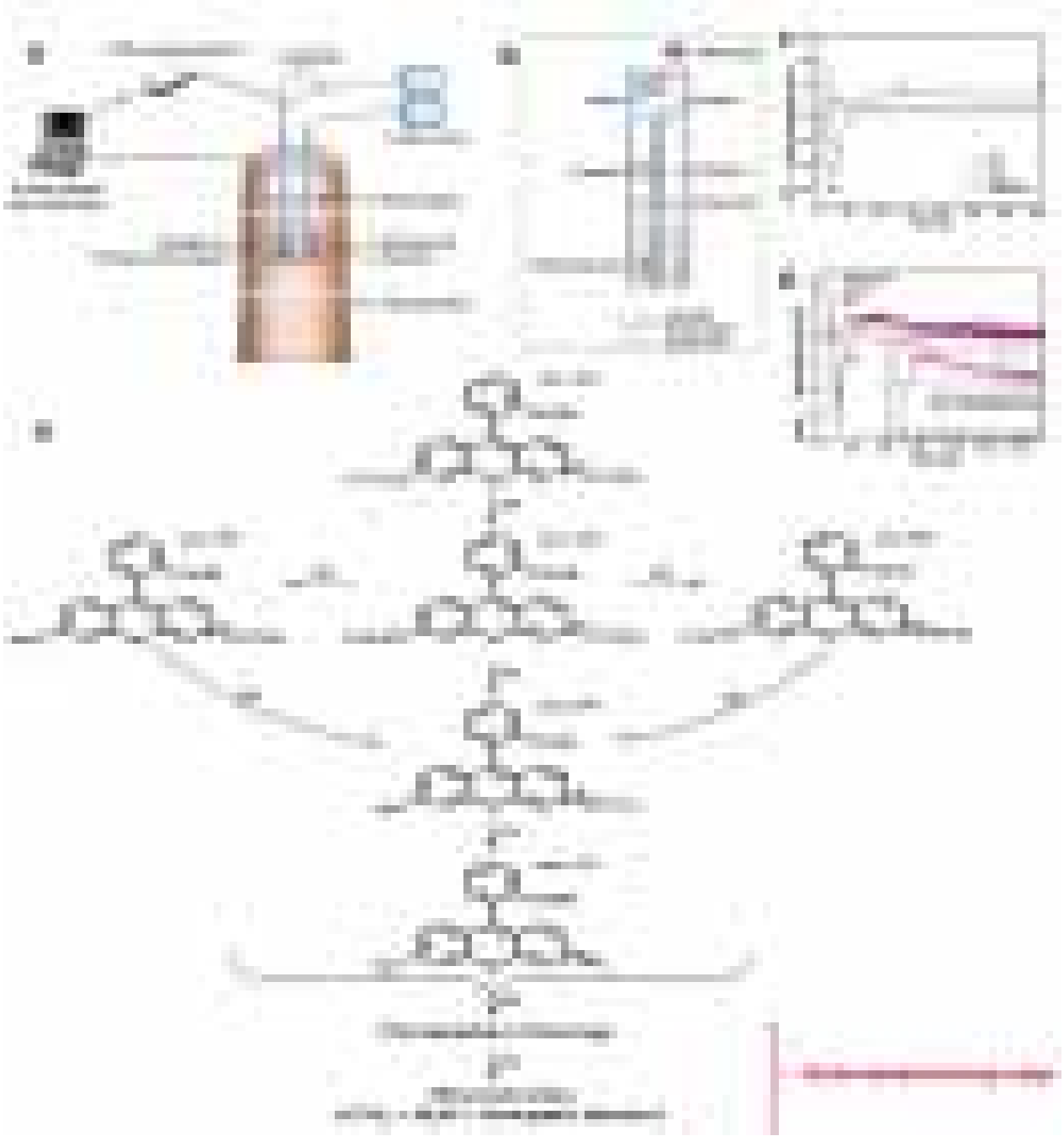

Fig. 11. A pseudo-zero-order in degradation of rhodamine B by Z-scheme g-C_3N_4@Ag@Ag_3PO_4 photocatalyst. Schematic illustration of a photocalorimeter-fluorescence spectroscopy (a) and optical probe in sample cell (b); Heat changes (c) and heat flow curves of RhB photocatalysis over CN, CNAP1, and CNAAP30% (d). (e) Degradation pathway of RhB

dye over Z-scheme g-C_3N_4@Ag@Ag_3PO_4 nanocomposites. Adapted with permission from ref. [226]. Copyright 2017 Elsevier B.V.

4.3 Sterilization and disinfection

Photocatalytic technology is a sustainable method for the inactivation of water-borne pathogens [227-229]. In this regard, nanoscale photocatalysts have exhibited great potential for photocatalytic sterilization and disinfection [230]. In the process of photocatalysis, photocatalyst mainly realizes the purpose of sterilization and disinfection by destroying pathogen groups and deconstructing the cell structure of individual pathogens [231]. Currently, the commonly used nanoscale metal-based nanomaterials may cause secondary pollution, which has aroused the concern of environmental management personnel and environmentalists [8,232,233]. Therefore, seeking efficient metal-free photocatalysts or selecting stable materials as carriers of metal-based catalysts for the inactivation of water-borne pathogens is of great significance.

Given that adjustable properties, g-C_3N_4-based photocatalyst can not only solve the key bottleneck of low activity caused by the rapid recombination of photogenerated carriers of original g-C_3N_4, but also can be used as a carrier or synergistic component of a metal photocatalyst to avoid the secondary pollution caused by metal ion leaching. Recent advances in g-C_3N_4-based photocatalyst photocatalytic sterilization and disinfection are summarized in Table 3. The g-C_3N_4-based photocatalyst generates charge carriers under sunlight irradiation that react with oxygen and water molecules, resulting in a variety of active species (h^+, •OH, $^1O_2$, $•O_2^-$, and H_2O_2) to inactivate pathogens in water (Fig. 12). To improve the efficiency of g-C_3N_4-based photocatalysts for photocatalytic inactivation of water-borne pathogens, one is

to change the interface between g-C_3N_4-based photocatalysts and the pathogen, use the photocatalyst surface to effectively capture the pathogen, and use the holes on the photocatalyst surface to inactivate the pathogen; The other is to adjust the photocatalytic properties of g-C_3N_4-based photocatalysts to increase the content of $^1O_2$, $\bullet O_2^-$, and H_2O_2 in the water environment, so that the photocatalyst can effectively inactivate the pathogen without touching the pathogen.

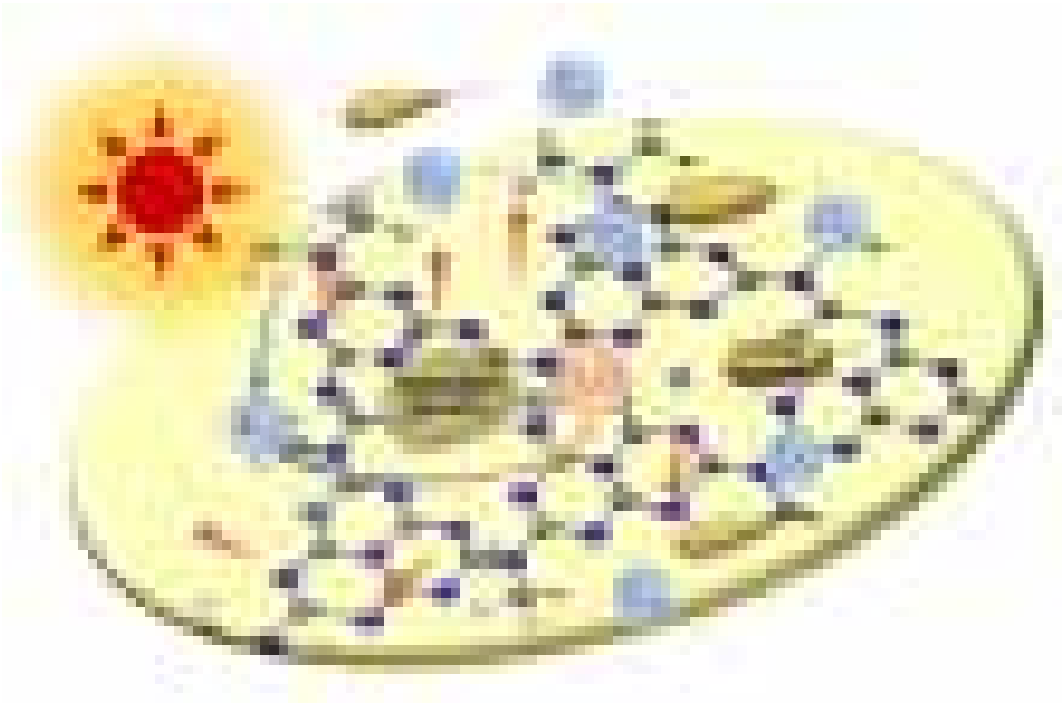

Fig. 12. Schematic diagram of the sterilization and disinfection mechanism of g-C_3N_4-based photocatalysts. Many active species such as h^+, $^1O_2$, $\bullet O_2^-$, and H_2O_2 are produced by g-C_3N_4-based photocatalysts which inactivate pathogen in the water body.

Polyethylenimine (PEI) PEI is a cationic polymer with rich amine groups. Modification of the surface of g-C_3N_4 nanosheets by PEI can greatly improve the photocatalytic disinfection activity of the g-C_3N_4-based composite [183]. As shown in Fig. 13a, the amine group is protonated in water, making the surface of the PEI-modified g-C_3N_4-based composites (PEI/C_3N_4) positively charged, which is conducive to capturing the pathogen in water, at the same

543 time, PEI on the g-C_3N_4 surface also promotes the separation of photogenerated electron-hole
544 pairs, and promotes the generation of H_2O_2 and $\bullet O_2^-$. Scanning electron microscopy (SEM,
545 Fig. 13b-d) showed that PEI/C_3N_4 was able to completely attach to the surface of pathogen
546 cells compared with pure g-C_3N_4 which could not contact pathogen cells. This is because the
547 abundant protonated groups on the surface of PEI/C_3N_4 provide anchoring sites for pathogen
548 cells through electrostatic binding. This is also demonstrated by the atomic force microscope
549 (AFM) measurement curve shown in Fig. 13e-g. Through this strategy, obtained PEI/C_3N_4
550 composites exhibited very high inactivation efficiency for *E. coli* and *E. faecalis* under
551 simulated light irradiation (Table 3, PEI/C_3N_4).

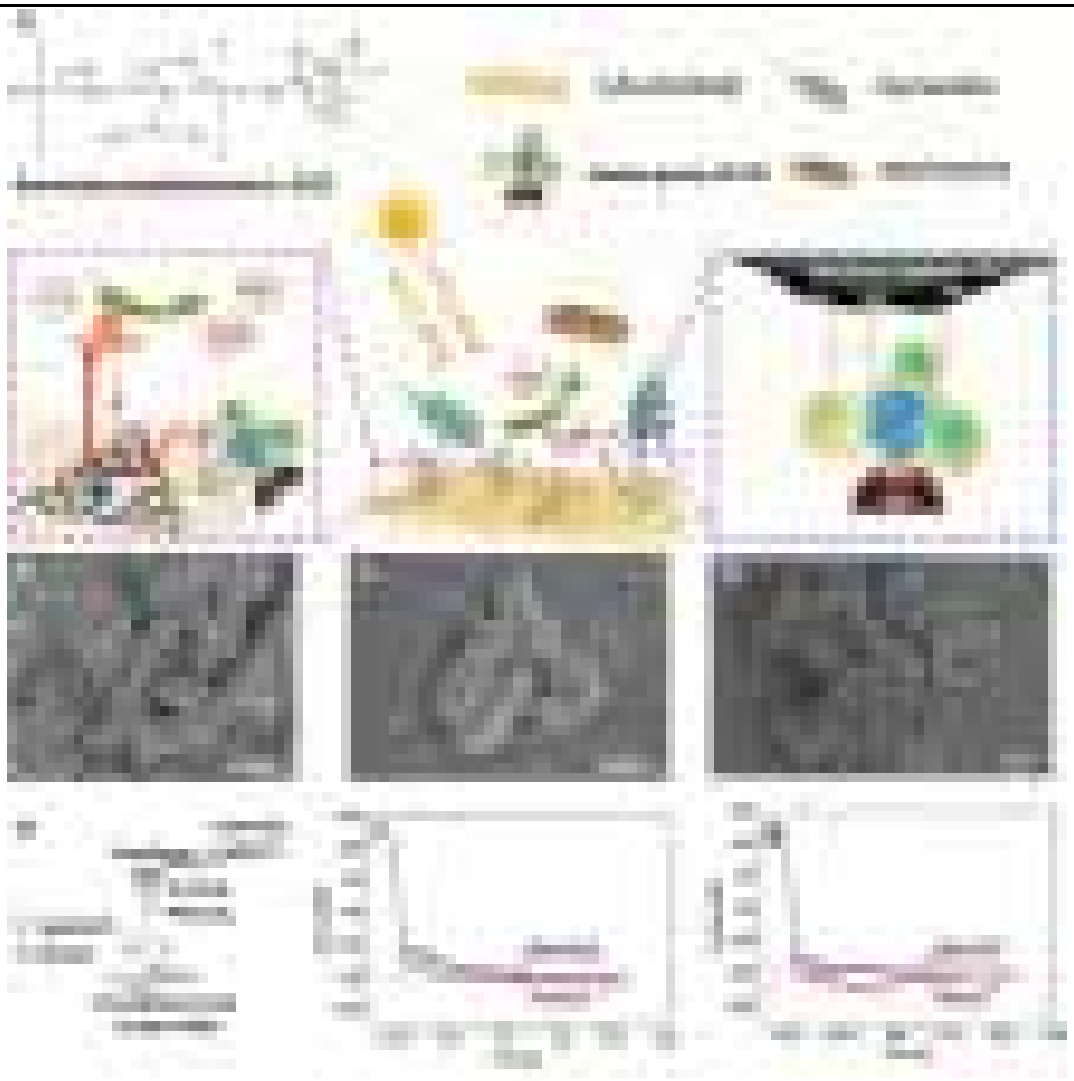

Fig. 13. PEI-modified g-C_3N_4-based composites for rapid photocatalytic water disinfection. (a) Illustration of the roles of PEI on g-C_3N_4 for improved photocatalytic bactericidal activity. SEM images of initial *E. coli* cells before mixing with photocatalysts (b), *E. coli* cells after mixing with C_3N_4 suspension (c), and after mixing with PEI/C_3N_4 suspension (d) for 45 min under dark. Illustration for the AFM force curve measurement process (e); Approach-Retract force curves of bare AFM Si probe towards *E. coli* cells (f); Approach-Retract force curves of PEI/C_3N_4 coated AFM Si probe towards *E. coli* cells (g). Adapted with permission from ref. [183]. Copyright 2020 Elsevier B.V.

Meanwhile, considering the influence of electron-withdrawing groups on the charge distribution of g-C_3N_4, the photogenerated hole-electron pair recombination can be inhibited by selectively introducing electron-withdrawing groups at the edge of g-C_3N_4 nanosheets to construct an anisotropic internal electric field in a 2D plane [182]. Compared with the charge loss at the edge of pure g-C_3N_4 nanosheets (Fig. 14d), the edges of g-C_3N_4-based composites

functionalized by -COOH and -C=O can accumulate electrons, thus increasing the thickness of the space charge region and strengthening the band curvature (Fig. 14a), and ultimately inhibits the recombination of photogenerated electron-hole pairs. Meanwhile, the photodeposition of Pt metal further confirms that edge functionalized -COOH and -C=O can accelerate charge transfer and enhance band bending this result (Fig. 14b, c, e, and f). The catalytic membrane prepared by the marginal functionalized g-C_3N_4 nanosheet (F-g-C_3N_4) could inactivate 99.9999% of *E. coli* within 30 min (Fig. 14g, a: F-g-C_3N_4-30; b: g-C_3N_4-r; c: F-g-C_3N_4-45; d: F-g-C_3N_4-60; e: bulk-g-C_3N_4). The cell structure of *E. coli* was gradually destroyed 45 min after F-g-C_3N_4-30 treatment under sunlight (Fig. 14h-k). Furthermore, compared with the currently reported g-C_3N_4-based photocatalyst (Table 3), F-g-C_3N_4-30-EP has ultra-high stability (stable cycling for more than 40 times) and practicability. F-g-C_3N_4-30-EP can be integrated into plastic film bags and fixed bed reactors for water purification production (Fig. 14l and m), which provides the basis for the industrial development of fully automated photocatalytic water disinfection systems.

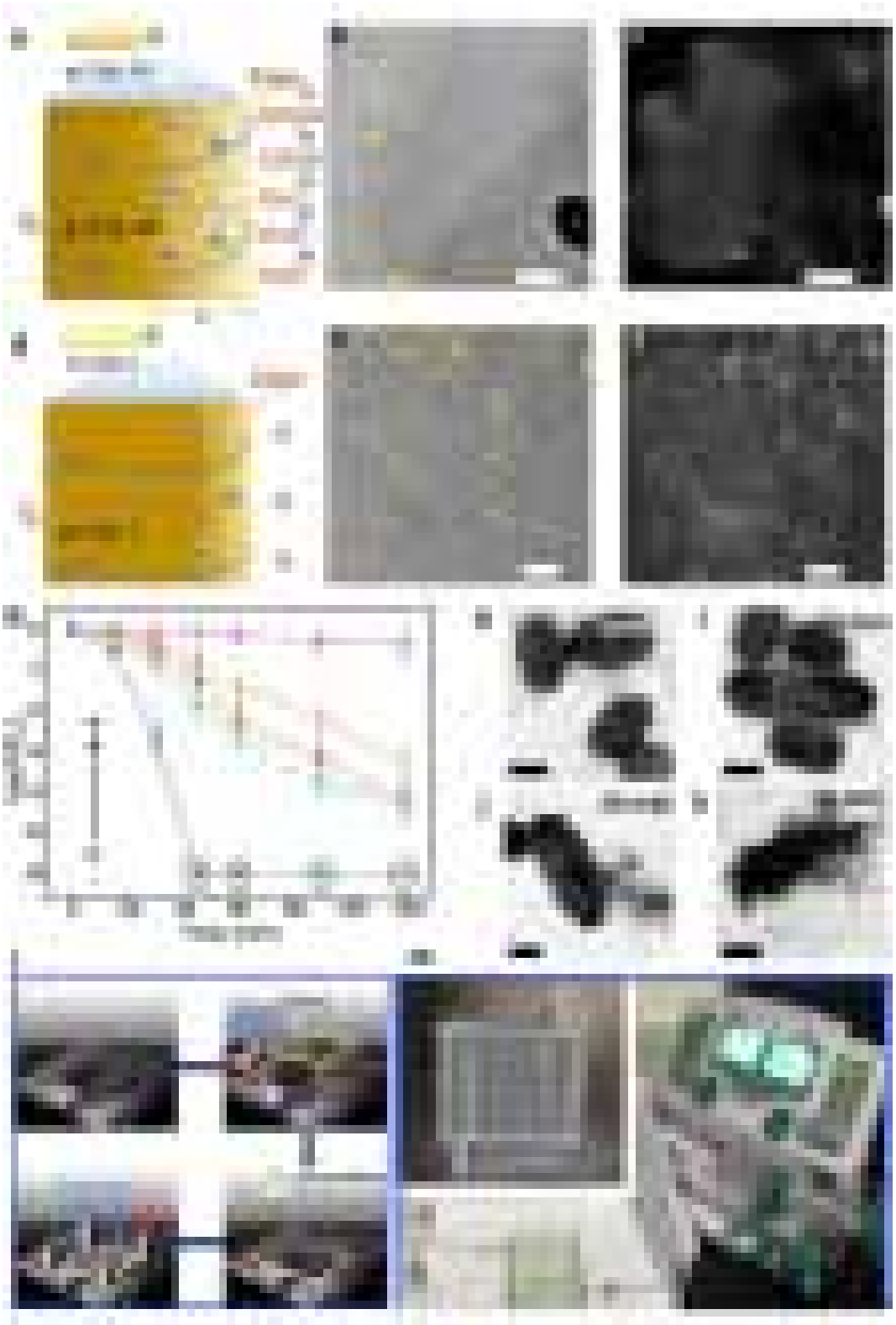

Fig. 14. Edge-functionalized g-C_3N_4-based photocatalyst for clean water supply. (a–f) Schematic diagram of possible depletion layer and the band-bending effects near the edge of (a) g-C_3N_4-30 and (d) g-C_3N_4-r. Shown are TEM images (b and e) and high-angle annular dark field (HAADF) images (c and f) of g-C_3N_4-30 and (e) g-C_3N_4-r after photo-deposition of Pt nanoparticles after photo-deposition of Pt nanoparticles. Point A is the burning trace of the

electron beam during HAADF measurement. (g) full-spectrum solar-light irradiation. (h–i) TEM images of *E. coli* with F-g-C_3N_4-30 as the photocatalyst. (l) Diagrammatic sketch of the modification process utilizing F-g-C_3N_4-30-EP coated onto a polyethylene bag modified by a silane coupling agent. (m) Flowing water disinfection device modified by nano-coating of F-g-C_3N_4-30-EP. Adapted with permission from ref. [182]. Copyright 2018 Elsevier B.V.

Analogously, the interface region near the CeO_2 component in CeO_2/PCN can also capture electrons, thus forming an electron accumulation layer and causing band bending [185]. Meanwhile, the electron depletion layer is formed in the interface region near the PCN component due to the loss of electrons, and the energy band is bent upward. Compared with CeO_2, the Fermi level of PCN is higher, which promotes the formation of an internal electric field at the CeO_2/PCN heterojunction and forms an S-shaped electron transport path. This mechanism is not only beneficial to the spatial separation of photoelectric-hole pairs, but also makes great use of the photoelectron and photoelectric hole in space. Meanwhile, the photoelectron reacts with O_2 molecules to produce a large number of $\bullet O_2^-$. These active species (h^+, $\bullet O_2^-$) can effectively destroy the bacterial cell wall, and further kill the pathogen. To illustrate, the S-scheme heterojunction photocatalyst can effectively inactivate 88.1% *S. aureus* within 15 min under visible light irradiation (Table 3, CeO_2/PCN).

Recently, combined with theoretical calculations, Zhou's group well predicted the role of nitrogen defects in the modulation of energy level and photocatalytic properties, and prepared porous nitrogen defects g-C_3N_4 ultrathin nanosheets (CN-x, x denoted the pH value) by thermal condensation of precursor after lyophilization [234]. Among them, the optimized CN-4 has the best photocatalytic disinfection effect (4.80 $\log_{10}$ CFU mL^{-1} for *E. coli*; 4.24 $\log_{10}$ CFU mL^{-1} for *S. aureus*) [234]. The hydrophilicity and protonation of the surface of CN-4 facilitate the capture of pathogens in water, and the sharp edge of the porous CN-4 nanosheet can destroy

610 the cell membrane of *E. coli* attached to its surface. Meanwhile, abundant pores and nitrogen
611 vacancies in CN-4 provide more active sites, which accelerate charge diffusion and transfer,
612 and thus accelerate the generation of active species. These photosensitive active species
613 produced by CN-4 attack pathogen cells, damaging their membranes, and attacking the internal
614 protective systems, ultimately causing pathogen to die.

615 **4.4 Reduction of hexavalent chromium**

616 Heavy metal ions contained in the wastewater of chemical plants have strong photothermal
617 stability and biodegradability, so it is difficult to remove them completely. Accumulation of
618 them through the food chain can cause damage to aquatic life and humans [8,209,230].
619 Hexavalent chromium Cr(VI) is a quintessential example, produced in various industrial
620 activities such as metal processing, electroplating, tanning, and steel production, which has
621 high toxicity and carcinogenicity [235]. Its allowable value in drinking water is 0.05 mg L^{-1}
622 [236]. Therefore, the degradation of Cr(VI) in wastewater is the focus of people's attention.
623 Presently, one of the most ideal methods is photocatalytic convert Cr(VI) to trivalent chromium
624 Cr(III) [237].

625 Due to the block-like and layered structure, the contact between Cr(VI) and the catalytic
626 active substances is prevented, so the reduction of Cr(VI) by g-C_3N_4 photocatalysts is less
627 efficient in actual water body remediation. To solve this problem, A series of bio-based carbon
628 microspheres (BPCMSs) coupled g-C_3N_4 nanosheets (g-C_3N_4/BPCMSs NSs) composite
629 materials were prepared to recover most of the total chromium (T-Cr) from wastewater through
630 a combination of adsorption and photo-reduction [210]. As shown in Fig. 15a and b, G-C_3N_4

631 prepared by high-temperature polycondensation of melamine has more than five layers of the
632 layered structure, and BPCMSs have many spherical microstructures uniformly distributed.
633 Meanwhile, BPCMSs have high thermal stability, and they as a dispersant can effectively
634 control the structure construction of the composites in the high-temperature polycondensation
635 process (Fig. 15c and d). Compared with other modified g-C_3N_4-based photocatalysts (Table
636 4), the prepared g-C_3N_4/BPCMSs composites can totally remove Cr(VI) in water and adsorb
637 most of the T-Cr in water. Furthermore, it is worth noting that the recycled Cr^{3+}/BPCMSs/g-
638 C_3N_4 composites have higher photocatalytic performance than the fresh composite. Especially
639 under acidic conditions, the secondhand Cr^{3+}/BPCMSs/g-C_3N_4 composites can show strong
640 reduction and degradation efficiency in Cr(VI)/4-FP system. Meanwhile, the recovered g-
641 C_3N_4-based composites have more stable photocatalytic activity, which is due to the
642 electrostatic interaction of surface CeOH and the stable adsorption of Cr(VI) on BPCMSs (Fig.
643 15e). As shown in Fig. 15e, the photocatalysts are excited by light to produce e^--h^+ pairs. Then,
644 oxidizing agents form an oxidizing active intermediate, and reducing agents form reducing
645 active intermediates under photogenic holes and electron redox. After the photocatalytic
646 reaction is completed, e^- are transferred from reducing active intermediates to oxidizing active
647 intermediate, and the photocatalyst returns to electric neutrality.

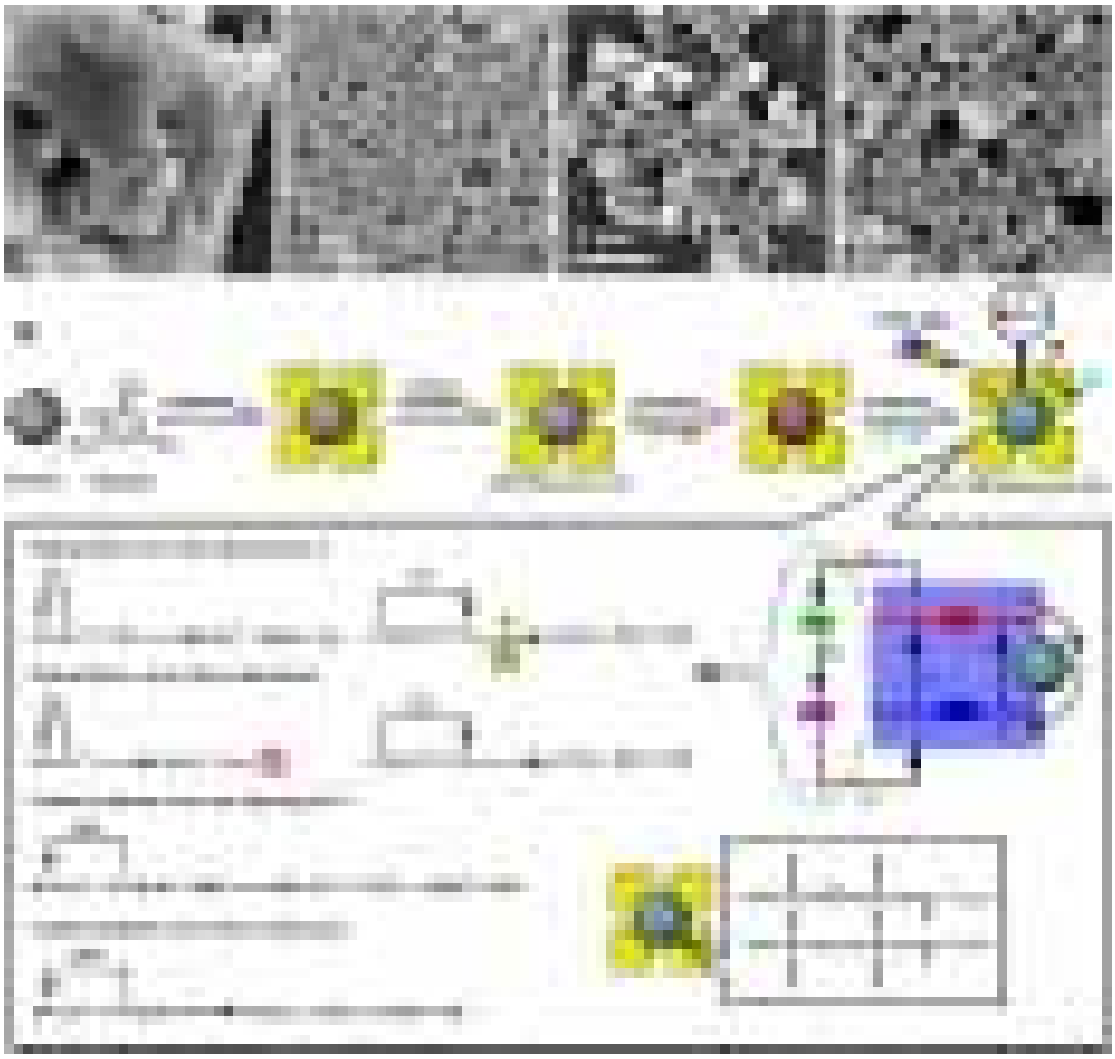

Fig. 15. Biochar-coupled g-C_3N_4-based photocatalyst for reduction of hexavalent chromium from water in single and combined pollution systems. FESEM images of as-prepared g-C_3N_4 (a), BPCMSs (b), BPCMSs(40)/g-C_3N_4 NSs (c), and BPCMSs(160)/g-C_3N_4 NSs (d). (e) The proposed fabrication route of BPCMSs/g-C_3N_4 NSs and recycled Cr^{3+}/BPCMSs/g-C_3N_4 NSs as well as the transfer of photogenerated electrons in different photocatalytic systems. Adapted with permission from ref. [210]. Copyright 2018 Elsevier B.V.

CoFe-LDH (LDH: layered double hydroxide) in the composite material has surface adsorption, which can quickly and in large capacity absorb Cr(VI) in water, and g-C_3N_4 nanosheets have many catalytic active sites that can in-situ reduce Cr(VI) [238]. The two form a typical magnetic recoverable heterojunction system (calcined CoFe-LDH/g-C_3N_4), which is favorable to the detachment of photoelectronic-holes, thus promoting the photoactivity of CoFe-LDH/g-C_3N_4. CoFe-LDH in the nanocomposite can be used to adsorb Cr(VI), and the

661 free radicals generated by the nanocomposite under visible light irradiation. Then, the free
662 radicals can be used to reduce Cr(VI). Compared with other g-C_3N_4-based composites (Table
663 4), CoFe-LDH/g-C_3N_4 has a relatively strong catalytic stability and can maintain a high
664 catalytic activity in the following ten operations.

665 Aside from the above examples, recently, we deposited black phosphorus quantum dots
666 (BPQDs) in porous g-C_3N_4 tubes to prepare metal-free composite nanomaterial (BPTCN) for
667 photo-reduction of Cr(VI) in wastewater [117]. Compared with BPQDs (17.61%), CN
668 (22.49%), and TCN (81.59%), the BPTCN has a better photo-reduction of Cr(VI) with 94.71%.
669 Meanwhile, the color of the aqueous solution containing Cr ions can be seen in the illustration
670 from purplish red to colorless, which appears that the sewage may have been purified.
671 Compared with CN (0.00369 min^{-1}) and TCN (0.0262 min^{-1}), BPTCN showed the highest
672 apparent removal rate constant of Cr(VI), which was 0.0404 min^{-1}. Furthermore, the pH value
673 of the water body is also one of the important aspects affecting the reduction rate of
674 photocatalytic Cr(VI) in the process of photodegradation. When the pH value was reduced from
675 5.65 to 2.65, the photo-reduction rate was increased from 91.25%/60 min to 93.11%/30 min,
676 respectively. The obvious improvement of photocatalytic effect may be mainly due to the
677 following two reasons [199,200,239]: first, under acidic conditions, H^+ in the solution is
678 conducive to the reduction of Cr(VI) (Equ. 1); Second, under neutral or alkaline conditions,
679 $Cr(OH)_3$ precipitation (Equ. 2) can often cover the photocatalyst's catalytic active site, thus
680 inhibiting its photocatalytic activity.

$$Cr_2O_7^{2-} + 14H^+ + 6e^- \rightarrow 2Cr^{3+} + 7H_2O \quad (1)$$

$$CrO_4^{2-} + 4H_2O + 3e^- \rightarrow Cr(OH)_3 + 5OH^- \quad (2)$$

Therefore, under acidic conditions, BPTCN can reduce Cr ions in raw water better under light conditions.

4.5 Metal-free Photocatalysis

Compared with traditional metal-based photocatalysts such as metal oxides and metal sulfides, metal-free polymeric g-C_3N_4 exhibit long stability under light irradiation and cost advantages [77,240,241]. As a metal-free photocatalyst, g-C_3N_4 can efficiently inactivate pathogens in water under visible light irradiation [242], providing a cost-effective approach for sustainable water treatment technology. However, pure g-C_3N_4 materials could be deactivation due to oxidative corrosion after prolonged exposure to light radiation and water [108]. Zhuang's group has synthesized a ternary metal-free g-C_3N_4-based photocatalyst using large-size graphene as the matrix by a simple hydrothermal method [243]. Because the steric hindrance effect of graphene blocks water and oxygen, the tight connection between graphene and carbon dots increases the specific surface area of the material, and the synergistic effect between the components accelerates the separation of photogenerated electron-hole pairs, the ternary metal-free g-C_3N_4-based photocatalyst not only has high photocatalytic oxidation of organic pollutants and reduction of heavy metals but also can resist photocorrosion to enhance photostability of the material in photocatalytic water purification.

In 2020, Sudhaik et al. prepared graphene supported g-C_3N_4 for metal-free photoactivation of peroxymonosulfate [240]. Compared with pure g-C_3N_4, the metal-free g-C_3N_4-based photocatalyst showed higher photocatalytic degradation (94%) of malathion and efficient

photocatalytic inactivation of *E. coli* [240]. Recently, Sahu et al. prepared metal-free oxygen-rich g-C_3N_4 for complete mineralization and degradation of organic pollutants under visible light [244]. The composition and structure of the metal-free g-C_3N_4-based photocatalyst can be adjusted by acid treatment under ultrasonication to increase its specific surface area and pore structure, visible light absorption capacity as well as the separation efficiency of photogenerated carriers. The metal-free g-C_3N_4-based photocatalysts, which are composed of elements (such as C and N) rich in the earth, meet the requirements of sustainable applications, and require further exploration and accumulation to assure that these materials have highly activity and stability in practical applications.

5. Chemical and Photocatalytic Stability

In the term of application, the recycling ability (Table 1-4, recycling) of g-C_3N_4-based photocatalysts is an important evaluation criterion. Incorporating g-C_3N_4-based photocatalysts into the photocatalytic water purification module with the continuous flow is required. This section briefly describes the stability of g-C_3N_4-based photocatalysts.

The g-C_3N_4 is a 2D flaky tri-*s*-triazines linked by tertiary amines, which can be found in air below 600°C [245]. However, the thermal stability of g-C_3N_4 is slightly affected by different preparation processes, which may be caused by different degrees of condensation [47,246,247]. Notably, g-C_3N_4 nanocrystals are usually negatively charged, which allows them to suspend stably in an aqueous solution without aggregation and precipitation [248-250]. Meanwhile, they also have good dispersion in strong acid solutions, and because of the strong van der Waals

721 interaction layer, g-C_3N_4 can maintain structural and chemical stability in strong acid solutions
722 [245,251].

723 In terms of composite materials, Shi et al. integrated g-C_3N_4 nanosheets and the materials
724 with interfacial hydrogen bond interactions into composite materials to improve the overall
725 thermal stability [252]. Wang et al. confirmed that g-C_3N_4 combined with reduced graphene
726 oxide can form a composite modified film with higher hydration properties [253]. As well as,
727 through fine adjustment, the compensating effect between the components of the composite
728 can enhance the activity and stability of the composite, to keep the crystal structure and surface-
729 active groups of the composite unchanged in the catalytic process [67,212,246]. Furthermore,
730 compared with the single Ag_3PO_4 material, Ag_3PO_4@g-C_3N_4 core-shell composite has higher
731 stability in the process of photocatalytic organic dyes in water, which demonstrates the
732 supporting effect of g-C_3N_4 shell on Ag_3PO_4 after the photocatalytic reaction [254].

733 **6. Conclusions and Perspectives**

734 As one of the candidate photocatalytic materials in the water purification field, g-C_3N_4-based
735 photocatalysts have received great attention over ten years. Investigations of g-C_3N_4-based
736 photocatalysts have provided a rich database of their design and synthesis as well as
737 environment-related applications. Various improved strategies to promote the performance and
738 ability of g-C_3N_4-based photocatalysts are introduced in this review. Undoubtedly, the g-C_3N_4-
739 based composites have unlimited potential for further improvement in the crystal structure,
740 light absorption capacity, electronic properties, and energy band arrangement.

741 At the atomic level, g-C_3N_4 can adjust HOMO and LUMO by element doping directionally
742 to reduce the bandgap of composite photocatalytic materials and enhance visible light capture.
743 At the molecular level, g-C_3N_4 can modify the link unit through copolymerization to expand
744 the visible light response, increase the electron-hole mobility, and improve the redox ability.
745 To improve the photoactivity, more types of g-C_3N_4-based Z-scheme/S-scheme heterojunction
746 and 2D g-C_3N_4-based photocatalysts are needed, which can hinder the photoinduced carrier
747 recombination rate and promote charge migration and separation. Improving the photocatalytic
748 stability of g-C_3N_4-based materials includes not only increasing the number of times in
749 complex environmental conditions and strong light irradiation, but also reducing the quality
750 loss in the continuous flow photocatalysis process. Suitable means to control the nanoparticle
751 size on the catalyst surface is deficient. Therefore, exploring different functionalization
752 strategies and specific chemical groups is needed to achieve the accurate adjustment of
753 interface contact points to enhance the anchoring capability of g-C_3N_4.

754 Although considerable potential material has been reported to date, the field of research in
755 g-C_3N_4-based composites for photocatalytic water purification is still at the preliminary stage
756 and far from meeting the demand of the industry. The theoretical calculation reveals the internal
757 properties of g-C_3N_4-based photocatalysts and explores the effect of modification strategies on
758 the overall performance of photocatalysts, accelerating the development of suitable g-C_3N_4-
759 based photocatalysts. To construct the composite material model to offer a theoretical
760 foundation for similar composite materials, the foresight to choose the parameters of the
761 calculation is needed. The adsorption of small organic molecules and heavy metal ions by g-
762 C_3N_4-based composites needs to be further investigated. Revealing the reasons for the

763 enhancement of photoactivity of g-C_3N_4-based composites from the perspective of
764 thermodynamics and reaction pathways is needed.

765 For applications, promising g-C_3N_4-based heterogeneous photocatalysts can remove
766 pollutants from different water bodies, but only a handful of pilot-scale studies have been
767 carried out, not implemented on a large scale [255,256]. Many issues are still to be resolved
768 before they can be applied on a large scale in the future. The first consideration is whether the
769 photocatalytic process should be used as a treatment unit in the sewage treatment plant or as
770 an independent system to undertake the whole sewage treatment process alone. In terms of the
771 photocatalytic process as an independent treatment system, the dynamics and photoutilization
772 efficiency of g-C_3N_4-based composites in the whole photocatalytic process need to be enhanced.

773 From the perspective of applications, the following areas need to be improved: (i) To ensure
774 that photocatalysts can maintain high photocatalytic activity after long flow operation, the
775 fixation strategy without negative influence in photocatalyst catalytic activity and/or cost-
776 effective solid-liquid separation technique is needed to be developed; (ii) For light use
777 efficiency, in addition to the need to increase the light response range of the photocatalysts
778 themselves, more efficient solar collectors are also needed to improve the light energy intensity
779 per unit area; (iii) For degradation target, besides the degradation of non-biological pollutants
780 in water, photocatalytic inactivation of pathogenic microorganisms in water by g-C_3N_4-based
781 composites has a great application prospect.

782 Furthermore, before the practical application of the g-C_3N_4-based heterogeneous

783 photocatalysts and photocatalytic equipment, pilot tests should be carried out to ensure that the
784 photocatalytic water purification technology developed is comprehensively assessed. For
785 example, the run of all the processes requires the actual device to provide a large amount of
786 technical and economic data for LCA, such as the photocatalyst usage, photocatalytic treatment
787 efficiency, floor space requirements, non-renewable energy consumption, secondary pollution
788 emissions, and other costs. Meanwhile, LCA also needs to consider the impact of photocatalytic
789 water purification technology on the environment, such as whether the g-C_3N_4-based
790 photocatalysts are bio-toxic, and whether their mass preparation and use have potential
791 ecological hazards.

792 Finally, the commercialization of g-C_3N_4-based photocatalysts still has a long way to go.
793 The collaboration of all disciplines worldwide, including materials science, physical science,
794 and chemical science, is an important weapon to break the bottleneck in the field of materials
795 chemistry and energy and will lead us to a sustainable world.

796 **Declaration of Competing Interest**

797 The authors declare no competing financial interest.

798 **Acknowledgment**

799 The study was financially supported by the Program for Changjiang Scholars and Innovative
800 Research Team in University (IRT-13R17), the National Natural Science Foundation of China
801 (U20A20323, 51521006, 51378190, 51979103, 51308200), the Fundamental Research Funds

for the Central Universities of China (531107051205), the Funds of Hunan Science and Technology Innovation Project (2018RS3115, 2020RC5012), Natural Science Foundation of Hunan Province, China (2020JJ5069), the Key Research and Development Project of Hunan Province of China (2017SK2241) and the Three Gorges Follow-up Research Project (2017HXXY-05).

References

[1] H. Mahmoudi, O. Abdellah, N. Ghaffour, Capacity building strategies and policy for desalination using renewable energies in Algeria, Renew. Sust. Energ. Rev. 13 (2009) 921-926. DOI: https://doi.org/10.1016/j.rser.2008.02.001

[2] T.A. Larsen, S. Hoffmann, C. Luthi, B. Truffer, M. Maurer, Emerging solutions to the water challenges of an urbanizing world, Science 352 (2016) 928-933. DOI: https://doi.org/10.1126/science.aad8641

[3] A.C. Johnson, X. Jin, N. Nakada, J.P. Sumpter, Learning from the past and considering the future of chemicals in the environment, Science 367 (2020) 384-387. DOI: https://doi.org/10.1126/science.aay6637

[4] G. Zeng, M. Chen, Z. Zeng, Risks of Neonicotinoid Pesticides, Science 340 (2013) 1403. DOI: https://doi.org/10.1126/science.340.6139.1403-a

[5] M. Chen, P. Xu, G.M. Zeng, C.P. Yang, D.L. Huang, J.C. Zhang, Bioremediation of soils contaminated with polycyclic aromatic hydrocarbons, petroleum, pesticides, chlorophenols and heavy metals by composting: Applications, microbes and future research needs, Biotechnol. Adv. 33 (2015) 745-755. DOI: https://doi.org/10.1016/j.biotechadv.2015.05.003

[6] H.R. Dong, G.M. Zeng, L. Tang, C.Z. Fan, C. Zhang, X.X. He, Y. He, An overview on limitations of TiO2-based particles for photocatalytic degradation of organic pollutants and the corresponding countermeasures, Water Res. 79 (2015) 128-146. DOI: https://doi.org/10.1016/j.watres.2015.04.038

[7] S. Ye, M. Cheng, G. Zeng, X. Tan, H. Wu, J. Liang, M. Shen, B. Song, J. Liu, H. Yang, Y. Zhang, Insights into catalytic removal and separation of attached metals from natural-aged microplastics by magnetic biochar activating oxidation process, Water Res. 179 (2020) 115876. DOI: https://doi.org/10.1016/j.watres.2020.115876

[8] S. Luo, Y. Liu, Y. Zhu, Q. Niu, M. Cheng, S. Ye, H. Yi, B. Shao, M. Shen, X. Wen, G. Zeng, Z. Liu, Perspectives on palladium-based nanomaterials: green synthesis, ecotoxicity, and risk assessment, Environmen. Sci.-Nano 8 (2021) 20-36. DOI: https://doi.org/10.1039/D0EN01048K

[9] D. Cambie, C. Bottecchia, N.J.W. Straathof, V. Hessel, T. Noel, Applications of Continuous-Flow Photochemistry in Organic Synthesis, Material Science, and Water Treatment, Chem. Rev. 116 (2016) 10276-10341. DOI: https://doi.org/10.1021/acs.chemrev.5b00707

[10] Y. Liu, M. Cheng, Z. Liu, G. Zeng, H. Zhong, M. Chen, C. Zhou, W. Xiong, B. Shao, B. Song, Heterogeneous Fenton-like catalyst for treatment of rhamnolipid-solubilized hexadecane wastewater, Chemosphere 236 (2019) 124387. DOI: https://doi.org/10.1016/j.chemosphere.2019.124387

[11] M. Duan, L. Jiang, G. Zeng, D. Wang, W. Tang, J. Liang, H. Wang, D. He, Z. Liu, L. Tang, Bimetallic nanoparticles/metal-organic frameworks: Synthesis, applications and

challenges, Applied Materials Today 19 (2020) 100564. DOI: https://doi.org/10.1016/j.apmt.2020.100564

[12] V. Hasija, A. Sudhaik, P. Raizada, A. Hosseini-Bandegharaei, P. Singh, Carbon quantum dots supported AgI /ZnO/phosphorus doped graphitic carbon nitride as Z-scheme photocatalyst for efficient photodegradation of 2, 4-dinitrophenol, Journal of Environmental Chemical Engineering 7 (2019) 103272. DOI: https://doi.org/10.1016/j.jece.2019.103272

[13] P. Raizada, A. Sudhaik, P. Singh, A. Hosseini-Bandegharaei, P. Thakur, Converting type II AgBr/VO into ternary Z scheme photocatalyst via coupling with phosphorus doped g-C3N4 for enhanced photocatalytic activity, Sep. Purif. Technol. 227 (2019) 115692. DOI: https://doi.org/10.1016/j.seppur.2019.115692

[14] B. Pare, P. Singh, S.B. Jonnalgadda, Degradation and mineralization of Victoria blue B dye in a slurry photoreactor using advanced oxidation process, Journal of Scientific & Industrial Research 68 (2009) 724-729. DOI: http://www.researchgate.net/profile/Pardeep_Singh6/publication/236667158_Degradation_and_mineralization_of_victoria_blue_B_dye_in_a_slurry_photoreactor_using_advanced_oxidation_process/links/0deec518c8cefe1c01000000

[15] H. Yi, D.L. Huang, L. Qin, G.M. Zeng, C. Lai, M. Cheng, S.J. Ye, B. Song, X.Y. Ren, X.Y. Guo, Selective Prepared Carbon Nanomaterials for Advanced Photocatalytic Application in Environmental Pollutant Treatment and Hydrogen Production, Appl. Catal. B 239 (2018) 408-424. DOI: https://doi.org/10.1016/j.apcatb.2018.07.068

[16] L. Qin, Z. Zeng, G. Zeng, C. Lai, A. Duan, R. Xiao, D. Huang, Y. Fu, H. Yi, B. Li, X. Liu, S. Liu, M. Zhang, D. Jiang, Cooperative catalytic performance of bimetallic Ni-Au

867 nanocatalyst for highly efficient hydrogenation of nitroaromatics and corresponding
868 mechanism insight, Appl. Catal. B 259 (2019) 118035. DOI:
869 https://doi.org/10.1016/j.apcatb.2019.118035
870 [17] C. Lai, M. Zhang, B. Li, D. Huang, G. Zeng, L. Qin, X. Liu, H. Yi, M. Cheng, L. Li, Z.
871 Chen, L. Chen, Fabrication of CuS/BiVO4 (040) binary heterojunction photocatalysts with
872 enhanced photocatalytic activity for Ciprofloxacin degradation and mechanism insight,
873 Chem. Eng. J. 358 (2019) 891-902. DOI: https://doi.org/10.1016/j.cej.2018.10.072
874 [18] H. Wang, H. Wang, Z. Wang, L. Tang, G. Zeng, P. Xu, M. Chen, T. Xiong, C. Zhou, X.
875 Li, D. Huang, Y. Zhu, Z. Wang, J. Tang, Covalent organic framework photocatalysts:
876 structures and applications, Chem. Soc. Rev. 49 (2020) 4135-4165. DOI:
877 https://doi.org/10.1039/D0CS00278J
878 [19] C. Liang, H.-Y. Niu, H. Guo, C.-G. Niu, Y.-Y. Yang, H.-Y. Liu, W.-W. Tang, H.-P.
879 Feng, Efficient photocatalytic nitrogen fixation to ammonia over bismuth monoxide quantum
880 dots-modified defective ultrathin graphitic carbon nitride, Chem. Eng. J. 406 (2021) 126868.
881 DOI: https://doi.org/10.1016/j.cej.2020.126868
882 [20] A. Habibi-Yangjeh, S. Asadzadeh-Khaneghah, S. Feizpoor, A. Rouhi, Review on
883 heterogeneous photocatalytic disinfection of waterborne, airborne, and foodborne viruses:
884 Can we win against pathogenic viruses?, J. Colloid. Interface. Sci. 580 (2020) 503-514. DOI:
885 https://doi.org/10.1016/j.jcis.2020.07.047
886 [21] S. Asadzadeh-Khaneghah, A. Habibi-Yangjeh, g-C3N4/carbon dot-based
887 nanocomposites serve as efficacious photocatalysts for environmental purification and energy

generation: A review, Journal of Cleaner Production 276 (2020) 124319. DOI: https://doi.org/10.1016/j.jclepro.2020.124319

[22] A. Akhundi, A. Badiei, G.M. Ziarani, A. Habibi-Yangjeh, M.J. Muñoz-Batista, R. Luque, Graphitic carbon nitride-based photocatalysts: Toward efficient organic transformation for value-added chemicals production, Molecular Catalysis 488 (2020) 110902. DOI: https://doi.org/10.1016/j.mcat.2020.110902

[23] M.N. Chong, B. Jin, C.W.K. Chow, C. Saint, Recent developments in photocatalytic water treatment technology: A review, Water Res. 44 (2010) 2997-3027. DOI: https://doi.org/10.1016/j.watres.2010.02.039

[24] A. Kumar, P. Raizada, P. Singh, R.V. Saini, A.K. Saini, A. Hosseini-Bandegharaei, Perspective and status of polymeric graphitic carbon nitride based Z-scheme photocatalytic systems for sustainable photocatalytic water purification, Chem. Eng. J. 391 (2020) 123496. DOI: https://doi.org/10.1016/j.cej.2019.123496

[25] P. Raizada, A. Sudhaik, P. Singh, P. Shandilya, V.K. Gupta, A. Hosseini-Bandegharaei, S. Agrawal, Ag3PO4 modified phosphorus and sulphur co-doped graphitic carbon nitride as a direct Z-scheme photocatalyst for 2, 4-dimethylphenol degradation, J. Photochem. Photobiol. A: Chem. 374 (2019) 22-35. DOI: https://doi.org/10.1016/j.jphotochem.2019.01.015

[26] P. Singh, P. Shandilya, P. Raizada, A. Sudhaik, A. Rahmani-Sani, A. Hosseini-Bandegharaei, Review on various strategies for enhancing photocatalytic activity of graphene based nanocomposites for water purification, Arabian Journal of Chemistry 13 (2020) 3498-3520. DOI: https://doi.org/10.1016/j.arabjc.2018.12.001

[27] Sonu, V. Dutta, S. Sharma, P. Raizada, A. Hosseini-Bandegharaei, V. Kumar Gupta, P. Singh, Review on augmentation in photocatalytic activity of CoFe2O4 via heterojunction formation for photocatalysis of organic pollutants in water, Journal of Saudi Chemical Society 23 (2019) 1119-1136. DOI: https://doi.org/10.1016/j.jscs.2019.07.003

[28] T. Hisatomi, J. Kubota, K. Domen, Recent advances in semiconductors for photocatalytic and photoelectrochemical water splitting, Chem. Soc. Rev. 43 (2014) 7520-7535. DOI: https://doi.org/10.1039/c3cs60378d

[29] T. Wu, X. Liu, Y. Liu, M. Cheng, Z. Liu, G. Zeng, B. Shao, Q. Liang, W. Zhang, Q. He, W. Zhang, Application of QD-MOF composites for photocatalysis: Energy production and environmental remediation, Coord. Chem. Rev. 403 (2020) 213097. DOI: https://doi.org/10.1016/j.ccr.2019.213097

[30] Y. Liu, H. Cheng, M. Cheng, Z. Liu, D. Huang, G. Zhang, B. Shao, Q. Liang, S. Luo, T. Wu, S. Xiao, The application of Zeolitic imidazolate frameworks (ZIFs) and their derivatives based materials for photocatalytic hydrogen evolution and pollutants treatment, Chem. Eng. J. In Press (2020) 127914. DOI: https://doi.org/10.1016/j.cej.2020.127914

[31] H. Wang, L. Zhang, Z. Chen, J. Hu, S. Li, Z. Wang, J. Liu, X. Wang, Semiconductor heterojunction photocatalysts: design, construction, and photocatalytic performances, Chem. Soc. Rev. 43 (2014) 5234-5244. DOI: https://doi.org/10.1039/c4cs00126e

[32] Z. Xing, J. Zhang, J. Cui, J. Yin, T. Zhao, J. Kuang, Z. Xiu, N. Wan, W. Zhou, Recent advances in floating TiO2-based photocatalysts for environmental application, Appl. Catal. B 225 (2018) 452-467. DOI: https://doi.org/10.1016/j.apcatb.2017.12.005

930 [33] Z. Wang, M. Chen, D. Huang, G. Zeng, P. Xu, C. Zhou, C. Lai, H. Wang, M. Cheng, W.
931 Wang, Multiply structural optimized strategies for bismuth oxyhalide photocatalysis and their
932 environmental application, Chem. Eng. J. 374 (2019) 1025-1045. DOI:
933 https://doi.org/10.1016/j.cej.2019.06.018
934 [34] S. Cao, J. Low, J. Yu, M. Jaroniec, Polymeric Photocatalysts Based on Graphitic Carbon
935 Nitride, Adv. Mater. 27 (2015) 2150-2176. DOI: https://doi.org/10.1002/adma.201500033
936 [35] W. Wang, M.O. Tadé, Z. Shao, Research progress of perovskite materials in
937 photocatalysis- and photovoltaics-related energy conversion and environmental treatment,
938 Chem. Soc. Rev. 44 (2015) 5371-5408. DOI: https://doi.org/10.1039/C5CS00113G
939 [36] C.B. Ong, L.Y. Ng, A.W. Mohammad, A review of ZnO nanoparticles as solar
940 photocatalysts: Synthesis, mechanisms and applications, Renew. Sust. Energ. Rev. 81 (2018)
941 536-551. DOI: https://doi.org/10.1016/j.rser.2017.08.020
942 [37] S. Luo, Z. Zeng, G. Zeng, Z. Liu, R. Xiao, P. Xu, H. Wang, D. Huang, Y. Liu, B. Shao,
943 Q. Liang, D. Wang, Q. He, L. Qin, Y. Fu, Recent advances in conjugated microporous
944 polymers for photocatalysis: designs, applications, and prospects, J. Mater. Chem. A 8 (2020)
945 6434-6470. DOI: https://doi.org/10.1039/D0TA01102A
946 [38] S. Luo, Z. Zeng, H. Wang, W. Xiong, B. Song, C. Zhou, A. Duan, X. Tan, Q. He, G.
947 Zeng, Z. Liu, R. Xiao, Recent Progress in Conjugated Microporous Polymers for Clean
948 Energy: Synthesis, Modification, Computer Simulations, and Applications, Prog. Polym. Sci.
949 115 (2021) 101374. DOI: https://doi.org/10.1016/j.progpolymsci.2021.101374
950 [39] Y. Wang, X. Wang, M. Antonietti, Polymeric Graphitic Carbon Nitride as a
951 Heterogeneous Organocatalyst: From Photochemistry to Multipurpose Catalysis to

952 Sustainable Chemistry, Angew. Chem. Int. Ed. 51 (2012) 68-89. DOI:
953 https://doi.org/10.1002/anie.201101182
954 [40] X. Wang, K. Maeda, A. Thomas, K. Takanabe, G. Xin, J.M. Carlsson, K. Domen, M.
955 Antonietti, A metal-free polymeric photocatalyst for hydrogen production from water under
956 visible light, Nat. Mater. 8 (2009) 76-80. DOI: https://doi.org/10.1038/nmat2317
957 [41] Z. Wang, H. Wang, Z. Zeng, G. Zeng, P. Xu, R. Xiao, D. Huang, X. Chen, L. He, C.
958 Zhou, Y. Yang, Z. Wang, W. Wang, W. Xiong, Metal-organic frameworks derived
959 Bi2O2CO3/porous carbon nitride: A nanosized Z-scheme systems with enhanced
960 photocatalytic activity, Appl. Catal. B 267 (2020) 118700. DOI:
961 https://doi.org/10.1016/j.apcatb.2020.118700
962 [42] W.J. Ong, L.L. Tan, Y.H. Ng, S.T. Yong, S.P. Chai, Graphitic Carbon Nitride (g-C3N4)-
963 Based Photocatalysts for Artificial Photosynthesis and Environmental Remediation: Are We
964 a Step Closer To Achieving Sustainability?, Chem. Rev. 116 (2016) 7159-7329. DOI:
965 https://doi.org/10.1021/acs.chemrev.6b00075
966 [43] H. Wang, X. Zhang, Y. Xie, Photoresponsive polymeric carbon nitride-based materials:
967 Design and application, Mater. Today 23 (2019) 72-86. DOI:
968 https://doi.org/10.1016/j.mattod.2018.05.001
969 [44] E. Vesali-Kermani, A. Habibi-Yangjeh, S. Ghosh, Visible-light-induced nitrogen
970 photofixation ability of g-C3N4 nanosheets decorated with MgO nanoparticles, Journal of
971 Industrial and Engineering Chemistry 84 (2020) 185-195. DOI:
972 https://doi.org/10.1016/j.jiec.2019.12.033

973 [45] E. Vesali-Kermani, A. Habibi-Yangjeh, H. Diarmand-Khalilabad, S. Ghosh, Nitrogen
974 photofixation ability of g-C3N4 nanosheets/Bi2MoO6 heterojunction photocatalyst under
975 visible-light illumination, J. Colloid. Interface. Sci. 563 (2020) 81-91. DOI:
976 https://doi.org/10.1016/j.jcis.2019.12.057
977 [46] S. Asadzadeh-Khaneghah, A. Habibi-Yangjeh, M.S. Asl, Z. Ahmadi, S. Ghosh,
978 Synthesis of novel ternary g-C3N4/SiC/C-Dots photocatalysts and their visible-light-induced
979 activities in removal of various contaminants, Journal of Photochemistry and Photobiology a-
980 Chemistry 392 (2020) 14. DOI: https://doi.org/10.1016/j.jphotochem.2020.112431
981 [47] Y. Yang, X. Li, C. Zhou, W. Xiong, G. Zeng, D. Huang, C. Zhang, W. Wang, B. Song,
982 X. Tang, X. Li, H. Guo, Recent advances in application of graphitic carbon nitride-based
983 catalysts for degrading organic contaminants in water through advanced oxidation processes
984 beyond photocatalysis: A critical review, Water Res. 184 (2020) 116200. DOI:
985 https://doi.org/10.1016/j.watres.2020.116200
986 [48] J. Liu, H. Wang, M. Antonietti, Graphitic carbon nitride "reloaded": emerging
987 applications beyond (photo)catalysis, Chem. Soc. Rev. 45 (2016) 2308-2326. DOI:
988 https://doi.org/10.1039/c5cs00767d
989 [49] Y. Cui, Z. Ding, X. Fu, X. Wang, Construction of Conjugated Carbon Nitride
990 Nanoarchitectures in Solution at Low Temperatures for Photoredox Catalysis, Angew. Chem.
991 Int. Ed. 51 (2012) 11814-11818. DOI: https://doi.org/10.1002/anie.201206534
992 [50] P. Niu, L. Zhang, G. Liu, H.-M. Cheng, Graphene-Like Carbon Nitride Nanosheets for
993 Improved Photocatalytic Activities, Adv. Funct. Mater. 22 (2012) 4763-4770. DOI:
994 https://doi.org/10.1002/adfm.201200922

995 [51] J. Xu, L. Zhang, R. Shi, Y. Zhu, Chemical exfoliation of graphitic carbon nitride for
996 efficient heterogeneous photocatalysis, J. Mater. Chem. A 1 (2013) 14766-14772. DOI:
997 https://doi.org/10.1039/C3TA13188B
998 [52] F. Shi, L. Chen, M. Chen, D. Jiang, A g-C3N4/nanocarbon/ZnIn2S4 nanocomposite: an
999 artificial Z-scheme visible-light photocatalytic system using nanocarbon as the electron
1000 mediator, Chem. Commun. 51 (2015) 17144-17147. DOI:
1001 https://doi.org/10.1039/C5CC05323D
1002 [53] R. Hao, G. Wang, H. Tang, L. Sun, C. Xu, D. Han, Template-free preparation of
1003 macro/mesoporous g-C3N4/TiO2 heterojunction photocatalysts with enhanced visible light
1004 photocatalytic activity, Appl. Catal. B 187 (2016) 47-58. DOI:
1005 https://doi.org/10.1016/j.apcatb.2016.01.026
1006 [54] D. Ma, J. Wu, M. Gao, Y. Xin, Y. Sun, T. Ma, Hydrothermal synthesis of an artificial Z-
1007 scheme visible light photocatalytic system using reduced graphene oxide as the electron
1008 mediator, Chem. Eng. J. 313 (2017) 1567-1576. DOI:
1009 https://doi.org/10.1016/j.cej.2016.11.036
1010 [55] H. Pan, Y.-W. Zhang, V.B. Shenoy, H. Gao, Ab Initio Study on a Novel Photocatalyst:
1011 Functionalized Graphitic Carbon Nitride Nanotube, ACS Catal. 1 (2011) 99-104. DOI:
1012 https://doi.org/10.1021/cs100045u
1013 [56] J. Xue, S. Ma, Y. Zhou, Z. Zhang, M. He, Facile Photochemical Synthesis of Au/Pt/g-
1014 C3N4 with Plasmon-Enhanced Photocatalytic Activity for Antibiotic Degradation, ACS
1015 Appl. Mater. Inter. 7 (2015) 9630-9637. DOI: https://doi.org/10.1021/acsami.5b01212

1016 [57] O. Fontelles-Carceller, M.J. Muñoz-Batista, M. Fernández-García, A. Kubacka,
1017 Interface Effects in Sunlight-Driven Ag/g-C3N4 Composite Catalysts: Study of the Toluene
1018 Photodegradation Quantum Efficiency, ACS Appl. Mater. Inter. 8 (2016) 2617-2627. DOI:
1019 https://doi.org/10.1021/acsami.5b10434
1020 [58] K. Wang, Q. Li, B. Liu, B. Cheng, W. Ho, J. Yu, Sulfur-doped g-C3N4 with enhanced
1021 photocatalytic CO2-reduction performance, Appl. Catal. B 176-177 (2015) 44-52. DOI:
1022 https://doi.org/10.1016/j.apcatb.2015.03.045
1023 [59] C. Xu, Q. Han, Y. Zhao, L. Wang, Y. Li, L. Qu, Sulfur-doped graphitic carbon nitride
1024 decorated with graphene quantum dots for an efficient metal-free electrocatalyst, J. Mater.
1025 Chem. A 3 (2015) 1841-1846. DOI: https://doi.org/10.1039/C4TA06149G
1026 [60] Y. Zhou, L. Zhang, J. Liu, X. Fan, B. Wang, M. Wang, W. Ren, J. Wang, M. Li, J. Shi,
1027 Brand new P-doped g-C3N4: enhanced photocatalytic activity for H2 evolution and
1028 Rhodamine B degradation under visible light, J. Mater. Chem. A 3 (2015) 3862-3867. DOI:
1029 https://doi.org/10.1039/C4TA05292G
1030 [61] Y. Zheng, L. Lin, B. Wang, X. Wang, Graphitic Carbon Nitride Polymers toward
1031 Sustainable Photoredox Catalysis, Angew. Chem. Int. Ed. 54 (2015) 12868-12884. DOI:
1032 https://doi.org/10.1002/anie.201501788
1033 [62] Y.-P. Zhu, T.-Z. Ren, Z.-Y. Yuan, Mesoporous Phosphorus-Doped g-C3N4
1034 Nanostructured Flowers with Superior Photocatalytic Hydrogen Evolution Performance, ACS
1035 Appl. Mater. Inter. 7 (2015) 16850-16856. DOI: https://doi.org/10.1021/acsami.5b04947
1036 [63] X. She, H. Xu, Y. Xu, J. Yan, J. Xia, L. Xu, Y. Song, Y. Jiang, Q. Zhang, H. Li,
1037 Exfoliated graphene-like carbon nitride in organic solvents: enhanced photocatalytic activity

and highly selective and sensitive sensor for the detection of trace amounts of Cu2+, J. Mater. Chem. A 2 (2014) 2563-2570. DOI: https://doi.org/10.1039/C3TA13768F

[64] D. Zheng, X.-N. Cao, X. Wang, Precise Formation of a Hollow Carbon Nitride Structure with a Janus Surface To Promote Water Splitting by Photoredox Catalysis, Angew. Chem. Int. Ed. 55 (2016) 11512-11516. DOI: https://doi.org/10.1002/anie.201606102

[65] C. Liu, H. Huang, L. Ye, S. Yu, N. Tian, X. Du, T. Zhang, Y. Zhang, Intermediate-mediated strategy to horn-like hollow mesoporous ultrathin g-C3N4 tube with spatial anisotropic charge separation for superior photocatalytic H-2 evolution, Nano Energy 41 (2017) 738-748. DOI: https://doi.org/10.1016/j.nanoen.2017.10.031

[66] B. Lin, H. An, X. Yan, T. Zhang, J. Wei, G. Yang, Fish-scale structured g-C3N4 nanosheet with unusual spatial electron transfer property for high-efficiency photocatalytic hydrogen evolution, Appl. Catal. B 210 (2017) 173-183. DOI: https://doi.org/10.1016/j.apcatb.2017.03.066

[67] X. Zhang, X. Yuan, L. Jiang, J. Zhang, H. Yu, W. Hou, G. Zeng, Powerful combination of 2D g-C3N4 and 2D nanomaterials for photocatalysis: Recent advances, Chem. Eng. J. 390 (2020) 124475. DOI: https://doi.org/10.1016/j.cej.2020.124475

[68] D. Huang, Z. Li, G. Zeng, C. Zhou, W. Xue, X. Gong, X. Yan, S. Chen, W. Wang, M. Cheng, Megamerger in photocatalytic field: 2D g-C3N4 nanosheets serve as support of 0D nanomaterials for improving photocatalytic performance, Appl. Catal. B 240 (2019) 153-173. DOI: https://doi.org/10.1016/j.apcatb.2018.08.071

[69] S. Chen, Y. Hu, S. Meng, X. Fu, Study on the separation mechanisms of photogenerated electrons and holes for composite photocatalysts g-C3N4-WO3, Appl. Catal. B 150-151 (2014) 564-573. DOI: https://doi.org/10.1016/j.apcatb.2013.12.053

[70] C. Chang, L. Zhu, S. Wang, X. Chu, L. Yue, Novel Mesoporous Graphite Carbon Nitride/BiOI Heterojunction for Enhancing Photocatalytic Performance Under Visible-Light Irradiation, ACS Appl. Mater. Inter. 6 (2014) 5083-5093. DOI: https://doi.org/10.1021/am5002597

[71] Y. Li, L. Fang, R. Jin, Y. Yang, X. Fang, Y. Xing, S. Song, Preparation and enhanced visible light photocatalytic activity of novel g-C3N4 nanosheets loaded with Ag2CO3 nanoparticles, Nanoscale 7 (2015) 758-764. DOI: https://doi.org/10.1039/C4NR06565D

[72] J. Fu, J. Yu, C. Jiang, B. Cheng, g-C3N4-Based Heterostructured Photocatalysts, Adv. Energy Mater. 8 (2018) 1701503. DOI: https://doi.org/10.1002/aenm.201701503

[73] T. Paul, D. Das, B.K. Das, S. Sarkar, S. Maiti, K.K. Chattopadhyay, CsPbBrCl2/g-C3N4 type II heterojunction as efficient visible range photocatalyst, J. Hazard. Mater. 380 (2019) 120855. DOI: https://doi.org/10.1016/j.jhazmat.2019.120855

[74] L.B. Jiang, X.Z. Yuan, G.M. Zeng, Z.B. Wu, J. Liang, X.H. Chen, L.J. Leng, H. Wang, H. Wang, Metal-free efficient photocatalyst for stable visible-light photocatalytic degradation of refractory pollutant, Appl. Catal. B 221 (2018) 715-725. DOI: https://doi.org/10.1016/j.apcatb.2017.09.059

[75] L. Jiang, X. Yuan, G. Zeng, J. Liang, Z. Wu, H. Wang, J. Zhang, T. Xiong, H. Li, A facile band alignment of polymeric carbon nitride isotype heterojunctions for enhanced

1079 photocatalytic tetracycline degradation, Environmen. Sci.-Nano 5 (2018) 2604-2617. DOI:
1080 https://doi.org/10.1039/c8en00807h
1081 [76] A. Sudhaik, P. Raizada, P. Singh, A. Hosseini-Bandegharaei, V.K. Thakur, V.-H.
1082 Nguyen, Highly effective degradation of imidacloprid by H2O2/ fullerene decorated P-doped
1083 g-C3N4 photocatalyst, Journal of Environmental Chemical Engineering 8 (2020) 104483.
1084 DOI: https://doi.org/10.1016/j.jece.2020.104483
1085 [77] A. Kumar, P. Raizada, V. Kumar Thakur, V. Saini, A. Aslam Parwaz Khan, N. Singh, P.
1086 Singh, An overview on polymeric carbon nitride assisted photocatalytic CO2 reduction:
1087 Strategically manoeuvring solar to fuel conversion efficiency, Chem. Eng. Sci. 230 (2021)
1088 116219. DOI: https://doi.org/10.1016/j.ces.2020.116219
1089 [78] A. Sudhaik, P. Raizada, S. Thakur, R.V. Saini, A.K. Saini, P. Singh, V. Kumar Thakur,
1090 V.-H. Nguyen, A.A.P. Khan, A.M. Asiri, Synergistic photocatalytic mitigation of
1091 imidacloprid pesticide and antibacterial activity using carbon nanotube decorated phosphorus
1092 doped graphitic carbon nitride photocatalyst, Journal of the Taiwan Institute of Chemical
1093 Engineers 113 (2020) 142-154. DOI: https://doi.org/10.1016/j.jtice.2020.08.003
1094 [79] F. Chen, Q. Yang, Y. Wang, J. Zhao, D. Wang, X. Li, Z. Guo, H. Wang, Y. Deng, C.
1095 Niu, G. Zeng, Novel ternary heterojunction photcocatalyst of Ag nanoparticles and g-C3N4
1096 nanosheets co-modified BiVO4 for wider spectrum visible-light photocatalytic degradation of
1097 refractory pollutant, Appl. Catal. B 205 (2017) 133-147. DOI:
1098 https://doi.org/10.1016/j.apcatb.2016.12.017
1099 [80] Z. Wan, G. Zhang, X. Wu, S. Yin, Novel visible-light-driven Z-scheme Bi12GeO20/g-
1100 C3N4 photocatalyst: Oxygen-induced pathway of organic pollutants degradation and proton

assisted electron transfer mechanism of Cr(VI) reduction, Appl. Catal. B 207 (2017) 17-26. DOI: https://doi.org/10.1016/j.apcatb.2017.02.014

[81] D. Xu, B. Cheng, S. Cao, J. Yu, Enhanced photocatalytic activity and stability of Z-scheme Ag2CrO4-GO composite photocatalysts for organic pollutant degradation, Appl. Catal. B 164 (2015) 380-388. DOI: https://doi.org/10.1016/j.apcatb.2014.09.051

[82] Y. Shang, X. Chen, W. Liu, P. Tan, H. Chen, L. Wu, C. Ma, X. Xiong, J. Pan, Photocorrosion inhibition and high-efficiency photoactivity of porous g-C3N4/Ag2CrO4 composites by simple microemulsion-assisted co-precipitation method, Appl. Catal. B 204 (2017) 78-88. DOI: https://doi.org/10.1016/j.apcatb.2016.11.025

[83] F. Chen, Q. Yang, S.N. Wang, F.B. Yao, J. Sun, Y.L. Wang, C. Zhang, X.M. Li, C.G. Niu, D.B. Wang, G.M. Zeng, Graphene oxide and carbon nitride nanosheets co-modified silver chromate nanoparticles with enhanced visible-light photoactivity and anti-photocorrosion properties towards multiple refractory pollutants degradation, Appl. Catal. B 209 (2017) 493-505. DOI: https://doi.org/10.1016/j.apcatb.2017.03.026

[84] M.R. Khan, T.W. Chuan, A. Yousuf, M.N.K. Chowdhury, C.K. Cheng, Schottky barrier and surface plasmonic resonance phenomena towards the photocatalytic reaction: study of their mechanisms to enhance photocatalytic activity, Catal. Sci. Technol. 5 (2015) 2522-2531. DOI: https://doi.org/10.1039/C4CY01545B

[85] S. Zhang, J. Li, X. Wang, Y. Huang, M. Zeng, J. Xu, In Situ Ion Exchange Synthesis of Strongly Coupled Ag@AgCl/g-C3N4 Porous Nanosheets as Plasmonic Photocatalyst for Highly Efficient Visible-Light Photocatalysis, ACS Appl. Mater. Inter. 6 (2014) 22116-22125. DOI: https://doi.org/10.1021/am505528c

[86] W. Jiang, W. Luo, J. Wang, M. Zhang, Y. Zhu, Enhancement of catalytic activity and oxidative ability for graphitic carbon nitride, J. Photochem. Photobiol., C 28 (2016) 87-115. DOI: https://doi.org/10.1016/j.jphotochemrev.2016.06.001

[87] W. Chen, T.-Y. Liu, T. Huang, X.-H. Liu, X.-J. Yang, Novel mesoporous P-doped graphitic carbon nitride nanosheets coupled with ZnIn2S4 nanosheets as efficient visible light driven heterostructures with remarkably enhanced photo-reduction activity, Nanoscale 8 (2016) 3711-3719. DOI: https://doi.org/10.1039/C5NR07695A

[88] Z.-A. Lan, G. Zhang, X. Wang, A facile synthesis of Br-modified g-C3N4 semiconductors for photoredox water splitting, Appl. Catal. B 192 (2016) 116-125. DOI: https://doi.org/10.1016/j.apcatb.2016.03.062

[89] C. Lu, P. Zhang, S. Jiang, X. Wu, S. Song, M. Zhu, Z. Lou, Z. Li, F. Liu, Y. Liu, Y. Wang, Z. Le, Photocatalytic reduction elimination of UO22+ pollutant under visible light with metal-free sulfur doped g-C3N4 photocatalyst, Appl. Catal. B 200 (2017) 378-385. DOI: https://doi.org/10.1016/j.apcatb.2016.07.036

[90] F. He, G. Chen, Y. Yu, Y. Zhou, Y. Zheng, S. Hao, The sulfur-bubble template-mediated synthesis of uniform porous g-C3N4 with superior photocatalytic performance, Chem. Commun. 51 (2015) 425-427. DOI: https://doi.org/10.1039/C4CC07106A

[91] Q. Fan, J. Liu, Y. Yu, S. Zuo, B. Li, A simple fabrication for sulfur doped graphitic carbon nitride porous rods with excellent photocatalytic activity degrading RhB dye, Appl. Surf. Sci. 391 (2017) 360-368. DOI: https://doi.org/10.1016/j.apsusc.2016.04.055

1143 [92] G. Liu, P. Niu, C. Sun, S.C. Smith, Z. Chen, G.Q. Lu, H.-M. Cheng, Unique Electronic
1144 Structure Induced High Photoreactivity of Sulfur-Doped Graphitic C3N4, J. Am. Chem. Soc.
1145 132 (2010) 11642-11648. DOI: https://doi.org/10.1021/ja103798k
1146 [93] S. Hu, L. Ma, Y. Xie, F. Li, Z. Fan, F. Wang, Q. Wang, Y. Wang, X. Kang, G. Wu,
1147 Hydrothermal synthesis of oxygen functionalized S–P codoped g-C3N4 nanorods with
1148 outstanding visible light activity under anoxic conditions, Dalton Transactions 44 (2015)
1149 20889-20897. DOI: https://doi.org/10.1039/C5DT04035C
1150 [94] Z. Li, C. Kong, G. Lu, Visible Photocatalytic Water Splitting and Photocatalytic Two-
1151 Electron Oxygen Formation over Cu- and Fe-Doped g-C3N4, J Phys. Chem. C 120 (2016)
1152 56-63. DOI: https://doi.org/10.1021/acs.jpcc.5b09469
1153 [95] G. Dong, K. Zhao, L. Zhang, Carbon self-doping induced high electronic conductivity
1154 and photoreactivity of g-C3N4, Chem. Commun. 48 (2012) 6178-6180. DOI:
1155 https://doi.org/10.1039/C2CC32181E
1156 [96] J. Zhang, Y. Wu, M. Xing, S.A.K. Leghari, S. Sajjad, Development of modified N doped
1157 TiO2 photocatalyst with metals, nonmetals and metal oxides, Energy Environ. Sci. 3 (2010)
1158 715-726. DOI: https://doi.org/10.1039/B927575D
1159 [97] S. Hu, J. Zhu, L. Wu, X. Wang, P. Liu, Y. Zhang, Z. Li, Effect of Fluorination on
1160 Photocatalytic Degradation of Rhodamine B over In(OH)ySz: Promotion or Suppression?, J
1161 Phys. Chem. C 115 (2011) 460-467. DOI: https://doi.org/10.1021/jp109578g
1162 [98] S. An, G. Zhang, T. Wang, W. Zhan, K. Li, C. Song, J.T. Miller, S. Miao, J. Wang, X.
1163 Guo, High-Density Ultra-small Clusters and Single-Atom Fe Sites Embedded in Graphitic

Carbon Nitride (g-C3N4) for Highly Efficient Catalytic Advanced Oxidation Processes, ACS Nano 12 (2018) 9441-9450. DOI: https://doi.org/10.1021/acsnano.8b04693

[99] L. Zhang, R. Long, Y. Zhang, D. Duan, Y. Xiong, Y. Zhang, Y. Bi, Direct Observation of Dynamic Bond Evolution in Single-Atom Pt/C3N4 Catalysts, Angew. Chem. Int. Ed. 59 (2020) 6224-6229. DOI: https://doi.org/10.1002/anie.201915774

[100] Z. Zhao, W. Zhang, W. Liu, Y. Li, J. Ye, J. Liang, M. Tong, Single-atom silver induced amorphization of hollow tubular g-C3N4 for enhanced visible light-driven photocatalytic degradation of naproxen, Sci. Total Environ. 742 (2020) 140642. DOI: https://doi.org/10.1016/j.scitotenv.2020.140642

[101] Y. Yang, G. Zeng, D. Huang, C. Zhang, D. He, C. Zhou, W. Wang, W. Xiong, B. Song, H. Yi, S. Ye, X. Ren, In Situ Grown Single-Atom Cobalt on Polymeric Carbon Nitride with Bidentate Ligand for Efficient Photocatalytic Degradation of Refractory Antibiotics, Small 16 (2020) 2001634. DOI: https://doi.org/10.1002/smll.202001634

[102] Z. Chen, Y. Bu, L. Wang, X. Wang, J.-P. Ao, Single-sites Rh-phosphide modified carbon nitride photocatalyst for boosting hydrogen evolution under visible light, Appl. Catal. B 274 (2020) 119117. DOI: https://doi.org/10.1016/j.apcatb.2020.119117

[103] J. Xu, X. Zheng, Z. Feng, Z. Lu, Z. Zhang, W. Huang, Y. Li, D. Vuckovic, Y. Li, S. Dai, G. Chen, K. Wang, H. Wang, J.K. Chen, W. Mitch, Y. Cui, Organic wastewater treatment by a single-atom catalyst and electrolytically produced H2O2, Nature Sustainability 4 (2020) 233-241. DOI: https://doi.org/10.1038/s41893-020-00635-w

[104] B. Qiao, A. Wang, X. Yang, L.F. Allard, Z. Jiang, Y. Cui, J. Liu, J. Li, T. Zhang, Single-atom catalysis of CO oxidation using Pt1/FeOx, Nat. Chem. 3 (2011) 634-641. DOI: https://doi.org/10.1038/nchem.1095

[105] J. Lu, C. Aydin, N.D. Browning, B.C. Gates, Imaging Isolated Gold Atom Catalytic Sites in Zeolite NaY, Angew. Chem. Int. Ed. 51 (2012) 5842-5846. DOI: https://doi.org/10.1002/anie.201107391

[106] Y. Lu, H. Wang, P. Yu, Y. Yuan, R. Shahbazian-Yassar, Y. Sheng, S. Wu, W. Tu, G. Liu, M. Kraft, R. Xu, Isolated Ni single atoms in nitrogen doped ultrathin porous carbon templated from porous g-C3N4 for high-performance CO2 reduction, Nano Energy 77 (2020) 105158. DOI: https://doi.org/10.1016/j.nanoen.2020.105158

[107] X.-F. Yang, A. Wang, B. Qiao, J. Li, J. Liu, T. Zhang, Single-Atom Catalysts: A New Frontier in Heterogeneous Catalysis, Acc. Chem. Res. 46 (2013) 1740-1748. DOI: https://doi.org/10.1021/ar300361m

[108] A. Kumar, P. Raizada, A. Hosseini-Bandegharaei, V.K. Thakur, V.-H. Nguyen, P. Singh, C-, N-Vacancy defect engineered polymeric carbon nitride towards photocatalysis: viewpoints and challenges, J. Mater. Chem. A 9 (2021) 111-153. DOI: https://doi.org/10.1039/D0TA08384D

[109] P. Raizada, V. Soni, A. Kumar, P. Singh, A.A. Parwaz Khan, A.M. Asiri, V.K. Thakur, V.-H. Nguyen, Surface defect engineering of metal oxides photocatalyst for energy application and water treatment, Journal of Materiomics 7 (2021) 388-418. DOI: https://doi.org/10.1016/j.jmat.2020.10.009

[110] S. Sharma, V. Dutta, P. Raizada, A. Hosseini-Bandegharaei, P. Singh, V.-H. Nguyen, Tailoring cadmium sulfide-based photocatalytic nanomaterials for water decontamination: a review, Environ. Chem. Lett. 19 (2021) 271-306. DOI: https://doi.org/10.1007/s10311-020-01066-x

[111] D. Zhao, C.-L. Dong, W. Bin, C. Chen, Y.-C. Huang, Z. Diao, S. Li, L. Guo, S. Shen, Synergy of Dopants and Defects in Graphitic Carbon Nitride with Exceptionally Modulated Band Structures for Efficient Photocatalytic Oxygen Evolution, Adv. Mater. 31 (2019) e1903545. DOI: https://doi.org/10.1002/adma.201903545

[112] J. Liao, W. Cui, J. Li, J. Sheng, H. Wang, X.a. Dong, P. Chen, G. Jiang, Z. Wang, F. Dong, Nitrogen defect structure and NO+ intermediate promoted photocatalytic NO removal on H2 treated g-C3N4, Chem. Eng. J. 379 (2020) 122282. DOI: https://doi.org/10.1016/j.cej.2019.122282

[113] Z. Zhang, L. Lu, Z. Lv, Y. Chen, H. Jin, S. Hou, L. Qiu, L. Duan, J. Liu, K. Dai, Porous carbon nitride with defect mediated interfacial oxidation for improving visible light photocatalytic hydrogen evolution, Appl. Catal. B 232 (2018) 384-390. DOI: https://doi.org/10.1016/j.apcatb.2018.03.086

[114] W. Lin, K. Lu, S. Zhou, J. Wang, F. Mu, Y. Wang, Y. Wu, Y. Kong, Defects remodeling of g-C3N4 nanosheets by fluorine-containing solvothermal treatment to enhance their photocatalytic activities, Appl. Surf. Sci. 474 (2019) 194-202. DOI: https://doi.org/10.1016/j.apsusc.2018.03.140

[115] Z. Wang, Y. Huang, M. Chen, X. Shi, Y. Zhang, J. Cao, W. Ho, S.C. Lee, Roles of N-Vacancies over Porous g-C3N4 Microtubes during Photocatalytic NOx Removal, ACS Appl. Mater. Inter. 11 (2019) 10651-10662. DOI: https://doi.org/10.1021/acsami.8b21987

[116] Y. Wu, H. Wang, Y. Sun, T. Xiao, W. Tu, X. Yuan, G. Zeng, S. Li, J.W. Chew, Photogenerated charge transfer via interfacial internal electric field for significantly improved photocatalysis in direct Z-scheme oxygen-doped carbon nitrogen/CoAl-layered double hydroxide heterojunction, Appl. Catal. B 227 (2018) 530-540. DOI: https://doi.org/10.1016/j.apcatb.2018.01.069

[117] W.J. Wang, Q.Y. Niu, G.M. Zeng, C. Zhang, D.L. Huang, B.B. Shao, C.Y. Zhou, Y. Yang, Y.X. Liu, H. Guo, W.P. Xiong, L. Lei, S.Y. Liu, H. Yi, S. Chen, X. Tang, 1D porous tubular g-C3N4 capture black phosphorus quantum dots as 1D/0D metal-free photocatalysts for oxytetracycline hydrochloride degradation and hexavalent chromium reduction, Appl. Catal. B 273 (2020) 119051. DOI: https://doi.org/10.1016/j.apcatb.2020.119051

[118] Y. Yang, G.M. Zeng, D.L. Huang, C. Zhang, D.H. He, C.Y. Zhou, W.J. Wang, W.P. Xiong, X.P. Li, B.S. Li, W.Y. Dong, Y. Zhou, Molecular engineering of polymeric carbon nitride for highly efficient photocatalytic oxytetracycline degradation and H2O2 production, Appl. Catal. B 272 (2020) 118970. DOI: https://doi.org/10.1016/j.apcatb.2020.118970

[119] L.M. Azofra, D.R. MacFarlane, C. Sun, A DFT study of planar vs. corrugated graphene-like carbon nitride (g-C3N4) and its role in the catalytic performance of CO2 conversion, PCCP 18 (2016) 18507-18514. DOI: https://doi.org/10.1039/C6CP02453J

[120] Y. Dou, S. Zhang, T. Pan, S. Xu, A. Zhou, M. Pu, H. Yan, J. Han, M. Wei, D.G. Evans, X. Duan, TiO2@Layered Double Hydroxide Core–Shell Nanospheres with Largely

1247 Enhanced Photocatalytic Activity Toward O2 Generation, Adv. Funct. Mater. 25 (2015)
1248 2243-2249. DOI: https://doi.org/10.1002/adfm.201404496
1249 [121] J. Li, W. Wei, C. Mu, B. Huang, Y. Dai, Electronic properties of g-C3N4/CdS
1250 heterojunction from the first-principles, Physica E 103 (2018) 459-463. DOI:
1251 https://doi.org/10.1016/j.physe.2018.04.023
1252 [122] J. Liu, E. Hua, High Photocatalytic Activity of Heptazine-Based g-C3N4/SnS2
1253 Heterojunction and Its Origin: Insights from Hybrid DFT, J Phys. Chem. C 121 (2017)
1254 25827-25835. DOI: https://doi.org/10.1021/acs.jpcc.7b07914
1255 [123] Y. Yu, W. Yan, X. Wang, P. Li, W. Gao, H. Zou, S. Wu, K. Ding, Surface Engineering
1256 for Extremely Enhanced Charge Separation and Photocatalytic Hydrogen Evolution on g-
1257 C3N4, Adv. Mater. 30 (2018) 1705060. DOI: https://doi.org/10.1002/adma.201705060
1258 [124] T. Di, B. Zhu, B. Cheng, J. Yu, J. Xu, A direct Z-scheme g-C3N4/SnS2 photocatalyst
1259 with superior visible-light CO2 reduction performance, J. Catal. 352 (2017) 532-541. DOI:
1260 https://doi.org/10.1016/j.jcat.2017.06.006
1261 [125] Z.-F. Huang, J. Song, X. Wang, L. Pan, K. Li, X. Zhang, L. Wang, J.-J. Zou, Switching
1262 charge transfer of C3N4/W18O49 from type-II to Z-scheme by interfacial band bending for
1263 highly efficient photocatalytic hydrogen evolution, Nano Energy 40 (2017) 308-316. DOI:
1264 https://doi.org/10.1016/j.nanoen.2017.08.032
1265 [126] Y. Gao, J. Zhu, H. An, P. Yan, B. Huang, R. Chen, F. Fan, C. Li, Directly Probing
1266 Charge Separation at Interface of TiO2 Phase Junction, J Phys. Chem. Lett. 8 (2017) 1419-
1267 1423. DOI: https://doi.org/10.1021/acs.jpclett.7b00285

[127] Z. Zhang, J.T. Yates, Band Bending in Semiconductors: Chemical and Physical Consequences at Surfaces and Interfaces, Chem. Rev. 112 (2012) 5520-5551. DOI: https://doi.org/10.1021/cr3000626

[128] P. Zhou, J. Yu, M. Jaroniec, All-Solid-State Z-Scheme Photocatalytic Systems, Adv. Mater. 26 (2014) 4920-4935. DOI: https://doi.org/10.1002/adma.201400288

[129] B. Shao, X. Liu, Z. Liu, G. Zeng, W. Zhang, Q. Liang, Y. Liu, Q. He, X. Yuan, D. Wang, S. Luo, S. Gong, Synthesis and characterization of 2D/0D g-C3N4/CdS-nitrogen doped hollow carbon spheres (NHCs) composites with enhanced visible light photodegradation activity for antibiotic, Chem. Eng. J. 374 (2019) 479-493. DOI: https://doi.org/10.1016/j.cej.2019.05.202

[130] C. Feng, L. Tang, Y. Deng, G. Zeng, J. Wang, Y. Liu, Z. Chen, J. Yu, J. Wang, Enhancing optical absorption and charge transfer: Synthesis of S-doped h-BN with tunable band structures for metal-free visible-light-driven photocatalysis, Appl. Catal. B 256 (2019) 117827. DOI: https://doi.org/10.1016/j.apcatb.2019.117827

[131] X. Tang, H. Chen, J.S. Ponraj, S.C. Dhanabalan, Q. Xiao, D. Fan, H. Zhang, Fluorination-Enhanced Ambient Stability and Electronic Tolerance of Black Phosphorus Quantum Dots, Adv. Sci. 5 (2018) 1800420. DOI: https://doi.org/10.1002/advs.201800420

[132] B. Feng, Z. Wu, J. Liu, K. Zhu, Z. Li, X. Jin, Y. Hou, Q. Xi, M. Cong, P. Liu, Q. Gu, Combination of ultrafast dye-sensitized-assisted electron transfer process and novel Z-scheme system: AgBr nanoparticles interspersed MoO3 nanobelts for enhancing photocatalytic performance of RhB, Appl. Catal. B 206 (2017) 242-251. DOI: https://doi.org/10.1016/j.apcatb.2017.01.029

[133] H. Gao, Y. Guo, Z. Yu, M. Zhao, Y. Hou, Z. Zhu, S. Yan, Q. Liu, Z. Zou, Incorporating p-Phenylene as an Electron-Donating Group into Graphitic Carbon Nitride for Efficient Charge Separation, ChemSusChem 12 (2019) 4285-4292. DOI: https://doi.org/10.1002/cssc.201901239

[134] K. Ding, L. Wen, M. Huang, Y. Zhang, Y. Lu, Z. Chen, How does the B,F-monodoping and B/F-codoping affect the photocatalytic water-splitting performance of g-C3N4?, PCCP 18 (2016) 19217-19226. DOI: https://doi.org/10.1039/C6CP02169G

[135] J. Zhang, F. Ren, M. Deng, Y. Wang, Enhanced visible-light photocatalytic activity of a g-C3N4/BiVO4 nanocomposite: a first-principles study, PCCP 17 (2015) 10218-10226. DOI: https://doi.org/10.1039/C4CP06089J

[136] L. Sun, Y. Qi, C.-J. Jia, Z. Jin, W. Fan, Enhanced visible-light photocatalytic activity of g-C3N4/Zn2GeO4 heterojunctions with effective interfaces based on band match, Nanoscale 6 (2014) 2649-2659. DOI: https://doi.org/10.1039/C3NR06104C

[137] L. Ruan, G. Xu, L. Gu, C. Li, Y. Zhu, Y. Lu, The physical properties of Li-doped g-C3N4 monolayer sheet investigated by the first-principles, Mater. Res. Bull. 66 (2015) 156-162. DOI: https://doi.org/10.1016/j.materresbull.2015.02.044

[138] J. Liu, B. Cheng, J. Yu, A new understanding of the photocatalytic mechanism of the direct Z-scheme g-C3N4/TiO2 heterostructure, PCCP 18 (2016) 31175-31183. DOI: https://doi.org/10.1039/C6CP06147H

[139] H.-X. Zhang, Y.F. Zhu, M. Zhao, Interface charge transfer and enhanced visible light response of graphene/anatase TiO2 (110) systems with and without oxygen vacancy: A

DFT+U calculation, Appl. Surf. Sci. 420 (2017) 105-109. DOI: https://doi.org/10.1016/j.apsusc.2017.05.142

[140] S. Lu, C. Li, H.H. Li, Y.F. Zhao, Y.Y. Gong, L.Y. Niu, X.J. Liu, T. Wang, The effects of nonmetal dopants on the electronic, optical and chemical performances of monolayer g–C3N4 by first-principles study, Appl. Surf. Sci. 392 (2017) 966-974. DOI: https://doi.org/10.1016/j.apsusc.2016.09.136

[141] L.-W. Ruan, Y.-J. Zhu, L.-G. Qiu, Y.-P. Yuan, Y.-X. Lu, First principles calculations of the pressure affection to g-C3N4, Comp. Mater. Sci. 91 (2014) 258-265. DOI: https://doi.org/10.1016/j.commatsci.2014.04.058

[142] J.J. Wang, L. Tang, G.M. Zeng, Y.C. Deng, Y.N. Liu, L.G. Wang, Y.Y. Zhou, Z. Guo, J.J. Wang, C. Zhang, Atomic scale g-C3N4/Bi2WO6 2D/2D heterojunction with enhanced photocatalytic degradation of ibuprofen under visible light irradiation, Appl. Catal. B 209 (2017) 285-294. DOI: https://doi.org/10.1016/j.apcatb.2017.03.019

[143] W.J. Wang, P. Xu, M. Chen, G.M. Zeng, C. Zhang, C.Y. Zhou, Y. Yang, D.L. Huang, C. Lai, M. Cheng, L. Hu, W.P. Xiong, H. Guo, M. Zhou, Alkali Metal-Assisted Synthesis of Graphite Carbon Nitride with Tunable Band-Gap for Enhanced Visible-Light-Driven Photocatalytic Performance, ACS Sustain. Chem. Eng. 6 (2018) 15503-15516. DOI: https://doi.org/10.1021/acssuschemeng.8b03965

[144] C. Zhou, C. Lai, D. Huang, G. Zeng, C. Zhang, M. Cheng, L. Hu, J. Wan, W. Xiong, M. Wen, X. Wen, L. Qin, Highly porous carbon nitride by supramolecular preassembly of monomers for photocatalytic removal of sulfamethazine under visible light driven, Appl. Catal. B 220 (2018) 202-210. DOI: https://doi.org/10.1016/j.apcatb.2017.08.055

[145] C.Y. Zhou, C. Lai, P. Xu, G.M. Zeng, D.L. Huang, Z.H. Li, C. Zhang, M. Cheng, L. Hu, J. Wan, F. Chen, W.P. Xiong, R. Deng, Rational Design of Carbon-Doped Carbon Nitride/Bi12O17Cl2 Composites: A Promising Candidate Photocatalyst for Boosting Visible-Light-Driven Photocatalytic Degradation of Tetracycline, ACS Sustain. Chem. Eng. 6 (2018) 6941-6949. DOI: https://doi.org/10.1021/acssuschemeng.8b00782

[146] X. Bai, Y. Li, L. Xie, X. Liu, S. Zhan, W. Hu, A novel Fe-free photo-electro-Fenton-like system for enhanced ciprofloxacin degradation: bifunctional Z-scheme WO3/g-C3N4, Environmen. Sci.-Nano 6 (2019) 2850-2862. DOI: https://doi.org/10.1039/c9en00528e

[147] J. Huang, D. Li, R. Li, Q. Zhang, T. Chen, H. Liu, Y. Liu, W. Lv, G. Liu, An efficient metal-free phosphorus and oxygen co-doped g-C3N4 photocatalyst with enhanced visible light photocatalytic activity for the degradation of fluoroquinolone antibiotics, Chem. Eng. J. 374 (2019) 242-253. DOI: https://doi.org/10.1016/j.cej.2019.05.175

[148] Y. Tian, L. Zhou, Q. Zhu, J. Lei, L. Wang, J. Zhang, Y. Liu, Hierarchical macro-mesoporous g-C3N4 with an inverse opal structure and vacancies for high-efficiency solar energy conversion and environmental remediation, Nanoscale 11 (2019) 20638-20647. DOI: https://doi.org/10.1039/c9nr06802c

[149] K. Wang, J. Li, G. Zhang, Ag-Bridged Z-Scheme 2D/2D Bi5FeTi3O15/g-C3N4 Heterojunction for Enhanced Photocatalysis: Mediator-Induced Interfacial Charge Transfer and Mechanism Insights, ACS Appl. Mater. Inter. 11 (2019) 27686-27696. DOI: https://doi.org/10.1021/acsami.9b05074

[150] W. Wang, Z. Zeng, G. Zeng, C. Zhang, R. Xiao, C. Zhou, W. Xiong, Y. Yang, L. Lei, Y. Liu, D. Huang, M. Cheng, Y. Yang, Y. Fu, H. Luo, Y. Zhou, Sulfur doped carbon

quantum dots loaded hollow tubular g-C3N4 as novel photocatalyst for destruction of Escherichia coli and tetracycline degradation under visible light, Chem. Eng. J. 378 (2019) 122132. DOI: https://doi.org/10.1016/j.cej.2019.122132

[151] W. Xue, D. Huang, J. Li, G. Zeng, R. Deng, Y. Yang, S. Chen, Z. Li, X. Gong, B. Li, Assembly of AgI nanoparticles and ultrathin g-C3N4 nanosheets codecorated Bi2WO6 direct dual Z-scheme photocatalyst: An efficient, sustainable and heterogeneous catalyst with enhanced photocatalytic performance, Chem. Eng. J. 373 (2019) 1144-1157. DOI: https://doi.org/10.1016/j.cej.2019.05.069

[152] Y. Yang, C. Zhang, D.L. Huang, G.M. Zeng, J.H. Huang, C. Lai, C.Y. Zhou, W.J. Wang, H. Guo, W.J. Xue, R. Deng, M. Cheng, W.P. Xiong, Boron nitride quantum dots decorated ultrathin porous g-C3N4: Intensified exciton dissociation and charge transfer for promoting visible-light-driven molecular oxygen activation, Appl. Catal. B 245 (2019) 87-99. DOI: https://doi.org/10.1016/j.apcatb.2018.12.049

[153] C.Y. Zhou, D.L. Huang, P. Xu, G.M. Zeng, J.H. Huang, T.Z. Shi, C. Lai, C. Zhang, M. Cheng, Y. Lu, A. Duan, W.P. Xiong, M. Zhou, Efficient visible light driven degradation of sulfamethazine and tetracycline by salicylic acid modified polymeric carbon nitride via charge transfer, Chem. Eng. J. 370 (2019) 1077-1086. DOI: https://doi.org/10.1016/j.cej.2019.03.279

[154] C.Y. Zhou, Z.T. Zeng, G.M. Zeng, D.L. Huang, R. Xiao, M. Cheng, C. Zhang, W.P. Xiong, C. Lai, Y. Yang, W.J. Wang, H. Yi, B.S. Li, Visible-light-driven photocatalytic degradation of sulfamethazine by surface engineering of carbon nitride : Properties,

1376 degradation pathway and mechanisms, J. Hazard. Mater. 380 (2019) 120815. DOI:
1377 https://doi.org/10.1016/j.jhazmat.2019.120815
1378 [155] J. Zheng, L. Zhang, Designing 3D magnetic peony flower-like cobalt oxides/g-C3N4
1379 dual Z-scheme photocatalyst for remarkably enhanced sunlight driven photocatalytic redox
1380 activity, Chem. Eng. J. 369 (2019) 947-956. DOI: https://doi.org/10.1016/j.cej.2019.03.131
1381 [156] M. Dou, J. Wang, B. Gao, C. Xu, F. Yang, Photocatalytic difference of amoxicillin and
1382 cefotaxime under visible light by mesoporous g-C3N4: Mechanism, degradation pathway and
1383 DFT calculation, Chem. Eng. J. 383 (2020) 123134. DOI:
1384 https://doi.org/10.1016/j.cej.2019.123134
1385 [157] Q. Chen, W. Yang, J. Zhu, L. Fu, D. Li, L. Zhou, Enhanced visible light photocatalytic
1386 activity of g-C3N4 decorated ZrO2-x nanotubes heterostructure for degradation of
1387 tetracycline hydrochloride, J. Hazard. Mater. 384 (2020) 121275. DOI:
1388 https://doi.org/10.1016/j.jhazmat.2019.121275
1389 [158] F. Gao, J. Chen, J. Zhao, Z. Chen, D. Xia, Z. Zhan, Q. Wang, Z-scheme heterojunction
1390 g-C3N4@PDA/BiOBr with biomimetic polydopamine as electron transfer mediators for
1391 enhanced visible-light driven degradation of sulfamethoxazole, Chem. Eng. J. 386 (2020)
1392 124014. DOI: https://doi.org/10.1016/j.cej.2020.124014
1393 [159] Q. Liang, X. Liu, J. Wang, Y. Liu, Z. Liu, L. Tang, B. Shao, W. Zhang, S. Gong, M.
1394 Cheng, Q. He, C. Feng, In-situ self-assembly construction of hollow tubular g-C3N4 isotype
1395 heterojunction for enhanced visible-light photocatalysis: Experiments and theories, J. Hazard.
1396 Mater. 401 (2020) 123355-123355. DOI: https://doi.org/10.1016/j.jhazmat.2020.123355

[160] M. Tang, Y. Ao, C. Wang, P. Wang, Facile synthesis of dual Z-scheme g-C3N4/Ag3PO4/AgI composite photocatalysts with enhanced performance for the degradation of a typical neonicotinoid pesticide, Appl. Catal. B 268 (2020) 118395. DOI: https://doi.org/10.1016/j.apcatb.2019.118395

[161] S. Ghodsi, A. Esrafili, R.R. Kalantary, M. Gholami, H.R. Sobhi, Synthesis and evaluation of the performance of g-C3N4/Fe3O4/Ag photocatalyst for the efficient removal of diazinon: Kinetic studies, Journal of Photochemistry and Photobiology a-Chemistry 389 (2020) 112279. DOI: https://doi.org/10.1016/j.jphotochem.2019.112279

[162] P. Qiu, J. Yao, H. Chen, F. Jiang, X. Xie, Enhanced visible-light photocatalytic decomposition of 2,4-dichlorophenoxyacetic acid over ZnIn2S4/g-C3N4 photocatalyst, J. Hazard. Mater. 317 (2016) 158-168. DOI: https://doi.org/10.1016/j.jhazmat.2016.05.069

[163] H. Wang, X.Z. Yuan, Y. Wu, G.M. Zeng, X.H. Chen, L.J. Leng, H. Li, Synthesis and applications of novel graphitic carbon nitride/metal-organic frameworks mesoporous photocatalyst for dyes removal, Appl. Catal. B 174 (2015) 445-454. DOI: https://doi.org/10.1016/j.apcatb.2015.03.037

[164] H. Wang, X.Z. Yuan, H. Wang, X.H. Chen, Z.B. Wu, L.B. Jiang, W.P. Xiong, G.M. Zeng, Facile synthesis of Sb2S3/ultrathin g-C3N4 sheets heterostructures embedded with g-C3N4 quantum dots with enhanced NIR-light photocatalytic performance, Appl. Catal. B 193 (2016) 36-46. DOI: https://doi.org/10.1016/j.apcatb.2016.03.075

[165] W. An, K. Sun, J. Hu, W. Cui, L. Liu, The Z-scheme Ag2CO3@g-C3N4 core-shell structure for increased photoinduced charge separation and stable photocatalytic degradation, Appl. Surf. Sci. 504 (2020) 144345. DOI: https://doi.org/10.1016/j.apsusc.2019.144345

[166] W. Bai, X. Yang, X. Du, Z. Qian, Y. Zhang, L. Liu, J. Yao, Robust and recyclable macroscopic g-C3N4/cellulose hybrid photocatalysts with enhanced visible light photocatalytic activity, Appl. Surf. Sci. 504 (2020) 144179. DOI: https://doi.org/10.1016/j.apsusc.2019.144179

[167] K.R.S. Devi, S. Mathew, R. Rajan, J. Georgekutty, K. Kasinathan, D. Pinheiro, S. Sugunan, Biogenic synthesis of g-C3N4/Bi2O3 heterojunction with enhanced photocatalytic activity and statistical optimization of reaction parameters, Appl. Surf. Sci. 494 (2019) 465-476. DOI: https://doi.org/10.1016/j.apsusc.2019.07.125

[168] F. Liu, N. Thien-Phap, Q. Wang, F. Massuyeau, Y. Dan, L. Jiang, Construction of Z-scheme g-C3N4/Ag/P3HT heterojunction for enhanced visible-light photocatalytic degradation of tetracycline (TC) and methyl orange (MO), Appl. Surf. Sci. 496 (2019) 143653. DOI: https://doi.org/10.1016/j.apsusc.2019.143653

[169] A. Mohammad, M.E. Khan, M.R. Karim, M.H. Cho, Synergistically effective and highly visible light responsive SnO2-g-C3N4 nanostructures for improved photocatalytic and photoelectrochemical performance, Appl. Surf. Sci. 495 (2019) 143432. DOI: https://doi.org/10.1016/j.apsusc.2019.07.174

[170] M. Pedrosa, M.J. Sampaio, T. Horvat, O.C. Nunes, G. Drazic, A.E. Rodrigues, J.L. Figueiredo, C.G. Silva, A.M.T. Silva, J.L. Faria, Visible-light-induced self-cleaning functional fabrics using graphene oxide/carbon nitride materials, Appl. Surf. Sci. 497 (2019) 143757. DOI: https://doi.org/10.1016/j.apsusc.2019.143757

[171] M. Wang, G. Tan, H. Ren, A. Xia, Y. Liu, Direct double Z-scheme O-g-C3N4/Zn2SnO4N/ZnO ternary heterojunction photocatalyst with enhanced visible

photocatalytic activity, Appl. Surf. Sci. 492 (2019) 690-702. DOI:
https://doi.org/10.1016/j.apsusc.2019.06.260
[172] L. Yang, X. Bai, J. Shi, X. Du, L. Xu, P. Jin, Quasi-full-visible-light absorption by D35-TiO2/g-C3N4 for synergistic persulfate activation towards efficient photodegradation of micropollutants, Appl. Catal. B 256 (2019) 117759. DOI:
https://doi.org/10.1016/j.apcatb.2019.117759
[173] J.-Y. Zhang, J.-Y. Mei, S.-S. Yi, X.-X. Guan, Constructing of Z-scheme 3D g-C3N4-ZnO@graphene aerogel heterojunctions for high-efficient adsorption and photodegradation of organic pollutants, Appl. Surf. Sci. 492 (2019) 808-817. DOI:
https://doi.org/10.1016/j.apsusc.2019.06.261
[174] S. Adhikari, D.-H. Kim, Heterojunction C3N4/MoO3 microcomposite for highly efficient photocatalytic oxidation of Rhodamine B, Appl. Surf. Sci. 511 (2020) 145595. DOI:
https://doi.org/10.1016/j.apsusc.2020.145595
[175] S. Feng, T. Chen, Z. Liu, J. Shi, X. Yue, Y. Li, Z-scheme CdS/CQDs/g-C3N4 composites with visible-near-infrared light response for efficient photocatalytic organic pollutant degradation, Sci. Total Environ. 704 (2020) 135404. DOI:
https://doi.org/10.1016/j.scitotenv.2019.135404
[176] K. Huang, C. Li, X. Zhang, X. Meng, L. Wang, W. Wang, Z. Li, TiO2 nanorod arrays decorated by nitrogen-doped carbon and g-C3N4 with enhanced photoelectrocatalytic activity, Appl. Surf. Sci. 518 (2020) 146219. DOI:
https://doi.org/10.1016/j.apsusc.2020.146219

1462 [177] T. Jia, F. Fu, J. Li, Z. Deng, F. Long, D. Yu, Q. Cui, W. Wang, Rational construction of
1463 direct Z-scheme SnS/g-C3N4 hybrid photocatalyst for significant enhancement of visible-
1464 light photocatalytic activity, Appl. Surf. Sci. 499 (2020) 143941. DOI:
1465 https://doi.org/10.1016/j.apsusc.2019.143941
1466 [178] G. Li, B. Wang, J. Zhang, R. Wang, H. Liu, Er-doped g-C3N4 for photodegradation of
1467 tetracycline and tylosin: High photocatalytic activity and low leaching toxicity, Chem. Eng. J.
1468 391 (2020) 123500. DOI: https://doi.org/10.1016/j.cej.2019.123500
1469 [179] G. Li, R. Wang, B. Wang, J. Zhang, Sm-doped mesoporous g-C3N4 as efficient
1470 catalyst for degradation of tylosin: Influencing factors and toxicity assessment, Appl. Surf.
1471 Sci. 517 (2020) 146212. DOI: https://doi.org/10.1016/j.apsusc.2020.146212
1472 [180] S. Velmurugan, S. Balu, S. Palanisamy, T.C.K. Yang, V. Velusamy, S.-W. Chen, E.-
1473 S.I. El-Shafey, Synthesis of novel and environmental sustainable AgI-Ag2S nanospheres
1474 impregnated g-C3N4 photocatalyst for efficient degradation of aqueous pollutants, Appl.
1475 Surf. Sci. 500 (2020) 143991. DOI: https://doi.org/10.1016/j.apsusc.2019.143991
1476 [181] X. Zhao, X. Zhang, D. Han, L. Niu, Ag supported Z-scheme WO2.9/g-C3N4 composite
1477 photocatalyst for photocatalytic degradation under visible light, Appl. Surf. Sci. 501 (2020)
1478 144258. DOI: https://doi.org/10.1016/j.apsusc.2019.144258
1479 [182] Z. Teng, N. Yang, H. Lv, S. Wang, M. Hu, C. Wang, D. Wang, G. Wang, Edge-
1480 Functionalized g-C3N4 Nanosheets as a Highly Efficient Metal-free Photocatalyst for Safe
1481 Drinking Water, Chem 5 (2019) 664-680. DOI: https://doi.org/10.1016/j.chempr.2018.12.009
1482 [183] X. Zeng, Y. Liu, Y. Xia, M.H. Uddin, D. Xia, D.T. McCarthy, A. Deletic, J. Yu, X.
1483 Zhang, Cooperatively modulating reactive oxygen species generation and bacteria-

1484 photocatalyst contact over graphitic carbon nitride by polyethylenimine for rapid water
1485 disinfection, Appl. Catal. B 274 (2020) 119095. DOI:
1486 https://doi.org/10.1016/j.apcatb.2020.119095
1487 [184] Y. Yan, X. Zhou, P. Yu, Z. Li, T. Zheng, Characteristics, mechanisms and bacteria
1488 behavior of photocatalysis with a solid Z-scheme Ag/AgBr/g-C3N4 nanosheet in water
1489 disinfection, Appl. Catal., A 590 (2020) 117282. DOI:
1490 https://doi.org/10.1016/j.apcata.2019.117282
1491 [185] P. Xia, S. Cao, B. Zhu, M. Liu, M. Shi, J. Yu, Y. Zhang, Designing a 0D/2D S-Scheme
1492 Heterojunction over Polymeric Carbon Nitride for Visible-Light Photocatalytic Inactivation
1493 of Bacteria, Angew. Chem. Int. Ed. 59 (2020) 5218-5225. DOI:
1494 https://doi.org/10.1002/anie.201916012
1495 [186] F. Wei, J. Li, C. Dong, Y. Bi, X. Han, Plasmonic Ag decorated graphitic carbon nitride
1496 sheets with enhanced visible-light response for photocatalytic water disinfection and organic
1497 pollutant removal, Chemosphere 242 (2020) 125201. DOI:
1498 https://doi.org/10.1016/j.chemosphere.2019.125201
1499 [187] X. Hu, X. Zeng, Y. Liu, J. Lu, S. Yuan, Y. Yin, J. Hu, D.T. McCarthy, X. Zhang,
1500 Nano-layer based 1T-rich MoS2/g-C3N4 co-catalyst system for enhanced photocatalytic and
1501 photoelectrochemical activity, Appl. Catal. B 268 (2020) 118466. DOI:
1502 https://doi.org/10.1016/j.apcatb.2019.118466
1503 [188] Q. Gao, J. Xu, Z. Wang, Y. Zhu, Enhanced visible photocatalytic oxidation activity of
1504 perylene diimide/g-C3N4 n-n heterojunction via pi-pi interaction and interfacial charge

separation, Appl. Catal. B 271 (2020) 118933. DOI: https://doi.org/10.1016/j.apcatb.2020.118933

[189] H. Ding, D. Han, Y. Han, Y. Liang, X. Liu, Z. Li, S. Zhu, S. Wu, Visible light responsive CuS/ protonated g-C3N4 heterostructure for rapid sterilization, J. Hazard. Mater. 393 (2020) 122423. DOI: https://doi.org/10.1016/j.jhazmat.2020.122423

[190] C. Zhang, M. Zhang, Y. Li, D. Shuai, Visible-light-driven photocatalytic disinfection of human adenovirus by a novel heterostructure of oxygen-doped graphitic carbon nitride and hydrothermal carbonation carbon, Appl. Catal. B 248 (2019) 11-21. DOI: https://doi.org/10.1016/j.apcatb.2019.02.009

[191] X. Zeng, S. Lan, I.M.C. Lo, Rapid disinfection of E-coli by a ternary BiVO4/Ag/g-C3N4 composite under visible light: photocatalytic mechanism and performance investigation in authentic sewage, Environmen. Sci.-Nano 6 (2019) 610-623. DOI: https://doi.org/10.1039/c8en01283k

[192] Y. Liu, X. Zeng, X. Hu, J. Hu, Z. Wang, Y. Yin, C. Sun, X. Zhang, Two-dimensional g-C3N4/TiO2 nanocomposites as vertical Z-scheme heterojunction for improved photocatalytic water disinfection, Catal. Today 335 (2019) 243-251. DOI: https://doi.org/10.1016/j.cattod.2018.11.053

[193] Z. Jiang, B. Wang, Y. Li, H.S. Chan, H. Sun, T. Wang, H. Li, S. Yuan, M.K.H. Leung, A. Lu, P.K. Wong, Solar-light-driven rapid water disinfection by ultrathin magnesium titanate/carbon nitride hybrid photocatalyst: Band structure analysis and role of reactive oxygen species, Appl. Catal. B 257 (2019) 117898. DOI: https://doi.org/10.1016/j.apcatb.2019.117898

1527 [194] S. Kang, L. Zhang, M. He, Y. Zheng, L. Cui, D. Sun, B. Hu, "Alternated cooling and
1528 heating" strategy enables rapid fabrication of highly-crystalline g-C3N4 nanosheets for
1529 efficient photocatalytic water purification under visible light irradiation, Carbon 137 (2018)
1530 19-30. DOI: https://doi.org/10.1016/j.carbon.2018.05.010
1531 [195] J. Xu, Z. Wang, Y. Zhu, Enhanced Visible-Light-Driven Photocatalytic Disinfection
1532 Performance and Organic Pollutant Degradation Activity of Porous g-C3N4 Nanosheets,
1533 ACS Appl. Mater. Inter. 9 (2017) 27727-27735. DOI:
1534 https://doi.org/10.1021/acsami.7b07657
1535 [196] L. Sung, T. Du, C. Hu, J. Chen, J. Lu, Z. Lu, H. Han, Antibacterial Activity of
1536 Grophene Oxide/g-C3N4 Composite through Photocatalytic Disinfection under Visible Light,
1537 ACS Sustain. Chem. Eng. 5 (2017) 8693-8701. DOI:
1538 https://doi.org/10.1021/acssuschemeng.7b01431
1539 [197] J. Li, Y. Yin, E. Liu, Y. Ma, J. Wan, J. Fan, X. Hu, In situ growing Bi2MoO6 on g-
1540 C3N4 nanosheets with enhanced photocatalytic hydrogen evolution and disinfection of
1541 bacteria under visible light irradiation, J. Hazard. Mater. 321 (2017) 183-192. DOI:
1542 https://doi.org/10.1016/j.jhazmat.2016.09.008
1543 [198] H. Zhao, H. Yu, X. Quan, S. Chen, Y. Zhang, H. Zhao, H. Wang, Fabrication of atomic
1544 single layer graphitic-C3N4 and its high performance of photocatalytic disinfection under
1545 visible light irradiation, Appl. Catal. B 152 (2014) 46-50. DOI:
1546 https://doi.org/10.1016/j.apcatb.2014.01.023
1547 [199] Y. Deng, L. Tang, G. Zeng, Z. Zhu, M. Yan, Y. Zhou, J. Wang, Y. Liu, J. Wang,
1548 Insight into highly efficient simultaneous photocatalytic removal of Cr(VI) and 2,4-

1549 dichlorophenol under visible light irradiation by phosphorus doped porous ultrathin g-C3N4
1550 nanosheets from aqueous media: Performance and reaction mechanism, Appl. Catal. B 203
1551 (2017) 343-354. DOI: https://doi.org/10.1016/j.apcatb.2016.10.046
1552 [200] X. Du, X. Yi, P. Wang, J. Deng, C.-c. Wang, Enhanced photocatalytic Cr(VI) reduction
1553 and diclofenac sodium degradation under simulated sunlight irradiation over MIL-100(Fe)/g-
1554 C3N4 heterojunctions, Chinese Journal of Catalysis 40 (2019) 70-79. DOI:
1555 https://doi.org/10.1016/S1872-2067(18)63160-2
1556 [201] H.-H. Wu, C.-W. Chang, D. Lu, K. Maeda, C. Hu, Synergistic Effect of Hydrochloric
1557 Acid and Phytic Acid Doping on Polyaniline-Coupled g-C3N4 Nanosheets for Photocatalytic
1558 Cr(VI) Reduction and Dye Degradation, ACS Appl. Mater. Inter. 11 (2019) 35702-35712.
1559 DOI: https://doi.org/10.1021/acsami.9b10555
1560 [202] X. Ding, D. Xiao, L. Ji, D. Jin, K. Dai, Z. Yang, S. Wang, H. Chen, Simple fabrication
1561 of Fe3O4/C/g-C3N4 two-dimensional composite by hydrothermal carbonization approach
1562 with enhanced photocatalytic performance under visible light, Catal. Sci. Technol. 8 (2018)
1563 3484-3492. DOI: https://doi.org/10.1039/c8cy00698a
1564 [203] D. Chen, J. Fang, S. Lu, G. Zhou, W. Feng, F. Yang, Y. Chen, Z. Fang, Fabrication of
1565 Bi modified Bi2S3 pillared g-C3N4 photocatalyst and its efficient photocatalytic reduction
1566 and oxidation performances, Appl. Surf. Sci. 426 (2017) 427-436. DOI:
1567 https://doi.org/10.1016/j.apsusc.2017.07.139
1568 [204] S. Patnaik, K.K. Das, A. Mohanty, K. Parida, Enhanced photo catalytic reduction of Cr
1569 (VI) over polymer-sensitized g-C3N4/ZnFe2O4 and its synergism with phenol oxidation

1570 under visible light, Catal. Today 315 (2018) 52-66. DOI:
1571 https://doi.org/10.1016/j.cattod.2018.04.008
1572 [205] M.-h. Wu, L. Li, Y.-c. Xue, G. Xu, L. Tang, N. Liu, W.-y. Huang, Fabrication of
1573 ternary GO/g-C3N4/MoS2 flower-like heterojunctions with enhanced photocatalytic activity
1574 for water remediation, Appl. Catal. B 228 (2018) 103-112. DOI:
1575 https://doi.org/10.1016/j.apcatb.2018.01.063
1576 [206] X. Zhou, C. Shao, S. Yang, X. Li, X. Guo, X. Wang, X. Li, Y. Liu, Heterojunction of
1577 g-C3N4/BiOI Immobilized on Flexible Electrospun Polyacrylonitrile Nanofibers: Facile
1578 Preparation and Enhanced Visible Photocatalytic Activity for Floating Photocatalysis, ACS
1579 Sustain. Chem. Eng. 6 (2018) 2316-2323. DOI:
1580 https://doi.org/10.1021/acssuschemeng.7b03760
1581 [207] D. Chen, J. Liu, Z. Jia, J. Fang, F. Yang, Y. Tang, K. Wu, Z. Liu, Z. Fang, Efficient
1582 visible-light-driven hydrogen evolution and Cr(VI) reduction over porous P and Mo co-doped
1583 g-C3N4 with feeble N vacancies photocatalyst, J. Hazard. Mater. 361 (2019) 294-304. DOI:
1584 https://doi.org/10.1016/j.jhazmat.2018.09.006
1585 [208] H.S. El-Sheshtawy, H.M. El-Hosainy, K.R. Shoeir, I.M. El-Mehasseb, M. El-Kemary,
1586 Facile immobilization of Ag nanoparticles on g-C3N4/V2O5 surface for enhancement of
1587 post-illumination, catalytic, and photocatalytic activity removal of organic and inorganic
1588 pollutants, Appl. Surf. Sci. 467 (2019) 268-276. DOI:
1589 https://doi.org/10.1016/j.apsusc.2018.10.109
1590 [209] J. Gu, H. Chen, F. Jiang, X. Wang, L. Li, All-solid-state Z-scheme Co9S8/graphitic
1591 carbon nitride photocatalysts for simultaneous reduction of Cr(VI) and oxidation of 2,4-

1592 dichlorophenoxyacetic acid under simulated solar irradiation, Chem. Eng. J. 360 (2019)
1593 1188-1198. DOI: https://doi.org/10.1016/j.cej.2018.10.137
1594 [210] K. Li, Z. Huang, S. Zhu, S. Luo, L. Yan, Y. Dai, Y. Guo, Y. Yang, Removal of Cr(VI)
1595 from water by a biochar-coupled g-C3N4 nanosheets composite and performance of a
1596 recycled photocatalyst in single and combined pollution systems, Appl. Catal. B 243 (2019)
1597 386-396. DOI: https://doi.org/10.1016/j.apcatb.2018.10.052
1598 [211] H. Zong, T. Zhao, G. Zhou, R. Qian, T. Feng, J.H. Pan, Revisiting structural and
1599 photocatalytic properties of g-C3N4/TiO2: Is surface modification of TiO2 by calcination
1600 with urea an effective route to "solar" photocatalyst?, Catal. Today 335 (2019) 252-261. DOI:
1601 https://doi.org/10.1016/j.cattod.2018.12.015
1602 [212] S. Wang, F. Li, X. Dai, C. Wang, X. Lv, G.I.N. Waterhouse, H. Fan, S. Ai, Highly
1603 flexible and stable carbon nitride/cellulose acetate porous films with enhanced photocatalytic
1604 activity for contaminants removal from wastewater, J. Hazard. Mater. 384 (2020) 121417.
1605 DOI: https://doi.org/10.1016/j.jhazmat.2019.121417
1606 [213] F. Zhao, Y. Liu, S. Ben Hammouda, B. Doshi, N. Guijarro, X. Min, C.-J. Tang, M.
1607 Sillanpaa, K. Sivula, S. Wang, MIL-101(Fe)/g-C3N4 for enhanced visible-light-driven
1608 photocatalysis toward simultaneous reduction of Cr(VI) and oxidation of bisphenol A in
1609 aqueous media, Appl. Catal. B 272 (2020) 119033. DOI:
1610 https://doi.org/10.1016/j.apcatb.2020.119033
1611 [214] M. Zhou, X.W. Lou, Y. Xie, Two-dimensional nanosheets for photoelectrochemical
1612 water splitting: Possibilities and opportunities, Nano Today 8 (2013) 598-618. DOI:
1613 https://doi.org/10.1016/j.nantod.2013.12.002

1614 [215] S. Ida, T. Ishihara, Recent Progress in Two-Dimensional Oxide Photocatalysts for
1615 Water Splitting, J. Phys. Chem. Lett. 5 (2014) 2533-2542. DOI:
1616 https://doi.org/10.1021/jz5010957
1617 [216] L. Liang, F. Lei, S. Gao, Y. Sun, X. Jiao, J. Wu, S. Qamar, Y. Xie, Single Unit Cell
1618 Bismuth Tungstate Layers Realizing Robust Solar CO2 Reduction to Methanol, Angew.
1619 Chem. Int. Ed. 54 (2015) 13971-13974. DOI: https://doi.org/10.1002/anie.201506966
1620 [217] Z. Zhang, J. Huang, M. Zhang, Q. Yuan, B. Dong, Ultrathin hexagonal SnS2
1621 nanosheets coupled with g-C3N4 nanosheets as 2D/2D heterojunction photocatalysts toward
1622 high photocatalytic activity, Appl. Catal. B 163 (2015) 298-305. DOI:
1623 https://doi.org/10.1016/j.apcatb.2014.08.013
1624 [218] J. Di, J. Xia, M. Ji, H. Li, H. Xu, H. Li, R. Chen, The synergistic role of carbon
1625 quantum dots for the improved photocatalytic performance of Bi2MoO6, Nanoscale 7 (2015)
1626 11433-11443. DOI: https://doi.org/10.1039/c5nr01350j
1627 [219] C. Feng, Y. Deng, L. Tang, G. Zeng, J. Wang, J. Yu, Y. Liu, B. Peng, H. Feng, J.
1628 Wang, Core-shell Ag2CrO4/N-GQDs@g-C3N4 composites with anti-photocorrosion
1629 performance for enhanced full-spectrum-light photocatalytic activities, Appl. Catal. B 239
1630 (2018) 525-536. DOI: https://doi.org/10.1016/j.apcatb.2018.08.049
1631 [220] S. Luo, Z. Zeng, G. Zeng, Z. Liu, R. Xiao, M. Chen, L. Tang, W. Tang, C. Lai, M.
1632 Cheng, B. Shao, Q. Liang, H. Wang, D. Jiang, Metal Organic Frameworks as Robust Host of
1633 Palladium Nanoparticles in Heterogeneous Catalysis: Synthesis, Application, and Prospect,
1634 ACS Appl. Mater. Inter. 11 (2019) 32579-32598. DOI:
1635 https://doi.org/10.1021/acsami.9b11990

1636 [221] Y. Liu, D. Huang, M. Cheng, Z. Liu, C. Lai, C. Zhang, C. Zhou, W. Xiong, L. Qin, B.
1637 Shao, Q. Liang, Metal sulfide/MOF-based composites as visible-light-driven photocatalysts
1638 for enhanced hydrogen production from water splitting, Coord. Chem. Rev. 409 (2020)
1639 213220. DOI: https://doi.org/10.1016/j.ccr.2020.213220
1640 [222] Y.C. Deng, L. Tang, C.Y. Feng, G.M. Zeng, J.J. Wang, Y. Lu, Y.N. Liu, J.F. Yu, S.
1641 Chen, Y.Y. Zhou, Construction of Plasmonic Ag and Nitrogen-Doped Graphene Quantum
1642 Dots Codecorated Ultrathin Graphitic Carbon Nitride Nanosheet Composites with Enhanced
1643 Photocatalytic Activity: Full-Spectrum Response Ability and Mechanism Insight, ACS Appl.
1644 Mater. Inter. 9 (2017) 42816-42828. DOI: https://doi.org/10.1021/acsami.7b14541
1645 [223] Y.C. Deng, L. Tang, C.Y. Feng, G.M. Zeng, J.J. Wang, Y.Y. Zhou, Y.N. Liu, B. Peng,
1646 H.P. Feng, Construction of plasmonic Ag modified phosphorous-doped ultrathin g-C3N4
1647 nanosheets/BiVO4 photocatalyst with enhanced visible-near-infrared response ability for
1648 ciprofloxacin degradation, J. Hazard. Mater. 344 (2018) 758-769. DOI:
1649 https://doi.org/10.1016/j.jhazmat.2017.11.027
1650 [224] H. Li, W. Tu, Y. Zhou, Z. Zou, Z-Scheme Photocatalytic Systems for Promoting
1651 Photocatalytic Performance: Recent Progress and Future Challenges, Adv. Sci. 3 (2016)
1652 1500389. DOI: https://doi.org/10.1002/advs.201500389
1653 [225] X. Li, Z. Huang, Z. Liu, K. Diao, G. Fan, Z. Huang, X. Tan, In situ photocalorimetry:
1654 An alternative approach to study photocatalysis by tracing heat changes and kinetics, Appl.
1655 Catal. B 181 (2016) 79-87. DOI: https://doi.org/10.1016/j.apcatb.2015.07.036
1656 [226] X. Li, T. Wan, J. Qiu, H. Wei, F. Qin, Y. Wang, Y. Liao, Z. Huang, X. Tan, In-situ
1657 photocalorimetry-fluorescence spectroscopy studies of RhB photocatalysis over Z-scheme g-

1658 C3N4@Ag@Ag3PO4 nanocomposites: A pseudo-zero-order rather than a first-order process,
1659 Appl. Catal. B 217 (2017) 591-602. DOI: https://doi.org/10.1016/j.apcatb.2017.05.086
1660 [227] D. Huang, S. Chen, G. Zeng, X. Gong, C. Zhou, M. Cheng, W. Xue, X. Yan, J. Li,
1661 Artificial Z-scheme photocatalytic system: What have been done and where to go?, Coord.
1662 Chem. Rev. 385 (2019) 44-80. DOI: https://doi.org/10.1016/j.ccr.2018.12.013
1663 [228] M. Cheng, G. Zeng, D. Huang, C. Lai, P. Xu, C. Zhang, Y. Liu, Hydroxyl radicals
1664 based advanced oxidation processes (AOPs) for remediation of soils contaminated with
1665 organic compounds: A review, Chem. Eng. J. 284 (2016) 582-598. DOI:
1666 https://doi.org/10.1016/j.cej.2015.09.001
1667 [229] H. Guo, C.-G. Niu, L. Zhang, X.-J. Wen, C. Liang, X.-G. Zhang, D.-L. Guan, N. Tang,
1668 G.-M. Zeng, Construction of Direct Z-Scheme AgI/Bi2Sn2O7 Nanojunction System with
1669 Enhanced Photocatalytic Activity: Accelerated Interfacial Charge Transfer Induced Efficient
1670 Cr(VI) Reduction, Tetracycline Degradation and Escherichia coli Inactivation, ACS Sustain.
1671 Chem. Eng. 6 (2018) 8003-8018. DOI: https://doi.org/10.1021/acssuschemeng.8b01448
1672 [230] P.J.J. Alvarez, C.K. Chan, M. Elimelech, N.J. Halas, D. Villagrán, Emerging
1673 opportunities for nanotechnology to enhance water security, Nat. Nanotechnol. 13 (2018)
1674 634-641. DOI: https://doi.org/10.1038/s41565-018-0203-2
1675 [231] B.C. Hodges, E.L. Cates, J.-H. Kim, Challenges and prospects of advanced oxidation
1676 water treatment processes using catalytic nanomaterials, Nat. Nanotechnol. 13 (2018) 642-
1677 650. DOI: https://doi.org/10.1038/s41565-018-0216-x
1678 [232] E. Valsami-Jones, I. Lynch, How safe are nanomaterials?, Science 350 (2015) 388.
1679 DOI: https://doi.org/10.1126/science.aad0768

[233] C. Liu, D. Kong, P.-C. Hsu, H. Yuan, H.-W. Lee, Y. Liu, H. Wang, S. Wang, K. Yan, D. Lin, P.A. Maraccini, K.M. Parker, A.B. Boehm, Y. Cui, Rapid water disinfection using vertically aligned MoS2 nanofilms and visible light, Nat. Nanotechnol. 11 (2016) 1098-1104. DOI: https://doi.org/10.1038/nnano.2016.138

[234] H. Liu, S. Ma, L. Shao, H. Liu, Q. Gao, B. Li, H. Fu, S. Fu, H. Ye, F. Zhao, J. Zhou, Defective engineering in graphitic carbon nitride nanosheet for efficient photocatalytic pathogenic bacteria disinfection, Appl. Catal. B 261 (2020) 118201. DOI: https://doi.org/10.1016/j.apcatb.2019.118201

[235] A. Zhitkovich, Chromium in Drinking Water: Sources, Metabolism, and Cancer Risks, Chem. Res. Toxicol. 24 (2011) 1617-1629. DOI: https://doi.org/10.1021/tx200251t

[236] J. Preethi, M.H. Farzana, S. Meenakshi, Photo-reduction of Cr(VI) using chitosan supported zinc oxide materials, Int. J. Biol. Macromol. 104 (2017) 1783-1793. DOI: https://doi.org/10.1016/j.ijbiomac.2017.02.082

[237] M.V. Dozzi, S. Marzorati, M. Longhi, M. Coduri, L. Artiglia, E. Selli, Photocatalytic activity of TiO2-WO3 mixed oxides in relation to electron transfer efficiency, Appl. Catal. B 186 (2016) 157-165. DOI: https://doi.org/10.1016/j.apcatb.2016.01.004

[238] B. Ou, J. Wang, Y. Wu, S. Zhao, Z. Wang, Efficient removal of Cr (VI) by magnetic and recyclable calcined CoFe-LDH/g-C3N4 via the synergy of adsorption and photocatalysis under visible light, Chem. Eng. J. 380 (2020) 122600. DOI: https://doi.org/10.1016/j.cej.2019.122600

[239] L. Zhang, C.-G. Niu, X.-J. Wen, H. Guo, X.-F. Zhao, D.-W. Huang, G.-M. Zeng, A facile strategy to fabricate hollow cadmium sulfide nanospheres with nanoparticles-textured

surface for hexavalent chromium reduction and bacterial inactivation, J. Colloid. Interface. Sci. 514 (2018) 396-406. DOI: 10.1016/j.jcis.2017.12.048

[240] A. Sudhaik, P. Raizada, S. Thakur, A.K. Saini, P. Singh, A. Hosseini-Bandegharaei, Metal-free photo-activation of peroxymonosulfate using graphene supported graphitic carbon nitride for enhancing photocatalytic activity, Mater. Lett. 277 (2020) 128277. DOI: https://doi.org/10.1016/j.matlet.2020.128277

[241] H. Heng, J. Yang, Y. Yin, P. Meng, X. Liu, Effect of precursor types on the performance of polyimide: A metal-free visible-light-driven photocatalyst for effective photocatalytic degradation of pollutants, Catal. Today 340 (2020) 225-235. DOI: https://doi.org/10.1016/j.cattod.2019.01.019

[242] Y. Li, C. Zhang, D. Shuai, S. Naraginti, D. Wang, W. Zhang, Visible-light-driven photocatalytic inactivation of MS2 by metal-free g-C3N4: Virucidal performance and mechanism, Water Res. 106 (2016) 249-258. DOI: https://doi.org/10.1016/j.watres.2016.10.009

[243] F. Zhang, Q. Wen, M. Hong, Z. Zhuang, Y. Yu, Efficient and sustainable metal-free GR/C3N4/CDots ternary heterostructrues for versatile visible-light-driven photoredox applications: Toward synergistic interaction of carbon materials, Chem. Eng. J. 307 (2017) 593-603. DOI: https://doi.org/10.1016/j.cej.2016.08.120

[244] R.S. Sahu, Y.-h. Shih, W.-L. Chen, New insights of metal free 2D graphitic carbon nitride for photocatalytic degradation of bisphenol A, J. Hazard. Mater. 402 (2021) 123509. DOI: https://doi.org/10.1016/j.jhazmat.2020.123509

[245] Y. Zheng, J. Liu, J. Liang, M. Jaroniec, S.Z. Qiao, Graphitic carbon nitride materials: controllable synthesis and applications in fuel cells and photocatalysis, Energy Environ. Sci. 5 (2012) 6717-6731. DOI: https://doi.org/10.1039/c2ee03479d

[246] T. Xu, R. Zou, X. Lei, X. Qi, Q. Wu, W. Yao, Q. Xu, New and stable g-C3N4/HAp composites as highly efficient photocatalysts for tetracycline fast degradation, Appl. Catal. B 245 (2019) 662-671. DOI: https://doi.org/10.1016/j.apcatb.2019.01.020

[247] H. Ji, P. Du, D. Zhao, S. Li, F. Sun, E.C. Duin, W. Liu, 2D/1D graphitic carbon nitride/titanate nanotubes heterostructure for efficient photocatalysis of sulfamethazine under solar light: Catalytic "hot spots" at the rutile–anatase–titanate interfaces, Appl. Catal. B 263 (2020) 118357. DOI: https://doi.org/10.1016/j.apcatb.2019.118357

[248] X. Zhang, H. Wang, H. Wang, Q. Zhang, J. Xie, Y. Tian, J. Wang, Y. Xie, Single-Layered Graphitic-C3N4 Quantum Dots for Two-Photon Fluorescence Imaging of Cellular Nucleus, Adv. Mater. 26 (2014) 4438-4443. DOI: https://doi.org/10.1002/adma.201400111

[249] B. Zhu, P. Xia, W. Ho, J. Yu, Isoelectric point and adsorption activity of porous g-C3N4, Appl. Surf. Sci. 344 (2015) 188-195. DOI: https://doi.org/10.1016/j.apsusc.2015.03.086

[250] X. Bai, S. Yan, J. Wang, L. Wang, W. Jiang, S. Wu, C. Sun, Y. Zhu, A simple and efficient strategy for the synthesis of a chemically tailored g-C3N4 material, J. Mater. Chem. A 2 (2014) 17521-17529. DOI: https://doi.org/10.1039/C4TA02781G

[251] Z. Zhou, J. Wang, J. Yu, Y. Shen, Y. Li, A. Liu, S. Liu, Y. Zhang, Dissolution and Liquid Crystals Phase of 2D Polymeric Carbon Nitride, J. Am. Chem. Soc. 137 (2015) 2179-2182. DOI: https://doi.org/10.1021/ja512179x

[252] Y. Shi, S. Jiang, K. Zhou, C. Bao, B. Yu, X. Qian, B. Wang, N. Hong, P. Wen, Z. Gui, Y. Hu, R.K.K. Yuen, Influence of g-C3N4 Nanosheets on Thermal Stability and Mechanical Properties of Biopolymer Electrolyte Nanocomposite Films: A Novel Investigation, ACS Appl. Mater. Inter. 6 (2014) 429-437. DOI: https://doi.org/10.1021/am4044932

[253] Y. Wang, R. Ou, H. Wang, T. Xu, Graphene oxide modified graphitic carbon nitride as a modifier for thin film composite forward osmosis membrane, J. Membr. Sci. 475 (2015) 281-289. DOI: https://doi.org/10.1016/j.memsci.2014.10.028

[254] L. Liu, Y. Qi, J. Lu, S. Lin, W. An, Y. Liang, W. Cui, A stable Ag3PO4@g-C3N4 hybrid core@shell composite with enhanced visible light photocatalytic degradation, Appl. Catal. B 183 (2016) 133-141. DOI: https://doi.org/10.1016/j.apcatb.2015.10.035

[255] M. Jourshabani, J.A. Dominic, G. Achari, Z. Shariatinia, Synergetic photocatalytic ozonation using modified graphitic carbon nitride for treatment of emerging contaminants under UVC, UVA and visible irradiation, Chem. Eng. Sci. 209 (2019) 115181. DOI: https://doi.org/10.1016/j.ces.2019.115181

[256] S. Gu, C.-T. Hsieh, Y. Ashraf Gandomi, J.-K. Chang, J. Li, J. Li, H. Zhang, Q. Guo, K.C. Lau, R. Pandey, Microwave growth and tunable photoluminescence of nitrogen-doped graphene and carbon nitride quantum dots, Journal of Materials Chemistry C 7 (2019) 5468-5476. DOI: https://doi.org/10.1039/C9TC00233B